

**UNIVERSIDADE DE SÃO PAULO**  
**CENTRO DE ENERGIA NUCLEAR NA AGRICULTURA**

**ALI MEHMANDOOST KOTLAR**

**Mitigation of nitrate leaching in tropical soils using  
Layered Double Hydroxide**

**Piracicaba**  
**2020**



**Ali MEHMANDOOST KOTLAR**

**Mitigation of nitrate leaching in tropical soils using  
Layered Double Hydroxide**

**Thesis presented to Center for Nuclear Energy in  
Agriculture of the University of São Paulo as a  
requisite to the Doctoral Degree in Sciences**

**Concentration Area: Nuclear Energy in  
Agriculture and Environment**

**Advisor: Prof. Dr. Quirijn de Jong Van Lier**

**Piracicaba  
2020**

AUTORIZO A DIVULGAÇÃO TOTAL OU PARCIAL DESTE TRABALHO, POR QUALQUER MEIO CONVENCIONAL OU ELETRÔNICO, PARA FINS DE ESTUDO E PESQUISA, DESDE QUE CITADA A FONTE.

International Cataloging Data on Publication (CIP)

**Seção Técnica de Biblioteca - CENA/USP**

Mehmandoost Kotlar, Ali

Mitigação da lixiviação de nitrato em solos tropicais usando hidróxidos duplos lamelares / Mitigation of nitrate leaching in tropical soils using layered double hydroxide / Ali Mehmandoost Kotlar; orientador Quirijn de Jong van Lier. - - Piracicaba, 2020.  
109 p. : il.

Tese (Doutorado – Programa de Pós-Graduação em Ciências. Área de Concentração: Energia Nuclear na Agricultura e no Ambiente) – Centro de Energia Nuclear na Agricultura, Universidade de São Paulo, 2020.

1. Condutividade hidráulica do solo 2. Lixiviação do solo 3. Nitratos 4. Pedologia – Transferência 5. Rizosfera 6. Simulação 7. Solos – Propriedades físicas I. Título.

CDU 631.432.3

**Elaborada por:**

Marilia Ribeiro Garcia Henyei

CRB-8/3631

Resolução CFB N° 184 de 29 de setembro de 2017

To four beloved people in my life: my parents, my brother Hossein and to Quirijn, my  
inspiration in life



## ACKNOWLEDGEMENT

I have been very fortunate to have met a terrific, generous and thoughtful supervisor, Quirijn, who has always inspired me to do my best and work my hardest in all I do. His extraordinary human qualities taught me a lot during these four years, how to be a friendly, charming and influential supervisor.

I am grateful to my friends in our lovely lab, starting from 2016 by knowing Andre Herman who just changed my life when he introduced Quirijn, Thalita who taught me how to tackle all difficulties within my PhD track, Everton, Victor, Leonardo, Marina and lastly Maria Eliza for all support she gave me. I am also thankful to my old but unforgettable friends in Iran, Farid and Pouya with whom I shared the greatest moments.

To Dr. Bo V. Iversen for the great and productive time I had during my visiting period between March 2018 to February 2019 at Aarhus university, Denmark.

To Dr. Hudson Carvalho who has ignited the first idea of this project in 2016 and his great first impression he made for me to come much more enthusiastic to CENA/USP to pursue my PhD.

I am also so grateful to FAPESP (Fundação de Amparo à Pesquisa do Estado de São Paulo), Brazil, for providing financial support (scholarship) for this project (Process n° 2016/18636-7) during my stay in Brazil and supporting a 10-month visiting period in Aarhus University in Denmark (Process n° 2017/21945-4) as well as CAPES (Coordination for the Improvement of Higher Education Personnel - Brazil) for funding part of this PhD thesis – Financing Code 001.

I am really proud of being student of USP/CENA where I was given this fabulous opportunity to do my PhD research.



## ABSTRACT

Mehmandoost Kotlar, Ali. **Mitigation of nitrate leaching in tropical soils using layered double hydroxide**. 2020. 109 p. Tese (Doutorado em Ciências) - Centro de Energia Nuclear na Agricultura, Universidade de São Paulo, Piracicaba, 2020.

Nitrate is the most intensively applied nutrient to agricultural land. Being a very mobile anion, even more in tropical acidic soils, its leaching easily contaminates surface and groundwater thus causing large financial loss for farmers. Estimation of water and solute fluxes using numerical models can be used to evaluate the efficiency of any hypothetical fertilizer management under a variety of soil and climatic conditions. As input, these models mainly require soil hydraulic properties, meteorological data and management scenarios. Therefore, the first objective of this study was to estimate soil hydraulic properties including water retention and hydraulic conductivity functions using easily measurable soil properties such as texture, organic matter or bulk density. Regarding nitrogen management practices, it is supposed that slow release fertilizers gradually release nitrate for root uptake leading to a reduction of nitrate loss, making them a good alternative to conventional fertilizers. This process was hypothetically modelled assuming application of slow-release fertilizers with different half-lives of 10, 20, 30 and 40 days under cultivation of summer maize and applying the commonly recommended  $180 \text{ kg N ha}^{-1}$ . The yield of maize under application of SRFs with half-lives of 30 and 40 days showed to increase up to  $200 \text{ kg N ha}^{-1}$  and reduce leaching of nitrogen by  $30$  to  $40 \text{ kg ha}^{-1}$ , unless bottom layers of the soil profile are very permeable. Finally, layered double hydroxides (LDH) which are supposed to be potentially applicable as slow release nitrate fertilizers were synthesized using a coprecipitation method and characterized by ICP-OES, XRD, FTIR and TGA analyses for nitrate release and leaching experiments. Batch experiments with LDH particles KCl,  $\text{K}_2\text{SO}_4$  or  $\text{CaCl}_2$  showed that 60 to 100% of intercalated nitrate is exchanged by anions within a few hours. Soil column studies with soils from temperate (Denmark) and tropical (Brazil) regions confirmed rapid release of nitrate from LDH. Application of LDH to a soil profile with bulk density of  $1300 \text{ kg m}^{-3}$ , 0.3 m rooting depth and a typical rate of field nitrogen application ( $120 \text{ kg ha}^{-1}$ ) caused an accumulation of 400 to 1050 kg Mg and 230 to 478 kg of Fe or Al depending on type of LDH. This high load of residual metals and the relatively quick release of nitrate may restrain the use of the LDH as slow release nitrate source.

Keywords: Layered double hydroxide. Nitrate leaching. Pedotransfer functions. Nitrate Transport modeling. Soil hydraulic properties.



## RESUMO

Mehmandoost Kotlar, Ali. **Mitigação da lixiviação de nitrato em solos tropicais usando hidróxidos duplos lamelares**. 2020. 109 p. Tese (Doutorado) - Centro de Energia Nuclear na Agricultura, Universidade de São Paulo, Piracicaba, 2020.

O nitrato é o nutriente mais intensamente aplicado às terras agrícolas. Sendo um ânion muito móvel, especialmente em solos ácidos tropicais, sua lixiviação pode contaminar as águas superficiais e subterrâneas e causar grandes perdas financeiras para os agricultores. A estimativa de fluxos de água e solutos usando modelos numéricos é uma alternativa para avaliar a eficiência de qualquer manejo hipotético de fertilizantes sob diversas condições climáticas e do solo. Esses modelos requerem como dados de entrada principalmente as propriedades hidráulicas do solo, dados meteorológicos e cenários de manejo. O primeiro objetivo deste estudo é estimar as propriedades hidráulicas do solo, incluindo funções de retenção de água e condutividade hidráulica, usando propriedades facilmente mensuráveis do solo, como textura, matéria orgânica e densidade do solo. Em relação às práticas de manejo do nitrogênio, supõe-se que os fertilizantes de liberação lenta (FLL) sejam alternativas ideais, liberando gradualmente o nitrato para ser absorvido pelas raízes, resultando na minimização da perda de nitrato. Esse processo foi hipoteticamente modelado, assumindo a aplicação de fertilizante de liberação lenta com tempos de meias-vida de 10, 20, 30 e 40 dias sob cultivo de milho de verão e 180 kg N ha<sup>-1</sup> usualmente recomendados. Os resultados demonstraram que o rendimento de milho sob aplicação de FLLs com meia-vida de 30 e 40 dias pode aumentar até 200 kg N ha<sup>-1</sup> e a lixiviação de nitrogênio diminui de 30 a 40 kg ha<sup>-1</sup>, a menos que as camadas inferiores do perfil do solo sejam muito permeáveis. Por fim, os hidróxidos duplos em camadas (LDH) são conhecidos por serem fertilizantes de liberação lenta de nitrato, sintetizados pelo método de coprecipitação e caracterizados pela análise de ICP-OES, DRX, FTIR e TGA para liberação de nitrato e experimentos que avaliam lixiviação. Experimentos em lotes com partículas de LDH KCl, K<sub>2</sub>SO<sub>4</sub> ou CaCl<sub>2</sub> mostraram que 60 a 100% do nitrato intercalado é trocado por ânions dentro de algumas horas. Estudos de coluna de solo com solos das regiões temperada (Dinamarca) e tropical (Brasil) confirmaram a liberação rápida de nitrato do LDH. A aplicação de LDH em um perfil de solo com densidade de 1300 kg m<sup>-3</sup>, profundidade de raízes de 0,3 m e uma taxa típica de aplicação de nitrogênio no campo (120 kg ha<sup>-1</sup>) causaram acúmulo de 400 a 1050 kg de Mg e 230 a 478 kg de Fe ou Al, dependendo do tipo de LDH. Essa alta carga de metais residuais pode restringir o uso do LDH como fonte de nitrato de liberação lenta.

Palavras-chave: Hidróxidos duplos lamelares. Lixiviação o nitrato. Funções de pedotransferência. Propriedades físicas do solo.



## LIST OF FIGURES

- Figure 2.1 Geographical position of sampled soils (A to H) and the University of São Paulo meteorological station (MS) in Piracicaba (SP), Brazil.
- Figure 2.2 Average monthly  $ET_0$  predicted by the calibrated Hargreaves equation -  $ET_{0H}$  and the Penman- Monteith equation -  $ET_{0P}$ , Precipitation (P) (a) and maximum, minimum temperature ( $T_{max}$  &  $T_{min}$ ) and Solar Radiation ( $R_s$ ) (b) for the University of São Paulo weather station in Piracicaba (SP), Brazil.
- Figure 2.3 Observed meteorological data versus simulated ones by LARS-WG: Left: Rainfall (P) and Evapotranspiration ( $ET_0$ ); Right: Radiation ( $R_a$ ) and Average Temperature ( $T_{ave}$ )
- Figure 2.4 Monthly observed and generated Dry and Wet Spell Length (DSL & WSL) (a) and Correlation of observed and generated DSL and WSL (b)
- Figure 2.5 Monthly drainage, evaporation and rainfall, averages and standard deviations for all soils under the bare soil (BS) scenario
- Figure 2.6 Soil Drainage Index (SDI) of each soil (A to H) calculated using  $h_{ms} = -1$  cm or  $h_{ms} = -3$  cm versus the average annual drainage under the bare soil (BS) scenario
- Figure 2.7 Performance of proposed models (RMSE and  $R^2$ ) for prediction of bare soil drainage
- Figure 2.8 Monthly average of drainage and evapotranspiration using real climatic data for 8 soils under BS, G30, G60 and G90 scenarios
- Figure 2.9 Ratio of actual to potential evapotranspiration for three grass scenarios, average monthly values from all soils.
- Figure 2.10 Performance of proposed models (RMSE and  $R^2$ ) for prediction of grass covered soil drainage
- Figure 3.1 Schematic design of the Automatic Drip Infiltrometer (ADI) apparatus for measuring unsaturated hydraulic conductivity.
- Figure 3.2 Response surfaces (2-D sensitivity analysis) of the objective function for pressure heads at three depths for parameter pairs (a)  $\alpha$ -n, (b)  $\alpha$ -  $\lambda$ , (c)  $\alpha$ -Ks, (d) n-  $\lambda$ , (e) n-Ks, (f) Ks-  $\lambda$
- Figure 3.3 (a) Simulated pressure head over time at three depths in simulated ADI experiments for three soil types; (b) example of the imposed stochastic bias added to the pressure heads for the silt soil. Numbers in the legend represent the depth (cm) of the tensiometers.
- Figure 3.4 Retention and hydraulic conductivity functions obtained in (a) soil column 7, the column with the highest deviation between  $K$  measured and obtained by inverse modeling, and (b) soil column 12, with the lowest respective deviation. Red circle in (a) shows the high deviation for some of the observed values.

- Figure 3.5 Average of water content at pF1, pF2, pF3 and pF4 obtained from SSM (steady state methods) versus corresponding values obtained from inverse modeling of ADI + PTF
- Figure 4.1 Quantification of released and required urea SRF applied in sowing date for scenario (i) and (ii)
- Figure 4.2 Changes in nitrogen uptake and leaching as well as yield under application of different SRFs with half-life of 10, 20, 30 and 40 days with the same weight of typical fertilizer compared to the corresponding values using typical
- Figure 4.3 Nitrogen uptake and leaching as well as grain yield of maize under application of different SRFs with half-life of 10, 20, 30 and 40 days and typical fertilizer with zero half-life
- Figure 5.1 XRD patterns of synthesized LDH
- Figure 5.2 FTIR spectra of synthesized LDH
- Figure 5.3 TGA and TDA curves of synthesized LDH
- Figure 5.4 Nitrate release fraction from LDH particles dispersed in of KCl, K<sub>2</sub>SO<sub>4</sub>, and CaCl<sub>2</sub> solutions with 0.01, 0.1 and 0.5 mol L<sup>-1</sup> ionic strength performed in the equilibrium (a) and in time dependent (kinetic) experiments (b)
- Figure 5.5 Dissolved fraction of Mg of LDH as a function of initial mass of LDH and pH of electrolyte background
- Figure 5.6 Breakthrough curves showing the relative loaded nitrate concentration ( $m/m_0$ ) as a function of the amount of leachate collected relative to the total pore volume (V/PV) after applying 3 g of LDH on the soil surface of columns with material from five Danish soils
- Figure 5.7 Breakthrough curves of (a) sand (L; large sand, S: small sand) and (b) real soil packed columns (with the name of locations as mentioned in Table 5.1), showing the relative loaded nitrate concentration ( $C/C_0$ ) as a function of the amount of leachate collected relative to the total pore volume (V/PV) after applying 3 g of LDH on the soil surface of columns with material from five Danish soils before and after addition of LDH
- Figure 5.8 Relative nitrate concentration ( $C/C_0$ ) as a function of the amount of leachate collected relative to the total pore volume (V/PV) after application of different doses of LDH (arrows show when and how many mg of LDH was applied) in various steps in loamy sandy (B1:a) and clay soil (B2:b)
- Figure 5.9 Mg (left) and Fe (right) intensities obtained from line scanning of two soil columns; sandy loam (B1: top) and clay (B2: bottom) by EDXRF; (L1; L2 and L3 are scanned lines)

## LIST OF TABLES

Table 2.1	Hydraulic parameters of the soils according to the van Genuchten (1980) equation
Table 2.2	Monthly averages (and, between brackets, standard deviations) of actual transpiration ( $T_a$ ), Drainage ( $D$ ) and Evaporation ( $E_v$ ), all in $\text{cm month}^{-1}$ , for G30, G60 and G90 scenarios in the wet (October to March) and dry season (April to September).
Table 3.1	Soil hydraulic parameters for reference soils (extracted from Vrugt et al., 2001). Values between brackets represent the range of values used in 1-D and 2-D Monte Carlo realizations
Table 3.2	RMSE and NSE of pressure heads obtained from simulations in sand, silt and clay soil (Table 3.1) scenarios in 100 Monte Carlo realizations for each of the VG parameters. Average (and standard deviations between brackets) for pressure heads at three depths (7, 10 and 13 cm), compared to values obtained with the reference parameter set.
Table 3.3	Soil hydraulic parameters estimated from synthesized data with and without added bias (standard deviation between parentheses if $\geq 0.5\%$ of average value), together with true values for sand, silt and clay reference soils.
Table 3.4	Statistical indicators of performance of the GPR pedotransfer functions for the prediction of $\theta_{pF1}$ , $\theta_{pF2}$ , $\theta_{pF3}$ , $\theta_{pF4.2}$ (volumetric water contents at pressure heads -0.1, -1, -10 and -158 m) for testing data and respective predictors (BD, bulk density; OM, organic matter content; sand, silt and clay contents)
Table 3.5	Average and coefficient of variation (CV) for measured soil physical and hydraulic properties and PTF-estimated water contents for the soil columns ( $n=15$ )
Table 3.6	Estimated parameters obtained from inverse modeling of ADI experiments in 15 soil columns, including GPR-PTF $\theta(h)$ values. (Standard deviations between parentheses if $\geq 0.5\%$ of true value)
Table 3.7	Statistical indicators for the performance of $\theta(h)$ prediction by inverse modeling of ADI experiments in 15 soil columns including GPR-PTF water contents and without GPR-PTF data
Table 4.1	Hydraulic parameters of the soils according to the van Genuchten (1980) equation
Table 4.2	Main calibrated crop data parameters

Table 5.1	Some properties of temperate (Denmark) and tropical (Brazil) soils used in soil column experiments
Table 5.2	Transport parameters obtained with STANMOD for temperate soil columns with and without (control) LDH
Table 5.3	LDH components ratio to the total mass of LDH

## LIST OF SYMBOLS

<b>Symbol</b>	<b>Description (unit)</b>
$R_n$	Surface radiation ( $\text{MJ m}^{-2} \text{d}^{-1}$ )
$R_s$	Solar radiation ( $\text{MJ m}^{-2} \text{d}^{-1}$ )
$G$	Soil heat flux density ( $\text{MJ m}^{-2} \text{d}^{-1}$ )
$e_s - e_a$	Vapour pressure deficit ( $\text{kPa}$ )
$\Delta$	Slope of the vapour pressure curve ( $\text{kPa } ^\circ\text{C}^{-1}$ )
$u_2$	Wind speed at 2 m ( $\text{m s}^{-1}$ )
$\text{ET}_{\text{OP}}$	Penman-Monteith evapotranspiration
$\text{ET}_{\text{OH}}$	Hargreaves evapotranspiration
$\theta$	Soil water content ( $\text{cm}^3 \text{cm}^{-3}$ )
$\theta_r$	Residual soil water content ( $\text{cm}^3 \text{cm}^{-3}$ )
$\theta_s$	Saturated soil water content ( $\text{cm}^3 \text{cm}^{-3}$ )
$S_e$	Saturation degree
$\lambda$	Fitting parameters
$K_s$	Saturated hydraulic conductivity ( $\text{cm d}^{-1}$ )
$K_s^{\text{sim}}$	Simulated saturated hydraulic conductivity ( $\text{cm d}^{-1}$ )
$t$	Time ( $d$ )
$h$	Pressure head ( $\text{cm}$ )
$S_p$	Potential water uptake rate ( $d^{-1}$ )
$T_p$	Potential transpiration rate ( $d^{-1}$ )
$\beta(z, t)$	Root density distribution function ( $\text{cm}^{-1}$ )
$\alpha(h)$	Dimensionless root water uptake stress reduction function
$k_{ex}$	Extinction coefficient
$X_{ik}^T$	Transpose of the variable vector
$\sigma$	Variance
$cov(f)$	Covariance or kernel function
$\sigma_f$	Amplitude
$\sigma_l$	Characteristic length scale
$\alpha^*$	Support vectors

$\varnothing_k^{\text{obs}}$	Observed values of a target parameter
$\varnothing_k^{\text{sim}}$	Simulated values of a target parameter
$K_{tr}$	Covariance of the training data
$K_{x_{ts}}^T$	Vector with the distances from $x_{ts}$ to each training point
$\theta_{pF1}$	Water content at -10 cm pressure head
$\theta_{pF2}$	Water content at -100 cm pressure head
$\theta_{pF4.2}$	Water content at -15848 cm pressure head
$H_{max}$	Plant maximum height (cm)
$C_{ref}$	Reflection coefficient, Albedo (-)
$RSC$	Minimum canopy resistance ( $s\ m^{-1}$ )
$T_{sum,ea}$	Temperature sum from emergence to anthesis ( $^{\circ}C$ )
$T_{sum,am}$	Temperature sum from anthesis to maturity ( $^{\circ}C$ )
$A_{max,d}$	Maximum $CO_2$ assimilation rate ( $kg\ ha^{-1}\ d^{-1}$ )
$R_{LAI}$	Maximum relative increase in LAI ( $m^2\ m^{-2}$ )
$K_{dif}$	Extinction coefficient for diffuse visible light (-)
$K_{dir}$	Extinction coefficient for direct visible light (-)
$e_{ff}$	Light use efficiency ( $kg\ CO_2\ j^{-1}$ )
$C_{vl}$	Assimilates conversion efficiency into leaves ( $kg\ kg^{-1}$ )
$C_{vo}$	Assimilates conversion efficiency into storage organs ( $kg\ kg^{-1}$ )
$C_{vr}$	Assimilates conversion efficiency into roots ( $kg\ kg^{-1}$ )
$C_{vs}$	Assimilates conversion efficiency into stems ( $kg\ kg^{-1}$ )
$R_{it}$	Relative increase in respiration rate with temperature ( $kg\ CH_2O\ j^{-1}\ d^{-1}$ )
$R_{ml}$	Relative maintenance respiration rate of leaves ( $kg\ CH_2O\ j^{-1}\ d^{-1}$ )
$R_{mo}$	Relative maintenance respiration rate of storage organs ( $kg\ CH_2O\ j^{-1}\ d^{-1}$ )
$R_{mr}$	Relative maintenance respiration rate of roots ( $kg\ CH_2O\ j^{-1}\ d^{-1}$ )
$R_{ms}$	Relative maintenance respiration rate of stems ( $kg\ CH_2O\ j^{-1}\ d^{-1}$ )
$P_{dl}$	Maximum relative death rate of leaves due to water stress( $d^{-1}$ )
$R_{rd,i}$	Maximum daily increase in rooting depth ( $cm\ d^{-1}$ )
$R_{d,m}$	Maximum root depth (cm)

$B_C$	Below ground plant coverage
$C_{NH_4}$	Concentration of $NH_4$ ( $kg\ m^{-3}$ )
$K_{sorp}$	Linear sorption constant ( $m^3\ kg$ )
$\rho_d$	Dry bulk density ( $kg\ m^{-3}$ )
$R_{NH_4;upt}$	$NH_4$ uptake rates ( $kg\ m^{-3}\ d^{-1}$ )
$R_{NH_4;nit}$	$NH_4$ nitrification rates ( $kg\ m^{-3}\ d^{-1}$ )
$R_{NO_3;upt}$	Nitrate uptake by plant roots ( $kg\ m^{-3}\ d^{-1}$ )
$\emptyset$	Soil column diameter (cm)
$v$	Pore water velocity ( $cm\ d^{-1}$ )
$P$	Péclet number
$D$	Effective dispersion coefficient ( $mg\ cm^{-2}$ )
$\beta$	Dimensionless non-equilibrium partitioning coefficient
$\omega$	Dimensionless mass transfer coefficient
$d_{003}$	Basal distance of layers (nm)



## LIST OF ABBREVIATIONS

<b>Symbol</b>	<b>Description (unit)</b>
SDI	Soil drainability index
CMIP5	Coupled Model Intercomparison Project phase 5
GCM	Representative Concentration Pathway
SWLM	Stepwise linear model
LM	Linear model
SVMs	support vector machines
GPR	Gaussian process regression
ENS	Ensemble method
LSboost	least squares boosting
BS	Bare soil
D	Drainage
ET	Evapotranspiration
LAI	Leaf Area Index
RMSE	Root mean square error
ADI	Automatic Drip Infiltrometer
SHP	Soil hydraulic properties
NSE	Nash–Sutcliffe efficiency
MSPE	Mean square percentage error
BD	Bulk Density
PTF	Pedotransfer function
SSM	Steady state methods
SWAP	Soil; Water; Atmosphere and Plant
SRF	Slow release fertilizer
XRF	X-ray fluorescence spectroscopy
LDH	Layered double hydroxide
DDW	Degassed deionized water
FT-IR	Fourier Transform Infrared

TGA	Thermogravimetric analyses
BTC	Breakthrough curve
ICP-OES	Inductively coupled plasma optical emission spectrometry

## Contents

1	General Introduction .....	23
1.1	Thesis structure .....	23
	References .....	24
2	Machine learning based prediction of drainage in layered soils using a soil drainability index .....	26
	Abstract .....	26
2.1	Introduction .....	27
2.3	Materials and Methods .....	28
2.3.1	Stochastic Weather Generation .....	28
2.3.2	Soil, Crop and Meteorological Data .....	29
2.3.3	HYDRUS-1D numerical modelling .....	31
2.3.4	Soil Drainability Index .....	33
2.3.5	Supervised Machine Learning .....	34
2.4.	Results .....	36
2.4.1	Climatic Data and Calibration of LARS-WG .....	36
2.4.2	Simulations with the bare soil scenario .....	37
2.4.3	Simulations with grass-covered lands (pasture) .....	41
2.5	Discussion .....	44
2.6	Conclusions .....	46
	References .....	47
3	Soil Hydraulic Properties Determined by Inverse Modeling of Drip Infiltration Experiments Extended with Pedotransfer Functions .....	50
	Abstract .....	50
3.1	Introduction .....	51
3.2	Materials and Methods .....	52
3.2.1	Sampling and experimental set up .....	52
3.2.2	Generation of Synthetic Data .....	54
3.2.3	Sensitivity Analysis .....	55
3.2.4	Inverse Modeling .....	56
3.2.5	Pedotransfer Function for Water Contents .....	57
3.3	Results and Discussion .....	58
3.3.1	Forward Modeling and Sensitivity Analysis .....	58
3.3.2	Inverse modeling using synthetic data .....	60
3.3.3	Pedotransfer function .....	62
3.3.4	Inverse modeling of actual measurements .....	63
3.4	Conclusions .....	67

References .....	68
4 Assessment of nitrogen fertilizer release half-life using crop modelling based experiments.....	72
Abstract .....	72
4.1. Introduction .....	73
4.2. Materials and Methods .....	75
4.2.1. Soil and meteorological data .....	75
4.2.2. SWAP-1D numerical modelling.....	76
4.2.3. N module paramters and Fertilizer application .....	78
4.3. Results and discussion .....	79
4.4. Conclusion.....	81
References .....	82
5 Nitrate leaching from layered double hydroxides in tropical and temperate soils .....	84
Abstract .....	84
5.1. Introduction .....	85
5.2. Materials and Methods .....	87
5.2.1. Synthesis of Mg-Fe-NO <sub>3</sub> LDH .....	87
5.2.2. Characterization of LDH .....	87
5.2.3. Nitrate release batch experiments.....	88
5.2.4. LDH dissolution experiment .....	88
5.2.5. Soil column study .....	88
5.2.6. Solute Transport Parameters Estimation .....	90
5.3. Results and Discussion .....	91
5.3.1. LDH Characterization.....	91
5.3.2. Nitrate release studies.....	94
5.3.3. LDH dissolution .....	96
5.3.4. Breakthrough curve analysis of temperate soils .....	97
5.3.5. Breakthrough curve analysis of tropical soils.....	100
5.3.6. LDH in practice .....	103
5.4. Conclusion.....	104
References .....	104
6 Final Remarks.....	108

# 1 General Introduction

## 1.1 Thesis structure

A largely agricultural-based economy has turned Brazil into one of the major consumers of fertilizer worldwide, with 9.65 million tons of imported NPK used by farmers in 2013. Recent data reveal around 16 million tons of NPK were imported in 2016, while Nitrogen fertilizer import increased 43% year over year. However, 40-70% of applied N and 80-90% of applied P are lost to the wider environment or become chemically bound to the soil making it practically unavailable to crops (de CASTRO et al., 2017; GIROTO et al., 2017).

Any soil water balance component such as precipitation, evaporation and evapotranspiration influences nitrate transport in soil, as more downward movement results in more nitrate leaching. Soil hydraulic properties and climate conditions besides cropping system can potentially describe possible nitrate leaching out of the root zone (WANG; LI 2019). Therefore, a simple and robust prediction of annual drainage from the soil profile under climate boundary conditions and cropping or bare soil systems can give sufficient information regarding potential nitrate leaching. **Chapter 2** of this thesis explains how annual drainage can be estimated from soil hydraulic properties under climatic conditions of São Paulo State introduces robust machine learning algorithms to predict them.

Since numerical models simulating nitrogen and water fluxes within a soil profile require soil hydraulic properties (SHP), the pedotransfer functions (PTFs) developed in Chapter 2 were calibrated to estimate SHPs from easily measured soil properties such as texture, organic matter and bulk density for an available dataset for Danish soils. Upon estimating drier water contents of soil samples using PTFs, they were combined with the results of automatic drip infiltrometer (ADI) experiments, measuring soil hydraulic conductivities near saturation, to obtain SHPs. The successful extension of ADI by predicted water contents of PTFs led to very accurate estimation of van Genuchten (1980) parameters, as described in **Chapter 3**.

The SWAP-1D hydrological model with a nitrogen balance module (KROES et al., 2009) was used in **Chapter 4** to model hypothetical slow release fertilizers with different half-lives 10, 20, 30 and 40 days. The soil hydraulic parameters of typical layered profiles nearby Piracicaba under cultivation of summer maize and the recommended  $180 \text{ kg N ha}^{-1}$  was considered as input of the model. Typical manure fertilization to provide  $180 \text{ kg N ha}^{-1}$  was simulated and then SRFs were applied in two different ways. First the  $180 \text{ kg N ha}^{-1}$  was added

in a single application on the sowing date and secondly we assumed the application of sufficient weight of SRFs to provide the plant with 180 kg N ha<sup>-1</sup> during the cropping period. The yield of maize under application of SRFs with half-lives of 30 and 40 days was shown to can increase yields up to 200 kg ha<sup>-1</sup> and leaching of nitrogen diminished by 30 to 40 kg ha<sup>-1</sup>.

Layered double hydroxides (LDH), natural or synthetic layered mineral compounds, with a structure identical to the mineral brucite Mg(OH)<sub>2</sub>, contain a fraction of trivalent cations beside divalent cations and can be expressed by the formula  $[M_{1-x}^{2+}M_x^{3+}(OH)_2]A_{x/m}^{n-}nH_2O$ , where  $M^{2+}$  and  $M^{3+}$  are divalent and trivalent metals and  $A^{n-}$  is the interlayer anion and  $x = M^{3+} / (M^{3+} + M^{2+})$  (BENÍCIO et al., 2017; TORRES-DORANTE et al., 2008). Great efforts have been made to confirm effective functionality of LDH in anion adsorption however, for agronomical purposes the retardation should be taken into account. Therefore, the main objective of the final **Chapter 5** was to investigate (i) how fast the intercalated nitrate can be released from LDH molecules? (ii) how strong the nitrate from mineral fertilizer can be absorbed by LDH particles and finally (iii) what is the amount LDH residues, including Mg and Fe hydroxides, that is accumulated in the soil profile? The main conclusions of this thesis and some recommendations for future studies are described in **Chapter 6**.

## References

- BENÍCIO; L. P. F.; CONSTANTINO; V. R. L.; PINTO; F. G.; VERGÜTZ; L.; TRONTO, J.; DA COSTA; L. M.: Layered Double Hydroxides: new technology in phosphate fertilizers based on nanostructured materials. **ACS Sustainable Chemistry & Engineering**, v. 5, n. 1, p. 399–409, 2017.
- DE CASTRO, S. G. Q.; DECARO, S. T.; FRANCO, H. C. J.; MAGALHÃES, P. S. G.; GARSIDE, A.; MUTTON, M. A. Best practices of nitrogen fertilization management for sugarcane under green cane trash blanket in Brazil. **Sugarcane Technology**, 19, n. 1, p. 51-56, 2017.
- GIROTO, A. S.; GUIMARÃES, G. G.; FOSCHINI, M.; RIBEIRO, C. Role of slow-release nanocomposite fertilizers on nitrogen and phosphate availability in soil. **Scientific Reports**, v. 7, p. 46032, 2017.
- KROES, J. G.; VAN DAM, J. C.; GROENENDIJK, P.; HENDRIKS, R. F. A.; JACOBS, C. M. J. **SWAP version 3.2**. Theory description and user manual. Wageningen: Alterra, 2009. (Alterra Report, 1649).
- TORRES-DORANTE, L.; LAMMEL, J.; KUHLMANN, H.; WITZKE, T.; OLFS, H. W. Capacity; selectivity; and reversibility for nitrate exchange of a layered double-hydroxide (LDH) mineral in simulated soil solutions and in soil. **Journal of Plant Nutrition and Soil Science**, v. 171, p. 777-784, 2008.

NYAMANGARA, J.; BERGSTROM, L. F.; PIHA, M. I.; GILLER, K. E. Fertilizer use efficiency and nitrate leaching in a tropical sandy soil. **Journal of Environmental Quality**, v. 32, n. 2, p. 599–606, 2003.

VAN GENUCHTEN, M. T. A closed-form equation for predicting the hydraulic conductivity of unsaturated soils. **Soil Science Society of America Journal**, v. 44, n. 5, p. 892–898, 1980.

WANG, Z. H.; LI, S. X. Nitrate N loss by leaching and surface runoff in agricultural land: A global issue (a review). **Advances in Agronomy**, v. 156, p. 159-217, 2019.

WU, C. L.; SHUKLA, S.; SHRESTHA, N. K. Evapotranspiration from drained wetlands with different hydrologic regimes: Drivers, modeling, and storage functions. **Journal of Hydrology**, v. 538, p. 416–428, 2016.

## 2 Machine learning based prediction of drainage in layered soils using a soil drainability index <sup>1</sup>

### Abstract

Numerical modelling of water flow allows predicting the rainwater partitioning into evaporation, deep drainage and transpiration for different seasonal, crop and soil type scenarios. We proposed and tested a single indicator for drainage estimation, the soil drainability index (SDI) based on the near saturated hydraulic conductivity of each layer. We studied rainfall partitioning for eight soils from Brazil and seven different real and generated weather datasets under scenarios without crop and with a permanent grass cover with three rooting depths, using the HYDRUS-1D model. The SDI showed a good correlation to simulated drainage of the soils. Moreover, well-trained machine-learning methods including linear and stepwise linear model (LM, SWLM) besides ensemble regression with boosting and bagging algorithm (ENS-LB, ENS-B), support vector machines (SVMs) and Gaussian process regression (GPR) predicted monthly drainage from bare soil (BS) and grass covered lands (G) using soil-plant-atmosphere parameters (i.e. SDI, monthly precipitation and evapotranspiration or transpiration). The RMSE values for testing data in BS and G were low, around 1.2 and 1.5 cm month<sup>-1</sup> for all methods.

**Keywords:** evapotranspiration; hydraulic conductivity; HYDRUS-1D; machine learning; subsurface drainage

---

<sup>1</sup> Kotlar, A.M., Iversen, B.V., De Jong van Lier, Q. 2019. Machine learning-based prediction of drainage in layered soils using a soil drainability index. *Soil Systems* 3:30, 2019. DOI:10.3390/soilsystems3020030.

## 2.1 Introduction

An increase of around 70% in food production could provide the required global food demand by 2050 for 9 billion people (FAO, 2009), however bottlenecks to increase the efficiency of agriculture should be mitigated by best management practices. Bottlenecks include the significant loss of water through evaporation, drainage and surface runoff, where the last two imply in the loss of nutrients as well (JÄGERMEYR et al., 2015). The effective factors on fluxes such drainage are broadly related to soil type, land use including vegetal cover and climatic characteristics such as rainfall duration and intensity. Soil features are summarized in soil hydraulic properties (SHP) including hydraulic conductivity and soil water retention curve. Climates with high temperatures, atmospheric demand, annual water excess and rainfall intensity favor these processes. This is the case for large parts of Brazil with a sub-humid climate and yearly rainfall ranging from 700 to 2100 mm. Brazil's position as a large producer of soybean, maize, among others (SENTELHAS et al., 2015), highlights the importance of in-depth knowledge of soil-plant atmosphere interaction to raise food production.

Understanding water fluxes like transpiration, evaporation and drainage in cultivated areas represents an ideal concept regarding the role of cultivation to minimize losses from drainage and to maximize productive water transpired by plants. Measurement techniques such as isotopic determinations, eddy covariance, lysimetry and sap flow measurements are used to trace fluxes in the soil-plant-atmosphere system. Zero flux plane method, single or double rings and well permeameter are also frequently used methods to estimate drainage or ground water recharge (WU; SHUKLA; SHRESTHA, 2016). These measurements are valuable but expensive and unavailable in the field testing cases.

Calibrated and validated computer-based modelling tools can add to the results of these direct methods. Numerical solutions of the Richards' equation with sink term (e.g. root water uptake) can be included in a model algorithm and serve as a robust tool to evaluate the partitioning of precipitation into evapotranspiration and percolation under various soil and cropping conditions. HYDRUS-1D (SIMUNEK; VAN GENUCHTEN; SEJNA, 2016) is such a model with a good performance in simulating water, solute and heat transport in variably saturated media, yielding acceptable predictions of the fate of water in the soil-plant-atmosphere system. HYDRUS-1D has been widely tested and calibrated and resulted in successful simulation of soil moisture dynamics (CHEN; WILLGOOSE; SACO, 2014; LIU et al., 2015), groundwater recharge (LETERME; MALLANTS; JACQUES., 2012;

RIES et al., 2015; PATLE et al., 2015), shallow groundwater contribution into soil moisture of root zone under various crop types (ZHU et al., 2009; SHOUSE; AYARS; SIMUNEK, 2011, ZHU et al., 2013; HOU et al., 2017) and water, solute and heat transport in soil combined with cropping systems (ZHAO et al., 2016; YANG et al., 2017; HE et al., 2017).

Using machine-learning methods to capture functional relation between input and output can improve the prediction of soil-plant-atmosphere phenomena with high complexities. These learning methods without prior knowledge of physical properties of variables have been used for simulation of soil hydraulic parameters such as water retention data and (near) saturated hydraulic conductivity prediction (LAMORSKI et al., 2008; ELBISY, 2015; KOTLAR; IVERSEN; DE JONG VAN LIER, 2019).

Comprehensive studies regarding rainfall partitioning over the soil water balance components in typical croplands in Brazil are missing, and the objective of this study is to develop an index capable of predicting the sharing of transpiration, evaporation and deep drainage fluxes under bare soil and cropped scenarios in layered soil. The indicator was evaluated for determining this rainfall sharing in rainfed scenarios for bare soil and grass-vegetated scenarios using real and downscaled generated daily meteorological data and detailed measured soil hydraulic properties. Finally, various parametric and nonparametric machine learning methods were compared in order to predict drainage from bottom of the soil profile by means of soil-atmosphere-(plant) input variables under bare and planting conditions.

## **2.3 Materials and Methods**

### **2.3.1 Stochastic Weather Generation**

To monitor the effect of various distributions of weather variables, synthetic daily weather series were generated using the downscaling based model LARS-WG (SEMENOV; BARROW; LARS, 2002). The weather generator utilizes input observed daily weather for a given site to determine parameters attributing probability distributions for weather variables as well as correlations between the variables. In contrast to LARS-WG, Markov chain-based algorithms have limited memory for rare events which is a vital parameter in agriculturally based problems, e.g. the strong effect of long dry days on yield and soil plant water availability. The simulation of rainfall occurrence is based on distributions of the length of continuous sequences, or series, of wet and dry days. The amount of precipitation is simulated by a

semi-empirical distribution for each month. Semi-empirical distributions are defined as a histogram with several intervals. Temperature and radiation are conditioned on the wet/dry status of a day and cross-correlated (SEMENOV; BARROW; LARS, 2002).

Future climate projections were generated from Coupled Model Intercomparison Project phase 5 (CMIP5) GCMs under both (Representative Concentration Pathway) RCP4.5 and RCP8.5 projections for 50 years by LARS-WG. RCP 4.5 and 8.5 are long-term scenarios by raising global emissions of greenhouse gases, short-lived species, and land-use/land-cover cause radiative forcing pathway leading to 4.5 and 8.5 ( $\text{W m}^{-2}$ ), equivalent to 650 and 1370 ppm  $\text{CO}_2$  in the year 2100.

### 2.3.2 Soil, Crop and Meteorological Data

Required soil hydraulic properties were retrieved from (DE JONG VAN LIER, 2017) for eight Southeast-Brazilian soils, latitudes around  $21^\circ \text{S}$  (Figure 2.1), covering a wide range of textures and soil classes. Retention data were obtained in undisturbed samples using standard laboratory procedures (tension table and pressure chamber) for several layers (between 5 and 10 layers covering the range between the surface and 1 m depth). Hydraulic conductivity data were achieved at the same depths from internal drainage experiments under field conditions. Hydraulic properties were expressed in terms of parameters of the van Genuchten (1980) equations' system (VAN GENUCHTEN, 1980) (Table 2.1).

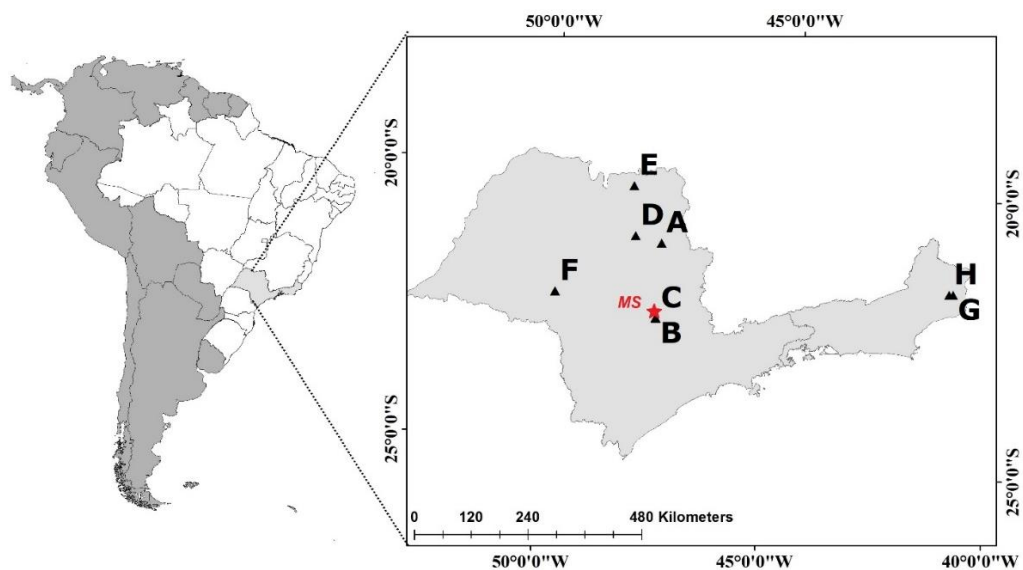


Figure 2.1. Geographical position of sampled soils (A to H) and the University of São Paulo meteorological station (MS) in Piracicaba (SP), Brazil.

Table 2.1 Hydraulic parameters of the soils according to the van Genuchten (1980) equation

Soil	Layer (cm)	$\theta_r$	$\theta_s$	$\alpha$ (cm <sup>-1</sup> )	$n$	$Ks$ (cm d <sup>-1</sup> )	$\lambda$
A Sandy Clay Loam	0-20	0.186	0.436	0.0263	2.328	27.18	2.02
	20-30	0.179	0.332	0.0275	1.697	25.49	0
	30-40	0.202	0.293	0.0070	2.919	42.29	7.17
	40-50	0.186	0.350	0.0262	1.523	42.77	0
	50-60	0.218	0.333	0.0154	2.570	34.12	0
	60-70	0.184	0.303	0.0181	1.869	43.24	0
	70-80	0.179	0.408	0.0269	2.754	118.79	1.99
	80-100	0.169	0.353	0.0289	1.735	79.29	0
B Clay	0-30	0.293	0.505	0.0172	1.525	10.43	8.21
	30-45	0.272	0.506	0.0169	1.415	11.12	8.82
	45-60	0.288	0.469	0.0219	1.397	24.00	5.12
	60-75	0.289	0.418	0.0095	1.901	27.25	3.83
	75-90	0.255	0.483	0.0201	1.535	75.11	0
	90-100	0.270	0.409	0.0092	2.377	97.38	0
C Sandy Clay Loam	0-15	0.113	0.469	0.0593	1.608	38.20	-0.36
	15-30	0.138	0.362	0.0421	1.759	32.80	1.13
	30-45	0.112	0.332	0.0373	1.551	24.00	2.16
	45-60	0.144	0.329	0.0392	1.527	17.50	1.30
	60-100	0.142	0.351	0.0424	1.487	17.50	1.76
D Clay	0-20	0.275	0.463	0.0232	1.389	76.42	3.93
	20-40	0.290	0.447	0.0181	1.356	113.85	4.71
	40-60	0.287	0.444	0.0136	1.443	120.54	4.98
	60-80	0.270	0.506	0.0254	1.590	1352.34	4.96
	80-100	0.257	0.513	0.0265	1.583	2014.19	4.97
E Clay	0-20	0.270	0.487	0.0647	1.925	163.1	3.41
	20-30	0.267	0.444	0.0212	2.014	46.62	1.70
	30-40	0.263	0.441	0.0223	1.843	53.62	1.25
	40-50	0.270	0.489	0.053	1.919	174.25	2.94
	50-60	0.262	0.558	0.0468	1.931	225.07	1.09
	60-70	0.253	0.439	0.0145	1.717	31.30	0.01
	70-80	0.231	0.516	0.0242	1.535	97.42	-0.28
	80-100	0.239	0.517	0.0211	1.494	88.55	-0.44
F Sandy Loam	0-15	0.086	0.428	0.079	1.360	23.28	-0.47
	15-40	0.123	0.370	0.0394	1.452	85.92	8.62
	40-65	0.152	0.340	0.0171	1.805	131.52	6.12
	65-90	0.132	0.360	0.0168	1.596	152.64	-3.02
	90-100	0.117	0.340	0.0131	1.482	102.72	0
G Sandy	0-10	0.094	0.398	0.0382	3.808	429.89	0
	20-30	0.068	0.468	0.0985	1.694	472.85	-1.70
	20-30	0.085	0.503	0.0778	1.800	522.89	-0.77
	30-40	0.048	0.480	0.0694	2.427	1075.9	0
	40-50	0.050	0.453	0.069	2.576	781.20	0
	50-60	0.044	0.441	0.0637	2.864	819.26	0
	60-70	0.099	0.395	0.0714	4.345	845.33	0
	70-80	0.072	0.426	0.0587	3.324	575.35	0
	80-90	0.054	0.447	0.0915	2.257	621.58	0
	90-100	0.054	0.443	0.0872	2.479	1074.03	0
H Clay	0-10	0.228	0.326	0.0225	1.656	12.94	0
	20-30	0.221	0.361	0.0311	1.457	49.08	0
	20-30	0.221	0.356	0.0233	1.668	238.99	8.71
	30-40	0.225	0.356	0.0452	1.378	184.30	6.19
	40-50	0.248	0.360	0.0213	1.816	106.01	9.69
	50-60	0.252	0.324	0.1184	1.364	781.08	0
	60-70	0.253	0.390	0.0184	1.545	54.58	4.34
	70-80	0.251	0.364	0.0335	1.497	34.61	0
	80-90	0.203	0.385	0.0483	1.483	457.82	-3.31
	90-100	0.254	0.377	0.0286	2.159	795.70	5.49

Daily meteorological data were obtained for a 38-year period (1978-2017) from the University of São Paulo weather station in Piracicaba, Brazil (22.703°S;47.624°W, Figure 2.1), representing the sub-tropical winter-dry climate (Koeppen Cwa) of southeast Brazil. Potential (reference) evapotranspiration for a hypothetical grass surface was calculated based on the Penman-Monteith ( $ET_{0P}$ , mm d<sup>-1</sup>) equation (2.1) (ALLEN et al., 1998):

$$ET_{0P} = \frac{0.408\Delta(R_n - G) + \gamma \frac{900}{T_{ave} + 273} u_2 (e_s - e_a)}{\Delta + \gamma(1 + 0.34u_2)} \quad (2.1)$$

Or, in case wind speed is unavailable, using the Hargreaves ( $ET_{0H}$ , mm d<sup>-1</sup>) equation:

$$ET_{0H} = 0.0055R_s(17.8 + T_{ave}) \quad (2.2)$$

In equations (2.1) and (2.2),  $R_n$  and  $R_s$  are the net radiation at the crop surface and solar radiation (MJ m<sup>-2</sup> d<sup>-1</sup>),  $G$  represents the soil heat flux density which is usually ignored in daily calculations (MJ m<sup>-2</sup> d<sup>-1</sup>),  $T$  (°C) and  $u_2$  (m s<sup>-1</sup>) are mean temperature and wind speed at 2 m height,  $(e_s - e_a)$  is the vapor pressure deficit (kPa),  $\Delta$  is the slope of the vapour pressure curve (kPa °C<sup>-1</sup>) and  $\gamma$  is the psychrometric constant, equal to 0.06317 kPa °C<sup>-1</sup> for the Piracicaba weather station.

### 2.3.3 HYDRUS-1D numerical modelling

The HYDRUS-1D model numerically simulates the temporal and spatial changes in water content by the Richards' equation:

$$\frac{\partial \theta}{\partial t} = \frac{\partial}{\partial z} \left[ k(h) \frac{\partial h}{\partial z} - k(h) \right] - S(h, z, t) \quad (2.1)$$

In this equation,  $\theta$  is soil water content (cm<sup>3</sup>cm<sup>-3</sup>),  $t$  is time (d),  $z$  is the vertical space coordinate (cm),  $k$  is the hydraulic conductivity (cm d<sup>-1</sup>),  $h$  represents pressure head (cm) and  $S$  is the sink term (d<sup>-1</sup>) accounting for the volume of water removed from the soil per unit of time due to crop water uptake and described by

$$S(h, z, t) = \alpha(h)S_p = \alpha(h)\beta(z, t)T_p \quad (2.2)$$

where  $S_p$  is the potential water uptake rate ( $d^{-1}$ ) calculated from the potential transpiration rate  $T_p$  ( $cm d^{-1}$ ) distributed over the root zone based on the normalized root density distribution function  $\beta(z, t)$  ( $cm^{-1}$ ).  $0 \leq \alpha(h) \leq 1$  is a dimensionless root water uptake stress reduction function proposed by Feddes et al. (1978) defined by crop dependent parameters described for grass in (FEDDES; KOWALIK; ZARADNY, 1978).  $T_p$  is calculated by

$$T_p(t) = ET_0(1 - \exp(-k_{ex}LAI(t))) \quad (2.3)$$

where  $k_{ex}$  is an extinction coefficient usually within the range between 0.5-0.75 and LAI is leaf area index.

The atmospheric boundary condition at the top of the soil surface is supplied to HYDRUS-1D by the daily variable potential evaporation  $E_p(t)$  (2.4) and precipitation  $P$ , besides a minimum and maximum allowed pressure head at the soil surface ( $h_{CritA}$  and  $h_s$ ).

$$E_p(t) = ET_0(t) - T_p(t) = ET_0(-\exp(-kLAI(t))) \quad (2.4)$$

A unit vertical hydraulic gradient or free drainage boundary condition was implemented for the lower boundary of the 100 cm soil profile as the groundwater level is very deep in these soils. For all scenarios, the initial condition was set to -100 cm pressure head in the entire profile. Temporal and spatial discretization for finite element method of HYDRUS-1D varied significantly to reach the lowest possible water balance error by the end of each simulation for each soil profile.

Simulations were performed for two standard conditions bare soil (BS; no crop, no transpiration) and for grass-covered soil (G). One real set of weather data for 38 years and six generated ones by LARS-WG for 50 years were used for the top boundary conditions. As reference crop, we simulated grass with a LAI equal to 2.88 (ALLEN et al., 1998) and with three different rooting depths (30, 60 or 90 cm), referred to as G30, G60 and G90 scenarios. Accordingly, four cropping/rooting scenarios (BS, G30, G60, G90) together with eight soils and seven weather data sets resulted in 224 different scenarios.

### 2.3.4 Soil Drainability Index

An a priori prediction of drainage throughout soil profile properties would be a useful tool for irrigation and fertilization management, but without experimentation or numerical modelling this is not an easy task, especially in nonuniform layered soils. In the drainage process, each soil layer has its own specific impact on water transmission to the bottom of the profile. There are many factors that could be considered to examine the effect of each layer on the overall drainability, summarized in their hydraulic properties such as saturated and unsaturated hydraulic conductivity and corresponding water contents. Additionally, the thickness of each layer is effective as it represents the flow domain. Consequently, a conceptual indicator could be defined under some assumptions that would correspond to overall drainability of a soil. It would give a general idea about to what extent leaching occurs under bare soil condition. We call this indicator the Soil Drainability Index (SDI).

Considering a soil with  $n$  layers, each with a thickness  $L_i$  (L) and a water content  $\theta_i$  ( $L^3 L^{-3}$ ), it is reasonable to assume that maximum water storage ( $\theta_{s,i}L_i$ ) is related to drainability. Furthermore, the water conducting properties of the layers will affect the rate at which drainage occurs. Hydraulic conductivity  $K$  may vary by orders of magnitude between soil layers, and the relative hydraulic conductivity ( $K/K_{sat}$ ) seems a more plausible alternative. Then, drainability might be correlated to the sum of products of water storage and relative  $K$  for all soil layers. To test this hypothesis, we considered the soil profile at near saturation ( $ns$  in parameter subscripts) with a static value of pressure head to be evaluated at values of -1 or -3 cm. These small tensions can remove the effect of macropore flow to a great extent, especially as saturated hydraulic conductivity measurements were performed on undisturbed samples. In order not to make the drainability to increase with increasing soil depth, the total sum of values was divided by the total depth, resulting in the following expression for the dimensionless Soil Drainability Index (SDI):

$$SDI = \left( \frac{1}{\sum L_i} \right) \left[ \sum_{i=1}^n \left( \frac{K(\theta_{ns})_i}{K_{s_i}} L_i \theta_{s_i} \right) \right] \quad (2.5)$$

### 2.3.5 Supervised Machine Learning

Supervised machine learning aims to map an input to an output based on example of input-output pairs including process uncertainty. Simulation of drainage in 8 soils combined to 7 weather scenarios and four cropping scenarios (BS, G30, 60 & 90) will result in 2688 number of monthly drainage values. Considering drainage related to reference evapotranspiration in bare soil and to transpiration in the grass scenarios, precipitation and the SDI of the soil, then the monthly drainage rate could be predicted through machine learning methods. For this purpose, parametric techniques including linear model (LM) and stepwise linear model (SWLM) in addition to nonparametric methods such as support vector machines (SVMs), Gaussian process regression (GPR), ensemble method (ENS) are utilized.

Parametric supervised machine learning optimizes the parameters of an *a priori* known learning function ( $f(\cdot)$ ) in equation 2.6 to achieve the best fit to data by minimizing the sum of squared errors (SSE).

$$y(X_i) = f(X_i) + \varepsilon_i = Bias + \sum_{k=1}^k X_{ik}^T w_k + \varepsilon_i \quad i = 1, 2, \dots, n \quad (2.6)$$

where  $w = (w_1, w_2, \dots, w_k)$  is the coefficient vector of parameters to be estimated,  $X_{ik}^T$  is the transpose of the variable vector for  $k$  variables, and  $\varepsilon$  is the error, with zero mean, normally and independently distributed with constant variance of  $\sigma^2$ .  $f(\cdot)$ , or the learning function is an *a priori* specified model in parametric supervised methods (KOTLAR; IVERSEN; DE JONG VAN LIER, 2019).

In nonparametric regression, any number of latent functions  $f(\cdot)$  in (2.6) for each pair of data can be generated and left unspecified, but these functions should be smooth and flexible. It means a particular subset of random latent functions  $f = \{f_1, \dots, f_n\}$  corresponds to input  $f = \{X_1, \dots, X_n\}$ . In Gaussian process regressions, it is *a priori* assumed that all  $f(\cdot)$  own a normal distribution looking like  $f(X) \sim GP(\bar{f}, cov(f))$ , where  $\bar{f}$  is the mean and  $cov(f)$  is covariance or kernel function.

Therefore, proper selection of kernel or covariance function is an important task since they determine the sample properties such as smoothness, length scale and amplitude, which are drawn from the GP to give a precise prediction for responses with inputs, which are close

to trained data points in training stage. For example, equation (2.7) is a squared exponential kernel function which is used in this study for GPR named GPR-SE.

$$k((x_i, x_j)) = \sigma_f^2 \exp \left[ -\frac{1}{2} \frac{(x_i - x_j)^T (x_i - x_j)}{\sigma_l^2} \right] \quad (2.6)$$

where amplitude  $\sigma_f$ , the characteristic length scale  $\sigma_l$  are kernel (hyper) parameters.

A Support Vector Machine (SVM) also maps output from a labelled training input-output dataset. The input data through kernel functions are projected into a higher dimensional space called feature space to find the output ( $y=f(x,w)+noise$ ) via  $f(x,w)=w.\varphi(X_i) + b$  where  $\varphi(X_i)$  is the projected input data into feature space,  $w$  and  $b$  are weight vector parameter and bias of the searched regression function. The SVR function can be obtained as:

$$f(x_i) = \sum_{i=1}^n (\alpha_i - \alpha_i^*) k(x_i, x) + b \quad (2.7)$$

These Lagrange multipliers ( $\alpha$  and  $\alpha^*$ ) are support vectors and different Gaussian, linear and second order polynomial kernel functions  $k(x_i, x) = \exp(-\frac{\|x_i - x\|^2}{2\sigma^2})$ ,  $k(x_i, x) = x_i x$ ,  $k(x_i, x) = (1 + (x_i x)^2)$  were selected to for SVMs.

Algorithms such as bootstrap aggregation (Bagging) proposed by Breiman (1996) or least squares boosting (LSboost) are the most commonly techniques used for ensemble learning regressions. Regression ensembles include many weak learners predicts the output via two algorithms Bagging or LSboost called ENS-B and ENS-L. A detailed explanation regarding machine learning methods used in this study can be found in (KOTLAR; IVERSEN; DE JONG VAN LIER, 2019).

To examine the effect of SDI on simulation of monthly drainage, two scenarios including predictors include SDI and without SDI (SDI, no SDI) were performed under the seven weather scenarios by machine learning algorithms. 70% of data were randomly chosen for training the model and the remaining unseen data verified the MLTs in the testing stage.

## 2.4. Results

### 2.4.1 Climatic Data and Calibration of LARS-WG

As wind speed is not a generated weather data by LARS-WG, using the Penman-Monteith equation (2.1) for prediction of  $ET_{OP}$  is not feasible, and equation (2.2) was used instead to predict  $ET_{OH}$ . However, without calibration of this equation, on average,  $ET_{OH}$  is  $7.95 \pm 3.75\%$  larger than the  $ET_{OP}$  except in August, September and October when it is about 1.8% smaller. After calibration, the coefficient in equation (2.2) is needed to change to 0.01266 where  $ET_{OH}$  is only  $2.9 \pm 2.04\%$  greater than  $ET_{OP}$  for the first half of year and for the second half of year  $ET_{OP}$  is  $5.10 \pm 3.52\%$  is larger than  $ET_{OH}$ , as shown in Figure 2.1.a. In general, the RMSE between  $ET_{OH}$  and  $ET_{OP}$  reduced from  $0.60$  to  $0.54 \text{ mm d}^{-1}$  after calibration. Figure 2.2.b also provides the observed values of monthly maximum and minimum temperature and solar radiation from 38 years of measured data.

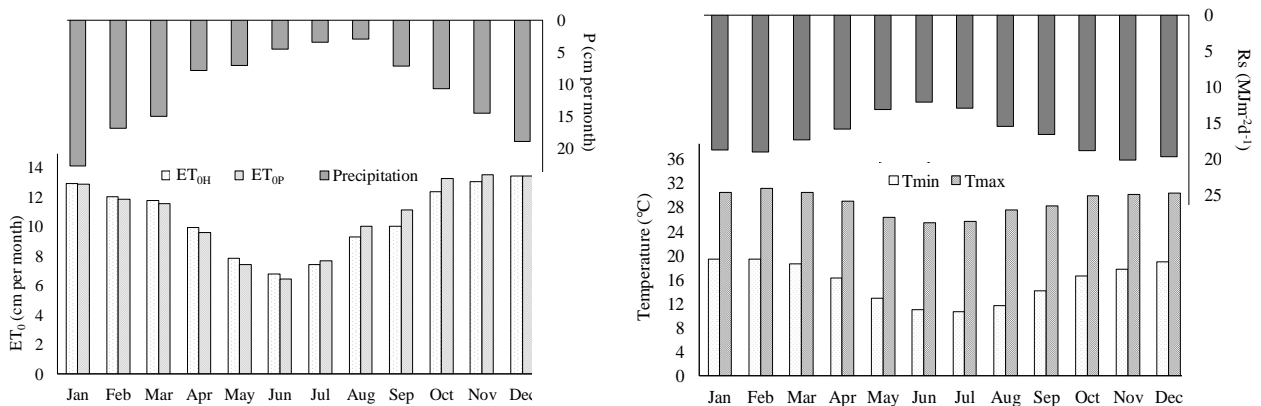


Figure 2.2. Average monthly  $ET_0$  predicted by the calibrated Hargraves equation -  $ET_{OH}$  and the Penman-Monteith equation -  $ET_{OP}$ , Precipitation (P) (a) and maximum, minimum temperature ( $T_{max}$  &  $T_{min}$ ) and Solar Radiation ( $R_s$ ) (b) for the University of São Paulo weather station in Piracicaba (SP), Brazil.

For calibration of LARS-WG, observed data from 1978-2015 were compared to simulated data by LARS-WG through baseline climate scenario. Monthly values of rainfall and reference evapotranspiration calculated using the Hargraves equation (2.2), as well as average temperature and solar radiation are simulated closely to observed values with  $R^2$  more than 98% for all cases) (Figure 2.3.a).

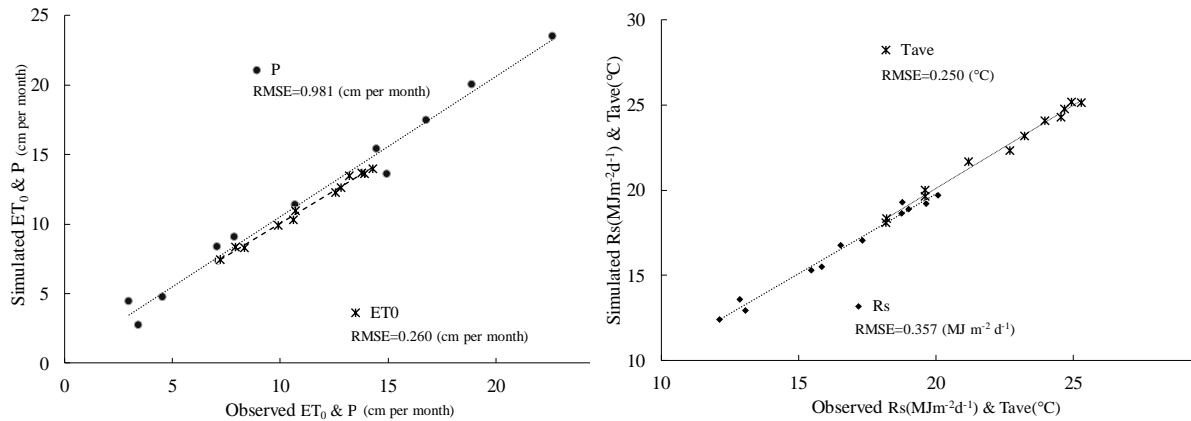


Figure 2.3. Observed meteorological data versus simulated ones by LARS-WG: Left: Rainfall (P) and Evapotranspiration ( $ET_0$ ); Right: Radiation ( $R_a$ ) and Average Temperature ( $T_{ave}$ )

In order to determine if the seasonal wet/dry series and the meteorological variables have a high probability of belonging to the same distribution as the observed data, the calibration was also verified by the Kolmogorov–Smirnov test close to 0 and p-values close to 1 for all cases (data not shown). For the assessment of drainage or plant water availability studies, the concept of wet and dry spell length (WSL or DSL) in weather data plays an important role. WSL and DSL were well simulated with high correlations (Figure 2.4.a), showing an excellent ability in proper weather data generation.

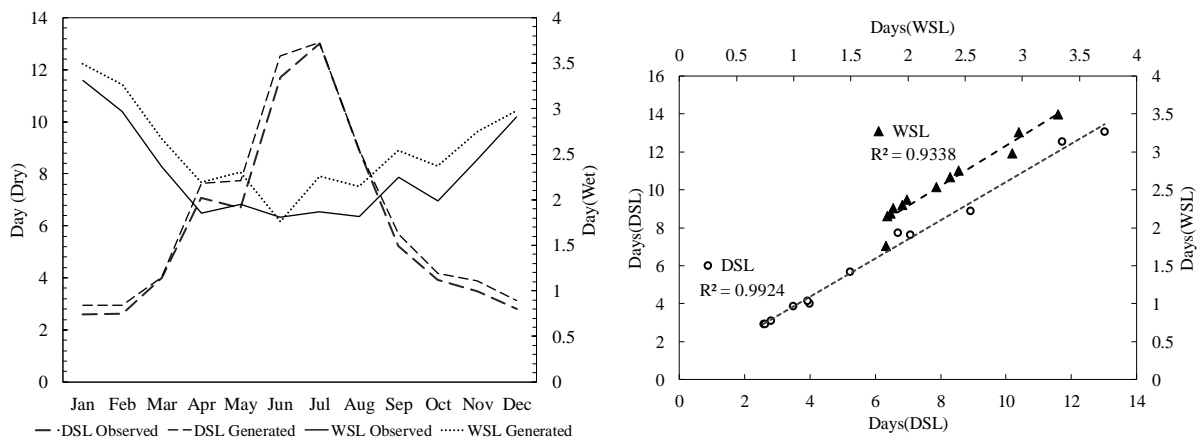


Figure 2.4. Monthly observed and generated Dry and Wet Spell Length (DSL & WSL) (a) and Correlation of observed and generated DSL and WSL (b)

#### 2.4.2 Simulations with the bare soil scenario

Figure 2.5 shows monthly drainage and evaporation with respective standard deviation versus rainfall evaluated from bare soil (BS) simulations using the 38 years of meteorological data for all eight soils (A to H). Higher drainage occurs in the rainy months October to March.

Monthly average of rainfall ( $10.6 \pm 6$  cm) shows larger standard deviation in drier- than in rainy- months. This is attributed to drainage and evaporation in bare soil with standard deviations of about 10 to 20% of the average value in rainy months versus 20-30% in dry months (Figure 2.5).

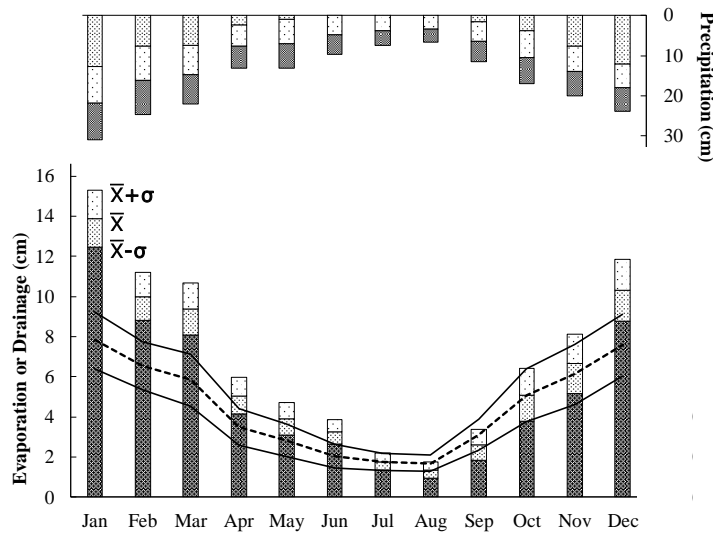


Figure 2.5. Monthly drainage, evaporation and rainfall, averages and standard deviations for all soils under the bare soil (BS) scenario

Regarding soil types, Figure 2.6 shows the SDI of each soil profile (A-H) calculated by equation (2.7) assuming two different pressure head criteria -1 and -3 cm. Resulting values are plotted against the average annual drainage predicted from respective bare soil profiles by the Hydrus simulations. The average annual precipitation for this 38-year series of weather data results in very close or more than 80 cm per year of drainage in bare soils E, G, A and B, decreasing to just above 55 cm in soil C. Standard deviations among years were close to 20 cm for all soils. This allows concluding that under this climate, differences in soil hydraulic properties among soils may lead to a variation in bare soil drainage partitioning of the order of 40 to 70% of the average annual rainfall.

Furthermore, Figure 2.6 shows an excellent correlation between SDI and annual drainage for both values of  $h_{ns}$ , with  $R^2$  around 0.9. This small changes near saturation matric potential is usually associated with great different in hydraulic conductivity while considering  $h_{ns}$  equal to zero matric potential ( $h_0=h_s$ ) results in a very weak correlation ( $R^2=0.42$ ) between SDI and annual drainage. This shows a good performance of SDI as predictor of annual drainage, even though for soils with lower SDI, around 0.2, there is less strong correlation.

Considering  $h_{ns} = -3$  cm, the correlation coefficient is slightly higher than for  $h_{ns} = -1$  cm (0.93 versus 0.88). Therefore, this near saturation-based index seems a good indicator of drainability, requiring the knowledge of water content at a fixed pressure head and the corresponding relative hydraulic conductivity.

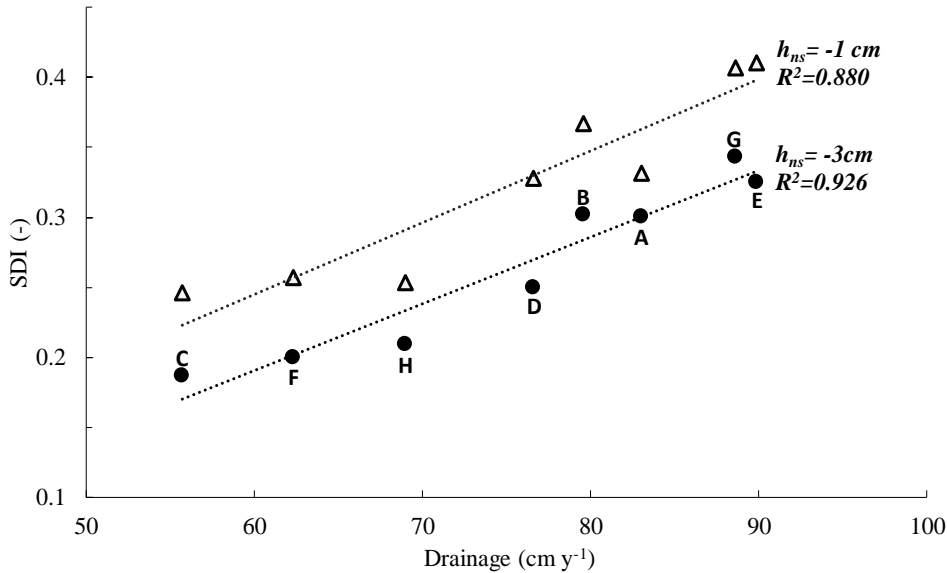


Figure 2.6. Soil Drainage Index (SDI) of each soil (A to H) calculated using  $h_{ns} = -1$  cm or  $h_{ns} = -3$  cm versus the average annual drainage under the bare soil (BS) scenario

From Figure 2.7 it is obvious that all the machine learning based models perform better when SDI is used among predictors. It can be inferred that including SDI in the model was less effective for SVM-L and SVM-P, showing a drop of 17 and 18% in RMSE and an increase of about 4% in  $R^2$  compared to the simulations with the same algorithms but without SDI.

The equations for prediction of monthly drainage prediction (D) using LM and SWLM are brought for both SDI and no-SDI scenarios as  $D_{LM}^{no-SDI}$ ,  $D_{SWLM}^{no-SDI}$ ,  $D_{LM}^{SDI}$  and  $D_{SWLM}^{SDI}$ . There is no interaction between  $ET_0$  and P which makes the obtained equation in order to predict monthly drainage for SWLM to be the same as for LM in no-SDI scenarios. However, introducing SDI forms interactions with P and  $ET_0$  to improve the model performance, as this better performance is also clear in Figure 2.7 where RMSE lessens from 1.427 for equation (2.11) to 1.148 and 1.137  $\text{cm month}^{-1}$  for equation (2.12) and equation (2.13) respectively. These equations are as follows:

$$D_{LM}^{no-SDI} = D_{SWLM}^{no-SDI} = 1.808 + 0.676P - 0.277ET_0 \quad (2.9)$$

$$D_{LM}^{SDI} = -1.793 + 0.671P - 0.259ET_0 + 13.847SDI \quad (2.10)$$

$$D_{SWLM}^{SDI} = 1.249 + 0.366P - 0.355ET_0 + 5.828SDI + 0.010P \times ET_0 + 0.739P \times SDI \quad (2.11)$$

The units are  $\text{cm month}^{-1}$  for  $D$ ,  $P$  and  $ET_0$ . Ensemble regression ENS-LB gives the best fit in SDI and no SDI scenarios. In the model with SDI as the third predictor,  $R^2$  of 0.983 and an RMSE of  $0.492 \text{ cm month}^{-1}$  are obtained in the testing stage, which means prediction of drainage is much more reliable in drier months with monthly drainage between 2 to 5 cm. This is expected since the incorporation of weak learners in an ensemble method makes estimations less likely to be biased (MØLLER et al., 2018).

Considering bagging and boosting algorithms in this study are based on decision tree learners, SDI parameter could enhance the decision-making capability of the ensemble model, especially when there is a strong relation between drainage and SDI as shown in Figure 2.6. Superiority of ENS-LB compared to ENS-B is due to this fact that at every step, the ensemble fits a new learner to the difference between the observed drainage and the aggregated prediction of all learners grown previously. Among kernel-based algorithms including SVMs and GPR, the latter shows better results with an  $R^2$  of 0.946 and RMSE of  $0.899 \text{ cm month}^{-1}$  for the model with SDI. However, in no-SDI, this accuracy decreased by 0.062 in  $R^2$  and  $0.421 \text{ cm month}^{-1}$  in RMSE. SVM-G with an RMSE of  $1.100 \text{ cm month}^{-1}$  is slightly better than other SVMs for prediction of annual drainage again where SDI is considered as an input.

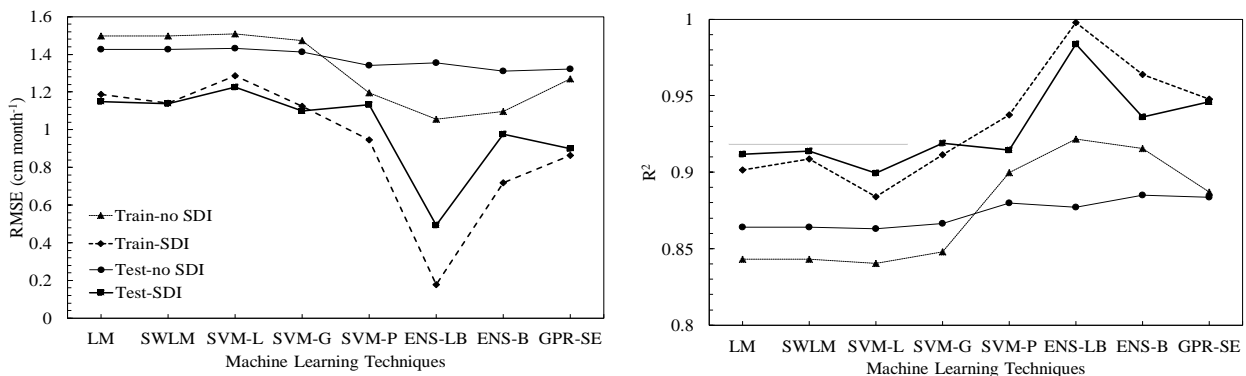


Figure 2.7. Performance of proposed models (RMSE and  $R^2$ ) for prediction of bare soil drainage

### 2.4.3 Simulations with grass-covered lands (pasture)

The presence of a vegetation cover reduces bottom drainage due to root water uptake, but the intensity of this drainage reduction depends on the hydraulic properties of soil layers and rooting depth and distribution. To illustrate this, Figure 2.8 shows monthly average drainage and evapotranspiration from soils covered with grass with three rooting depths (30, 60 and 90 cm, scenarios G30, G60, and G90) together with the values (drainage and evaporation) for BS. Comparing BS to the grass scenarios, monthly drainage was reduced by 30 to 50% with G30, G60 and G90 scenarios.

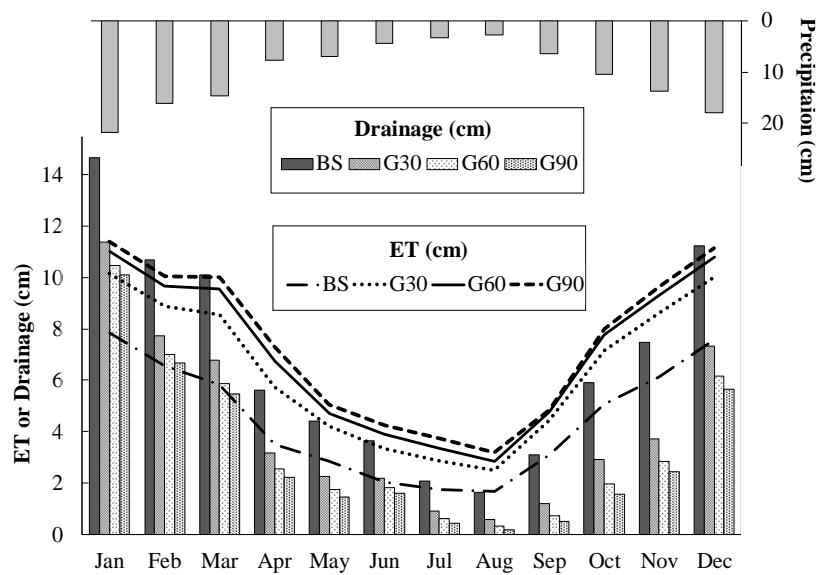


Figure 2.8. Monthly average of drainage and evapotranspiration using real climatic data for 8 soils under BS, G30, G60 and G90 scenarios

Figure 2.8 also gives the details and comparisons of evapotranspiration (*ET*) due to climatic conditions under all grass types simulations and evaporation from bare soil. *ET* increases from G30 to G60 to G90, but the increase between G30 and G60 is higher than between G60 and G90. This shows that increasing rooting depth beyond a certain depth leads to a very modest increase in transpiration, as also confirmed by the data in Table 2.2. This depth then corresponds to an available water content capable of maintaining potential transpiration for most of the occurring weather conditions.

Seasonally speaking, actual transpiration in rainy months is just above twice that of dry months because of the higher amount of available water in the root zone. Averaging between G30, G60 and G90,  $5.6 (\pm 2.4)$  cm month<sup>-1</sup> of transpiration results from  $7.7 (\pm 0.9)$  cm (corresponding to 68% of total  $T_a$ ) transpiration in rainy months and  $3.6 (\pm 1.1)$  cm (32%) in the

dry months, from April to September. The seasonal dependency of transpiration demonstrates the typical response to atmospheric demand and soil moisture supply on grass. Higher rainfall amounts return to the atmosphere at maximum rates by evapotranspiration. In dry months with a higher vapor pressure deficit, atmospheric demand increases but transpiration is less due to limiting soil water supply.

Table 2.2. Monthly averages (and, between brackets, standard deviations) of actual transpiration ( $T_a$ ), Drainage (D) and Evaporation ( $E_v$ ), all in  $\text{cm month}^{-1}$ , for G30, G60 and G90 scenarios in the wet (October to March) and dry season (April to September)

Scenario	$T_a$		D		$E_v$	
Season	Wet	Dry	Wet	Dry	Wet	Dry
G30	7.2( $\pm 0.9$ )	3.2( $\pm 1.0$ )	6.6 ( $\pm 3.0$ )	1.7( $\pm 1.0$ )	1.7( $\pm 1.2$ )	0.7( $\pm 0.25$ )
G60	7.8( $\pm 0.95$ )	3.6( $\pm 1.2$ )	5.7( $\pm 1.0$ )	1.3( $\pm 0.9$ )	1.85( $\pm 1.3$ )	0.75( $\pm 0.23$ )
G90	8.1 ( $\pm 1.0$ )	3.9( $\pm 1.2$ )	5.3( $\pm 3.0$ )	1.1( $\pm 0.8$ )	1.9( $\pm 1.35$ )	0.8( $\pm 0.23$ )

Overall, predicted evapotranspiration for these scenarios ranges from 761 and 844 to 886  $\text{mm y}^{-1}$  (standard deviations around 35  $\text{mm y}^{-1}$ ) for G30, G60 and G90. The observed reduction of evapotranspiration when rooting depth is shallower allows to understand the effect of conversion of deeply rooted crops to shallow rooted ones or land cover change as results, for example, from deforestation.

The ratio of actual to potential ET for different grass scenarios as in Figure 2.9 shows that rainfed crops are under frequent drought stress, even in the wetter months, and irrigation could improve crop yield and subsequently water use efficiency. The use of a fixed and constant LAI of 2.88 results in equal potential evapotranspiration predictions for G30, G60 and G90, and increasing the rooting depth from 30 to 60 cm allows increasing  $ET_a$  by about 10%. In the case of endoalic soils, common in Precambrian surfaces under a tropical humid climate, an increase of rooting depth can be sometimes accomplished by increasing soil pH using chalk, thus decreasing soluble aluminum contents.

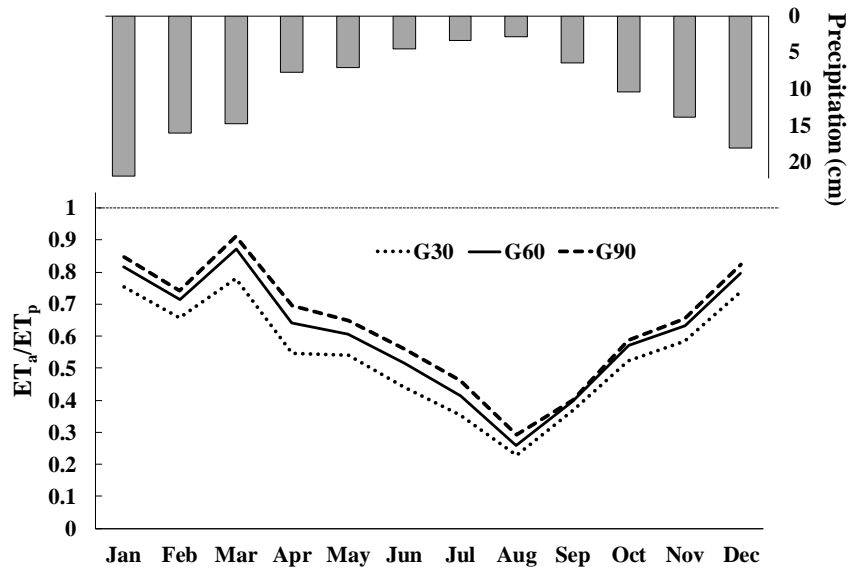


Figure 2.9. Ratio of actual to potential evapotranspiration for three grass scenarios, average monthly values from all soils.

Similar to the procedure for the prediction of drainage from a bare soil profile, drainage prediction from grass covered lands (G30, G60 & G90) was performed by machine learning methods, replacing  $ET_0$  by the actual transpiration of grass ( $T_p$ ) obtained by simulation with the Richards equation under different atmospheric boundary conditions. The values of RMSE and  $R^2$  for all algorithms are shown in 2.10. In the bare soil scenario, there is no trace of soil effect if SDI is not considered and the system would be only plant atmosphere, however, in the grass-based scenarios, Hydrus obtains plant transpiration through numerical simulation, recalling equation (2.5), where the hydraulic parameters of the soil affect the value of  $T_p$  in different times and different soils. In this way, SDI addition can be the soil representative in the grass scenario besides  $T_p$  and the system even without SDI is soil-plant atmosphere. Therefore, for machine learning methods the introduction of SDI to predict drainage for grass-based scenarios should not be the same as it was for bare soil.

Plant participation intensively affects the accuracy of parametric models, where RMSE of LM and SWLM on testing data increased by 20.7 and 21.21% in the model with SDI. These models are shown in equations (2.14), (2.15), (2.16) and (2.17) with and without SDI.

$$D_{LM}^{no-SDI} = -0.560 + 0.564P - 0.343T_p \quad (2.12)$$

$$D_{swLM}^{no-SDI} = 314 + 0.438P - 0.483T_p + 0.01P \times T_p \quad (2.13)$$

$$D_{LM}^{SDI} = -1.233 + 0.5641P - 0.335T_p + 2.651SDI \quad (2.14)$$

$$D_{SWLM}^{SDI} = -0.356 + 0.433P - 0.478T_p + 2.709SDI + 0.017P \times T_p \quad (2.15)$$

As already mentioned, SDI engagement in the model did not make a significant difference in better prediction of drainage as clear from comparison of Figure 2.7 and Figure 2.10, except for ENS-BL. For this algorithm, RMSE of predicted and observed values for testing dataset decreased from 0.629 to 0.448 cm month<sup>-1</sup>.

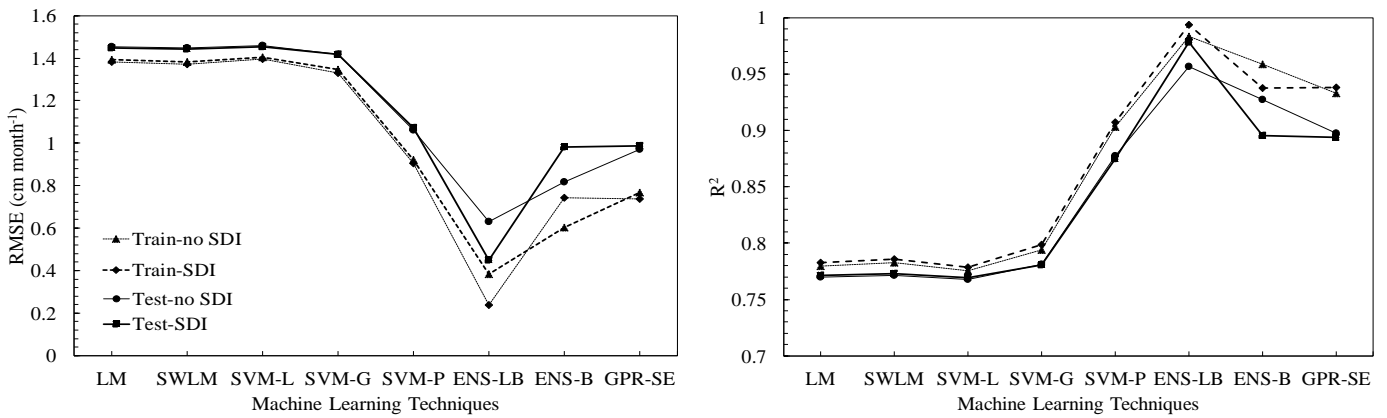


Figure 2.10. Performance of proposed models (RMSE and  $R^2$ ) for prediction of grass covered soil drainage

## 2.5 Discussion

In present work a new index to approximate annual drainage from a layered soil under no cropping was proposed. To the best of our knowledge there is no study focusing on simple methods to estimate drainage in tropical soils and only few studies are available for measurement of drainage flux. The main hypothesis was to relate the drainage under atmospheric boundary condition with hydraulic properties of the soil. This link was made by the soil drainability index (SDI) composed of near saturated (e.g. at - 1 and -3 cm) and saturated hydraulic conductivities beside saturated water content of every single layer. The index requires fewer parameters to estimate annual drainage compared to typical modelling and experimental methods. However, the SDI concept needs more verification through experimental data, not easily available for most scenarios.

We found that any prediction of rainfall dependent problems will be less precise in the drier months. The eight analysed soil types drained 56.5% ( $\pm 9\%$ ) of monthly rainfall if left bare, whereas the remaining portion of the water budget was lost via evaporation. Thus 40 to 70% of the average annual rainfall could be lost due to bottom drainage from bare soils similar to the results reported in (FARIA; BOWEN, 2003) where drainage could be 35% of precipitation in bare soils with a clayey texture. In a modelling study (OLIVEIRA et al., 2015), authors showed 65% of precipitation during 1961-1990 to be drained from a bare Cambisol as well.

Deep drainage may be a water saving measure in groundwater irrigation; nevertheless, it accounts for non-productive loss of water in deep groundwater scenarios, common in most soils in Brazil. Under these conditions, higher drainage results in lower transpiration and reduced biomass production. Intensive fertilization may pose a serious risk of groundwater contamination because of drainage and leaching.

Moreover, having a single soil hydraulic related parameter such SDI representing soil profile role in water flow could be used as a single predictor besides atmospheric and plant related parameters to predict fluxes such as drainage. SDI engagement ameliorated the performance of parametric machine learning models (linear and stepwise model) by about 20% in terms of RMSE, though RMSE of  $0.492 \text{ cm month}^{-1}$  proved the robust method of ensemble for prediction of drainage with SDI.

Simulated bottom drainage for grass covered scenarios with rooting depth of 30, 60 and 90 cm was  $501 \pm 40.3$ ,  $420 \pm 31.5$  and  $382 \pm 30.8 \text{ mm y}^{-1}$ , respectively, within the range between  $145\text{-}703 \text{ mm y}^{-1}$  reported for recharge rate data in grass cultivated lands in (OLIVEIRA et al., 2015). Referring to land use change in Brazil, one could consider the effect of a change from native vegetation with more than 90 cm root depth such as savannah to a shallower rooted grass for grazing purposes, resulting in a 25% of drainage increase and more non-productive loss of water according to our simulations. There is on average 40% reduction in monthly drainage due to plantation.

Comparing the simulated ET of  $3.2 \pm 0.4 \text{ mm d}^{-1}$  for rainy months and  $1.4 \pm 0.45 \text{ mm d}^{-1}$  for dry months for all grass covered scenarios, regardless of root depth, to measured values, good agreement is found. Using remote sensing techniques, Andrade et al. (2014) measured evapotranspiration in grass cover areas of Brazil to be less than  $1.5 \text{ mm d}^{-1}$  between May and October. Feltrin et al., (2017) used lysimeters and recorded  $2.95 \text{ mm d}^{-1}$  of evapotranspiration in a grass covered location in Rio Grande do Sul State, Brazil.

The value of 2.25-2.43 mm d<sup>-1</sup> was reported from a macroscale analysis for Mato Grosso State, Brazil (LATHUILLIÈRE; JOHNSON; DONNER, 2012).

Considering a leaf area index (LAI) between 0.4 and 1.1 resulted in a measured ET of 2.6 ± 0.9 mm d<sup>-1</sup> for grass cultivated in the cerrado biome of central Brazil (MEIRELLES et al., 2011). However, a LAI of 3.2 (close to our assumption of LAI 2.88) for an ungrazed *Brachiaria* pasture in central Brazil increased calculated ET to 3.4 mm d<sup>-1</sup> (SANTOS et al., 2004). High infiltration rate of very sandy soils with grass cultivation in the study by Nóbrega et al. (2017) resulted in 1.19 ± 0.52 mm d<sup>-1</sup> and 2.15 ± 0.58 mm d<sup>-1</sup> evapotranspiration in the Cerrado. The reported value of evapotranspiration for wet months in our study is within the comprehensive finding of 3-4 mm d<sup>-1</sup> as reported in (SANCHES et al., 2011) for grass cultivation in a tropical condition. We did not observe significant improvement in prediction of drainage by incorporation of SDI factor in machine learning models, although it was expected because the T<sub>p</sub> factor carries the role of soil profile behavior hence SDI does not seem to be influential.

## 2.6 Conclusions

A soil drainability index (SDI) is defined in order to predict the annual drainage from bare soils and grass cultivated soil. Fewer parameters are required to estimate annual drainage based on SDI compared to typical modelling and experimental methods. When SDI is used as a predictor for monthly drainage from bare soils using machine-learning models, performance of these models improved significantly. The introduction of SDI for drainage prediction from planted soils enhanced the robustness of models but less than bare soil. Among machine learning methods, ensemble regression with least squares boosting aggregation algorithm predicted monthly drainage better than Gaussian process regression and support vector machines. The RMSE values for testing data in bare soil scenarios were low, around 1.2 cm month<sup>-1</sup>. In grass-cropped scenarios, the accuracy of the models was lower, with RMSE up to about 1.5 cm month<sup>-1</sup>, probably due to errors associated to the prediction of actual crop transpiration.

## References

- ALLEN, R. G.; PEREIRA, L. S.; RAES, D.; SMITH, M. **Crop evapotranspiration**. Guidelines for computing crop water requirements. Rome: FAO, 1998. 300 p. (FAO Irrigation and Drainage Paper, 56).
- ANDRADE, R. G.; TEIXEIRA, A. H. de C.; SANO, E. E.; LEIVAS, J. F.; VICTORIA, D. C.; NOGUEIRA, S. F. Pasture evapotranspiration as indicators of degradation in the Brazilian Savanna. In: SPIE Remote Sensing Conference, 16., 2014, Amsterdam. **Proceedings...** Bellingham, WA, 2014.
- BREIMAN; L. Bagging predictors. **Machine Learning**, v. 24, n. 2, p. 123–140, 1996.
- CHEN, M.; WILLGOOSE, G. R.; SACO, P. M. Spatial prediction of temporal soil moisture dynamics using HYDRUS-1D. **Hydrological Processes**, v. 28, n. 2, p. 171–185, 2014.
- DE JONG VAN LIER, Q. Field capacity; a valid upper limit of crop available water? **Agricultural Water Management**, v. 193; p. 214–220, 2017.
- ELBISY, M. S. Support Vector Machine and regression analysis to predict the field hydraulic conductivity of sandy soil. **KSCE Journal of Civil Engineering**, v. 19, n. 7, p. 2307–2316, 2015.
- FAO. **How to feed the World in 2050?** Rome, 2015.
- FARIA, R. T. DE; BOWEN, W. T. Evaluation of DSSAT soil-water balance module under cropped and bare soil conditions. **Brazilian Archives of Biology and Technology**, v. 46, n. 4, p. 489–498, 2015.
- FEDDES, R. A.; KOWALIK, P. J.; ZARADNY, H. **Simulation of field water use and crop yield**. New York: Wiley, 1978. (Simulation Monographs).
- FELTRIN, R. M.; DE PAIVA, J. B. D.; DE PAIVA, E. M. C. D.; MEISSNER, R.; RUPP, H.; BORG, H. Use of Lysimeters to Assess Water Balance Components in Grassland and Atlantic Forest in Southern Brazil. **Water, Air, & Soil Pollution**, v. 228, n. 7, p. 247, 2017.
- HE, K.; YANG, Y.; YANG, Y.; CHEN, S.; HU, Q.; LIU, X.; GAO, F. HYDRUS Simulation of Sustainable Brackish Water Irrigation in a Winter Wheat-Summer Maize Rotation System in the North China Plain. **Water**, v. 9, n. 7, p. 536, 2017.
- HOU, L.; ZHOU, Y.; BAO, H.; WENNINGER, J. Simulation of maize (*Zea mays* L.) water use with the HYDRUS-1D model in the semi-arid Hailiutu River catchment, Northwest China. **Hydrological Sciences Journal**, v. 62, n. 1, p. 93–103, 2017.
- JÄGERMEYR, J.; GERTEN, D.; HEINKE, J.; SCHAPHOFF, S., KUMMU; M.; & LUCHT, W. Water savings potentials of irrigation systems: global simulation of processes and linkages. **Hydrology and Earth System Sciences**, v. 19, n. 7, p. 3073–3091, 2015.
- KOTLAR, A. M.; IVERSEN, B. V.; DE JONG VAN LIER, Q. Evaluation of Parametric and Nonparametric Machine-Learning Techniques for Prediction of Saturated and Near-Saturated Hydraulic Conductivity. **Vadose Zone Journal**, v. 18, n. 1, 13 p., 2019.
- LAMORSKI, K.; PACHEPSKY, Y.; SŁAWIŃSKI, C.; WALCZAK, R. T. Using support vector machines to develop pedotransfer functions for water retention of soils in Poland. **Soil Science Society of America Journal**, v. 72, n. 5, p. 1243–1247, 2008.

LATHUILLIÈRE, M. J.; JOHNSON, M. S.; DONNER, S. D. Water use by terrestrial ecosystems: temporal variability in rainforest and agricultural contributions to evapotranspiration in Mato Grosso, Brazil. **Environmental Research Letters**, v. 7, n. 2, p. 24024, 2012.

LETERME, B.; MALLANTS, D.; JACQUES, D. Sensitivity of groundwater recharge using climatic analogues and HYDRUS-1D. **Hydrology and Earth System Sciences**, v. 16, n. 8, p. 2485–2497, 2012.

LIU, T.; LAI, J.; LUO, Y.; LIU, L. Study on extinction depth and steady water storage in root zone based on lysimeter experiment and HYDRUS-1D simulation. **Hydrology Research**, v. 46, n. 6, p. 871–879, 2015.

MEIRELLES, M. L.; FRANCO, A. C.; FARIAS, S. E. M.; BRACHO, R. Evapotranspiration and plant-atmospheric coupling in a *Brachiaria brizantha* pasture in the Brazilian savannah region. **Grass and Forage Science**, v. 66, n. 2, p. 206–213, 2011.

MØLLER, A. B.; BEUCHER, A.; IVERSEN, B. V.; GREVE, M. H. Predicting artificially drained areas by means of a selective model ensemble. **Geoderma**, v. 320, p. 30–42, 2018.

NÓBREGA, R. L. B.; GUZHA, A. C.; TORRES, G. N.; KOVACS, K.; LAMPARTER, G.; AMORIM, R. S. S.; GEROLD, G. Effects of conversion of native Cerrado vegetation to pasture on soil hydro-physical properties, evapotranspiration and streamflow on the Amazonian agricultural frontier. **PloS One**, v. 12, n. 6, p. 0179414, 2017.

OLIVEIRA, P. T. S.; WENDLAND, E.; NEARING, M. A.; SCOTT, R. L.; ROSOLEM, R.; DA ROCHA, H. R. The water balance components of undisturbed tropical woodlands in the Brazilian cerrado. **Hydrology and Earth System Sciences**, v. 19, n. 6, p. 2899–2910, 2015.

PATLE, G. T.; SINGH, D. K.; SARANGI, A.; SAHOO, R. Modelling of groundwater recharge potential from irrigated paddy field under changing climate. **Paddy and Water Environment**, v. 15, n. 2, p. 413–423, 2017.

RIES, F.; LANGE, J.; SCHMIDT, S.; PUHLMANN, H.; SAUTER, M. Recharge estimation and soil moisture dynamics in a Mediterranean, semi-arid karst region. **Hydrology and Earth System Sciences**, v. 19, n. 3, p. 1439–1456, 2015.

SANCHES, L.; VOURLITIS, G. L.; DE CARVALHO ALVES, M.; PINTO-JÚNIOR, O. B.; DE SOUZA NOGUEIRA, J. Seasonal patterns of evapotranspiration for a *Vochysia divergens* forest in the Brazilian Pantanal. **Wetlands**, v. 31, n. 6, p. 1215–1225, 2011.

SANTOS, A. J. B.; QUESADA, C. A.; DA SILVA, G. T.; MAIA, J. F.; MIRANDA, H. S.; CARLOS MIRANDA, A.; LLOYD, J. High rates of net ecosystem carbon assimilation by *Brachiaria* pasture in the Brazilian Cerrado. **Global Change Biology**, v. 10, n. 5, p. 877–885, 2004.

SEMENOV, M. A.; BARROW, E. M. **LARS-WG**: A stochastic weather generator for use in climate impact studies. Hertfordshire, UK: Rothamsted Research, 2002.

SENTELHAS, P. C.; BATTISTI, R.; CÂMARA, G. M. S.; FARIAS, J. R. B.; HAMPF, A. C.; NENDEL, C. The soybean yield gap in Brazil—magnitude; causes and possible solutions for sustainable production. **The Journal of Agricultural Science**, v. 153, n. 8, p. 1394–1411, 2015.

SHOUSE, P. J.; AYARS, J. E.; ŠIMŮNEK, J. Simulating root water uptake from a shallow saline groundwater resource. **Agricultural Water Management**, v. 98, n. 5, p. 784–790, 2011.

ŠIMŮNEK, J.; VAN GENUCHTEN, M. T.; ŠEJNA, M. Recent Developments and Applications of the HYDRUS Computer Software Packages. **Vadose Zone Journal**, v. 15, n. 7, 2016.

VAN GENUCHTEN, M. T. A closed-form equation for predicting the hydraulic conductivity of unsaturated soils. **Soil Science Society of America Journal**, v. 44, n. 5, p. 892–898, 1980.

WU, C. L.; SHUKLA, S.; SHRESTHA, N. K. Evapotranspiration from drained wetlands with different hydrologic regimes: Drivers, modeling, and storage functions. **Journal of Hydrology**, v. 538, p. 416–428, 2016.

YANG, R.; TONG, J.; HU, B. X.; LI, J.; WEI, W. Simulating water and nitrogen loss from an irrigated paddy field under continuously flooded condition with Hydrus-1D model. **Environmental Science and Pollution Research**, v. 24, n. 17, p. 15089–15106, 2017.

ZHAO, Y.; SI, B.; HE, H.; XU, J.; PETH, S.; & HORN, R. Modeling of Coupled Water and Heat Transfer in Freezing and Thawing Soils, Inner Mongolia. **Water**, v. 8, n. 10, p. 424, 2016.

ZHU, Y.; REN, L.; HORTON, R.; LÜ, H.; CHEN, X.; JIA, Y.; SUDICKY, E. A. Estimating the contribution of groundwater to root zone soil moisture. **Hydrology Research**, v. 44, n. 6, p. 1102–1113, 2013.

ZHU, Y.; REN, L.; ZHANG, Q.; YU, Z.; WU, Y.; FENG, H. The contribution of groundwater to soil moisture in *Populus euphratica* root zone layer. *Ecohydrology of Surface and Groundwater Dependent Systems*. **IAHS Publication**, n. 328, p. 181–188, 2009.

### 3 Soil Hydraulic Properties Determined by Inverse Modeling of Drip Infiltrometer Experiments Extended with Pedotransfer Functions<sup>2</sup>

#### Abstract

A transient flow experiment using automated drip infiltrometers (ADIs) was performed on soil columns (about 6 dm<sup>3</sup>) large enough to incorporate macropore flow effects. We investigated to what extent the estimated soil hydraulic parameters obtained from inverse modeling of these experiments are reliable. A machine learning based pedotransfer function (PTF) for prediction of water content at  $-1$ ,  $-10$ , and  $-158$  m pressure head was developed. Sensitivity analysis of the van Genuchten parameters (residual and saturated water content  $\theta_r$  and  $\theta_s$ , fitting parameters  $\alpha$ ,  $n$ , and  $\lambda$ , and saturated hydraulic conductivity  $K_s$ ) in soils of sandy, silty, and clayey textures showed that the temporal variation of pressure heads in ADI scenarios was not sensitive to  $\theta_r$  and  $\theta_s$ . The other parameters were accurately estimated from numerically synthesized data. The uniqueness of the estimated parameters did not change when a bias, representing experimental error, was added to the data set. In actual columns, using the temporal and spatial pressure head data from the ADIs and the water contents in the drier range predicted by the developed PTF resulted in a precise estimation of the van Genuchten parameters. Not including the PTF water contents resulted in non-uniquely estimated van Genuchten parameters.

Keywords: Hydraulic conductivity function, Gaussian process regression, Inverse modelling, HYDRUS 1D, Drip infiltrometer.

---

<sup>2</sup> Kotlar, A.M., Varvaris, I., De Jong van Lier, Q., De Jong, L.W., Møldrup, P., Iversen, B.V. Soil Hydraulic Properties Determined by Inverse Modeling of Drip Infiltrometer Experiments Extended with Pedotransfer Functions. *Vadose Zone Journal*, 18 (1), 2019. DOI: 10.2136/vzj2018.12.0215.

### 3.1 Introduction

The accurate modeling of water flow and budgeting of solute and heat transport in the vadose zone based on a numerical solution of the Richards equation depends on precise knowledge of the fundamental soil hydraulic properties (SHPs): water retention [ $\theta(h)$ ] and hydraulic conductivity [ $K(h)$ ] (GROH et al., 2018; WENINGER et al., 2018). Direct measurement of  $K(h)$  is laborious, therefore  $K(h)$  is most commonly indirectly derived by using the measured saturated hydraulic conductivity, the  $\theta(h)$  function, and an empirical parameter related to tortuosity and connectivity, which, in its turn, exhibits a very large spatial variability (DURNER et al., 1999). Consequently, any method to directly quantify  $K(h)$  represents an improvement of modeling quality, but this is predominantly neglected (WENINGER et al., 2018; WELLER et al., 2011).

Both soil heterogeneity at different scales, from millimeters to kilometers, and the large amount of required data restrict the use of pedotransfer functions for the determination of SHPs and especially the soil water retention function [ $\theta(h)$ ] (GRAHAM et al., 2018). Methods to measure SHPs, including pressure plates and in situ techniques like internal drainage experiments, are commonly laborious and costly. Most of these methods are inadequate to describe water dynamics at larger scales because they require hydraulic equilibrium, restricting experiments to small sample sizes (SCHARNAGL et al., 2011). A proper and real estimation of SHPs requires experiments performed on sample sizes larger than the representative elementary volume under transient water flow conditions. Subsequent inverse modeling of the observed data allows hydraulic properties to be effectively lumped for the scale of interest (HOPMANS; NIELSEN; BRISTOW, 2002; MALLANTS et al., 1997; PACHEPSKY; HILL, 2017).

Numerical methods to inversely model transient flow methods under diverse boundary conditions have recently gained considerable attention (LI et al., 2018; RASHID et al., 2015; ARORA; MOHANTY; MCGUIRE, 2011). In the upward infiltration method, a constant upward flux from the bottom is established as a boundary condition to obtain SHPs in the wetting branch. This method was proposed by Hudson et al. (1996) and modified through an applied constant bottom suction, allowing the cumulative flux data to be included as an auxiliary variable in the objective function (YOUNG et al., 2002). The latest improvement in the upward infiltration method was to impose multiple tensions at the lower boundary

(MORET-FERNÁNDEZ et al., 2016) and estimate SHPs without using tensiometers but small ring soil cores (100 cm<sup>3</sup>).

Another boundary condition is established in evaporation scenarios, initially proposed on horizontal (GARDNER; MIKLICH, 1962) and vertical columns (WIND, 1969) and now frequently used for the simultaneous determination of retention and conductivity functions (SIMUNEK; VAN GENUCHTEN; WENDROTH, 1998; ROMANO; SANTINI, 1999; SCHELLE; IDEN; DURNER, 2011). These methods tend to fail in providing conductivities under near-saturated conditions.

Outflow experiments inversely model the measured outflow of water from a soil sample under established pressure or suction conditions. For instance, inverse modeling of one-step outflow experiments (KOOL; PARKER; VAN GENUCHTEN, 1985) supplied with further information of water content (VAN DAM et al., 1992) was improved by multistep outflow experiments (VAN DAM; STRICKER; DROOGERS, 1994).

Similar to outflow experiments, a group of methods is based on the crust method (BOUMA and BAKER, 1974), in which vertical flow is established under a gravitational gradient alone, without a pressure head gradient. As an alternative to the original crust method, which requires a semi-infinite soil column, automated drip infiltrometers (IVERSEN; KOPPELGAARD; JACOBSON, 2004) allow similar boundary conditions in a finite geometry. In automatic drip infiltrometer (ADI) experiments, data on  $K(h)$  can be obtained for the wet range. The extension of these pressure head data with information on water content may improve the well-posedness of the inverse modeling problem (ZHANG; WARD; GEE, 2003). The objective of this study was to analyze ADI experimental data using inverse modeling techniques and to investigate if the extension of retention data to the drier range using prediction by a Gaussian process regression pedotransfer function trained on a local data set may result in a better assessment of SHPs.

## **3.2 Materials and Methods**

### **3.2.1 Sampling and experimental set up**

Fifteen undisturbed soil columns (20 cm high and 20 cm in diameter, volume 6.283 dm<sup>3</sup>) were sampled from the top layer of an experimental field located in Lund, Denmark (coordinates 55.24 N, 12.29 E), which belongs to the Danish Pesticide Leaching Assessment

Program (LINDHARDT et al., 2001). The soil has a sandy loam texture (64% sand, 23% silt, and 13% clay, organic matter content 2.5%) (KOTLAR; IVERSEN; DE JONG VAN LIER., 2019a). Winter wheat was cultivated at the location during the 5 yr before sampling. In the same field, small ring samples (100 cm<sup>3</sup>) were taken for water retention analysis using a sand box for pressure heads from  $-0.1$  to  $-1$  m and ceramic plate equipment for pressure heads between  $-1.6$  and  $-150$  m. Water content for the very dry soil was determined after one night of oven drying using a WP4-T dew point potentiometer (METER Group).

Analogous to the studies of McKenzie et al. (2001) and Weller et al. (2011), unsaturated hydraulic conductivity was measured using automated (step flow) drip infiltrometers (Figure 3.1) as reported by Iversen, Koppelgaard and Jacobson (2004). In the ADI setup, tensiometers recorded pressure heads at five depths in the column under step flow. A suction was applied at the bottom of the sample, and the inflow was adjusted until a steady state was established in which the five tensiometers showed similar readings and flow was due to a gravitational gradient only. Subsequently, suction was increased and the process repeated. Five to eight bottom suctions were applied, varying between  $-0.1$  to  $-1$  m pressure head, allowing determination of  $K(h)$  in this range of pressure heads. Saturated hydraulic conductivity was independently measured using the constant-head method as described by Iversen et al. (2004).

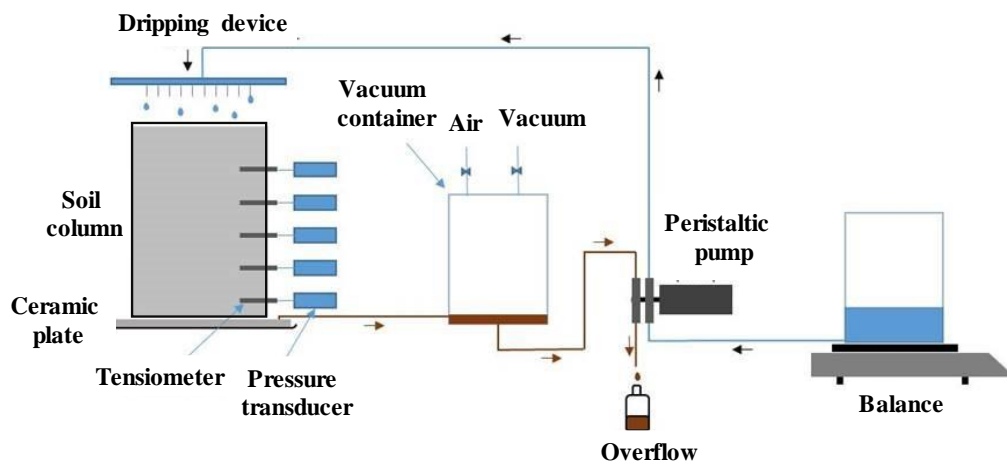


Figure 3.1. Schematic design of the Automatic Drip Infiltrometer (ADI) apparatus for measuring unsaturated hydraulic conductivity

### 3.2.2 Generation of Synthetic Data

To evaluate the reliability of the SHPs estimated by inverse modeling of ADI scenarios, ADI experiments similar to the experimental setup were simulated numerically by HYDRUS-1D for three reference soils used by Vrugt et al. (2001) (Table 3.1).

The HYDRUS-1D model numerically simulates the temporal and spatial changes in water content or pressure head by solving the Richards' equation (SIMUNEK et al., 2008):

$$\frac{\partial \theta}{\partial t} = \frac{\partial}{\partial z} \left[ k(h) \frac{\partial h}{\partial z} + k(h) \right] \quad (3.1)$$

where  $\theta$  is the volumetric soil water content,  $t$  is time (d),  $z$  is the vertical space coordinate (cm),  $K$  is the hydraulic conductivity ( $\text{cm d}^{-1}$ ), and  $h$  is pressure head (cm). The soil hydraulic properties were modeled using the van Genuchten–Mualem constitutive relationships (VAN GENUCHTEN, 1980):

$$S_e(h) = \frac{\theta(h) - \theta_r}{\theta_s - \theta_r} = (1 + |\alpha h|^n)^{-m} \quad (3.2)$$

$$K(h) = K_s S_e^\lambda [1 - (1 - S_e^{1/m})^m]^2 \quad (3.3)$$

where  $S_e$  is the saturation degree,  $\theta_s$  and  $\theta_r$  are volumetric saturated and residual water contents, and  $\alpha$  ( $\text{cm}^{-1}$ ),  $m = 1 - 1/n$ , and  $\lambda$  are fitting parameters.

The simulated scenarios were chosen to represent the ADI experiment in 20-cm-high soil columns with three tensiometers (at depths of 7, 10, and 13 cm), discretized into 100 elements. A finer grid size was chosen near the virtual tensiometers. At the bottom of the soil column, a 1-cm-thick porous plate with  $K_s$  equal to  $2.7 \text{ cm d}^{-1}$  was simulated with van Genuchten (1980) parameters  $n = 1.001$  and  $\alpha = 10^{-20} \text{ cm}^{-1}$ , thus ensuring that it remained fully saturated for the pressure heads applied (SIMUNEK et al., 2008). Boundary conditions were multistep flux [always less than  $K$  ( $-1 \text{ cm}$ )] and zero evaporation. The bottom boundary condition was a stepwise varying pressure head, never lower than  $-100 \text{ cm}$ .

### 3.2.3 Sensitivity Analysis

To study the parameter sensitivity of the described ADI scenario and to evaluate if insensitive parameters might be removed (RITTER et al., 2003; LAMBOT et al., 2004), one-parameter analyses as well as two-parameter analyses were performed using the same scenarios described for synthetic data generation. In the one-parameter analysis, 100 forward simulations (Monte Carlo) were performed by changing one of the parameters  $\theta_r$ ,  $\theta_s$ ,  $\alpha$ ,  $n$ ,  $\lambda$ , or  $K_s$  within an interval around the respective true value. Similarly, in the two-parameter analysis, parameter pairs  $\alpha$ - $n$ ,  $\alpha$ - $K_s$ ,  $\alpha$ - $\lambda$ ,  $n$ - $K_s$  and  $n$ - $\lambda$  were simultaneously changed, resulting in  $100 \times 100 = 10,000$  realizations. The two-parameter analyses allowed assessment of the corresponding response surfaces. In both one- and two-parameter analyses, the remaining parameters were kept at their true value.

Table 3.1. Soil hydraulic parameters for reference soils (extracted from Vrugt et al., 2001). Values between brackets represent the range of values used in 1-D and 2-D Monte Carlo realizations

texture	VG parameters <sup>†</sup>					
	$\theta_r$	$\theta_s$	$\alpha$ (cm <sup>-1</sup> )	$n$	$K_s$ (cm d <sup>-1</sup> )	$\lambda$
<b>Sand</b>	0.02	0.38	0.0214	2.075	15.56	0.039
	(0-0.07)	(0.3-0.5)	(0.001-0.03)	(1.4-3.0)	(7-50)	(-3-3)
<b>Silt</b>	0.034	0.46	0.0160	1.370	6.00	0.5
	(0-0.1)	(0.3-0.5)	(0.001-0.04)	(1.2-1.9)	(4-25)	(-3-3)
<b>Clay</b>	0.00	0.42	0.0191	1.152	13.80	-1.384
	(0-0.1)	(0.3-0.5)	(0.009-0.09)	(1.1-2.5)	(7.5-35)	(-3-3)

<sup>†</sup>  $\theta_r$ , residual volumetric water content;  $\theta_s$ , saturated volumetric water content;  $\alpha$ ,  $n$  and  $\lambda$ : fitting parameters;  $K_s$ , saturated hydraulic conductivity

Two statistical indicators were used to compare the Monte Carlo realizations of simulated pressure head readings ( $h_{sim}$ ) with the pressure heads simulated with the reference values ( $h_{ref}$ ): the root mean square error (RMSE) and the Nash–Sutcliffe efficiency (NSE):

$$RMSE = \sqrt{\frac{\sum_{i=1}^s (h_{sim} - h_{ref})^2}{s - 1}} \quad (3.4)$$

$$NSE = 1 - \frac{\sum_{i=1}^s (h_{sim} - h_{ref})^2}{\sum_{i=1}^s (h_{ref} - h_{ref})^2} \quad (3.5)$$

### 3.2.4 Inverse Modeling

The inverse modeling to obtain the SHP functions  $\theta(h)$  and  $K(h)$  aimed to minimize the following objective function  $F(\phi)$ :

$$F(\phi) = \sum_{j=1}^p \sum_{i=1}^n \{ [\phi_k^{obs}(z_j, t_i) - \phi_k^{sim}(z_j, t_i)]^2 \} \quad (3.6)$$

where  $\phi_k^{obs}$  and  $\phi_k^{sim}$  are the observed and simulated values, respectively, of a target parameter (e.g., pressure head) at depth  $z_j$  and time  $t_i$ . Minimization of the objective function was performed using HYDRUS-1D (SIMUNEK et al., 2008). HYDRUS-1D uses the Levenberg–Marquardt non-linear minimization method, a local gradient-type search algorithm, as opposed to global search algorithms that search the entire parameter space. Local search algorithms are generally sensitive to the initial parameter estimates (SIMUNEK et al., 2005; KELLENNERS et al., 2005).

To reduce the number of parameters to be estimated by inverse modeling, parameters  $\theta_r$  and  $\theta_s$  were fixed at experimentally observed values. Saturated water content was calculated based on bulk density and particle density ( $2650 \text{ kg m}^{-3}$ ). Estimated water content at  $pF = 5$  using a WP4 psychrometric tensiometer was used as the residual water content. A stochastic bias was introduced, applying a 1-cm noise to the observed pressure heads to evaluate the sensitivity to experimental errors (KOOL; PARKER, 1988; PETERS; DURNER, 2008).

In this study, two sets of data were used in inverse modeling to estimate the SHPs: (i) the traditional ADI data set consisting of measured pressure head data from the three most central tensiometers (eliminating the top and bottom tensiometers, thus avoiding possible boundary disturbance); and (ii) the ADI data set consisting of measured pressure head data from the three most central tensiometers extended with water contents predicted by a pedotransfer function.

The testing of inverse modeling and obtained parameters was accomplished by comparison of  $K(h)$  observed in ADI experiments and simulated by estimated parameters using the RMSE and the mean square percentage error (MSPE):

$$MSPE = \frac{100\%}{n} \sum_{i=1}^n \left[ \frac{K_{sim,i} - K_{obs,i}}{K_{obs,i}} \right]^2 \quad (3.7)$$

where  $K_{obs,i}$  is the  $i$ th hydraulic conductivity measured in the ADI experiment,  $K_{sim,i}$  is the corresponding  $K(h)$  calculated using parameters obtained by inverse modeling, and  $n$  is the number of observations. For the cases where water contents predicted by PTF and simulated ones obtained from the van Genuchten parameters or the measured ones from small rings were compared with each other, the RMSE was the evaluation criterion.

### 3.2.5 Pedotransfer Function for Water Contents

A machine learning based pedotransfer function (PTF) was developed by Gaussian process regression (GPR) to obtain retention data for the dry range. Gaussian process regression uses nearest neighbors, considering the distance between neighbors based on covariance (or kernel) function. Closeness or similarity between two points (distance) is given by kernel functions (RASMUSSEN; WILLIAMS, 2006). Kernel similarities between a test point and each point of the training data are found to predict the target of the test point, thus kernel values of far points approach zero. Briefly, the mathematical form of GPR is

$$\begin{bmatrix} Y_{tr} \\ Y_{ts} \end{bmatrix} = GP \left[ 0, \begin{bmatrix} K_{tr} & K_{trs} \\ K_{trs}^T & K_{ts} \end{bmatrix} \right] \quad (3.8)$$

where  $Y_{tr}$  and  $Y_{ts}$  are training and test targets (e.g., here water content points) and  $K_{tr}$  is the covariance of the training data,  $K_{ts}$  of the test data, and  $K_{trs}$  between test and training data. Considering a Gaussian likelihood function, the predictive mean  $y_{ts}$  for a given test point ( $x_{ts}$ ) is

$$y_{ts} = K_{x_{ts}}^T K_{x_{tr}}^{-1} Y_{tr} \quad (3.9)$$

where  $\mathbf{K}_{x_{ts}}^T$  is the vector with the distances from  $x_{ts}$  to each training point. Optimization of kernel parameters and other details are explained in Kotlar et al. (2019a, 2019c).

The developed PTF allows prediction of water contents  $\theta_{pF1}$ ,  $\theta_{pF2}$ ,  $\theta_{pF3}$  and  $\theta_{pF4.2}$  corresponding to pressure heads of  $-0.1$  (pF1),  $-1$  (pF2),  $-10$  (pF3) and  $-158$  m (pF4.2), respectively. For each water content ( $\theta_{pF1}$ ,  $\theta_{pF2}$ ,  $\theta_{pF3}$  and  $\theta_{pF4.2}$ ), easily measurable soil properties including texture (sand, silt, and clay contents), organic matter, and bulk density (BD) were used as predictors. Gaussian process regression was trained by a random selection of 70% of the data set including 452 soils from Denmark retrieved from Kotlar et al. (2019b). Considering the performance of the PTFs for the four tensions, some of them were selected to be used as additional data for the drier part in the inverse simulation.

### 3.3 Results and Discussion

#### 3.3.1 Forward Modeling and Sensitivity Analysis

Table 3.2 shows averages of the statistical indicators RMSE and NSE of pressure heads for the 100 one-parameter Monte Carlo simulations performed for each van Genuchten (VG) parameter for the reference sand, silt, and clay soils from Table 3.1. Results show that the prediction of pressure head is relatively insensitive to the residual water content, corroborating the report by Kelleners et al. (2005), as well as to saturated water content. Higher sensitivity is shown for  $n$ ,  $K_s$ ,  $\lambda$ , and especially  $\alpha$ .

For silt and clay soils, the model showed less sensitivity to  $\lambda$  compared with the sand soil. This could be expected because  $\lambda$  especially affects the prediction of  $K(h)$  in the dry range, which occurs more commonly in ADI experiments in a sandy soil. Parameter  $\alpha$  is the most sensitive parameter in the model for the sand and silt soils; this parameter strongly affects the pressure heads observed at the tensiometers. For the clay soil, the model is more sensitive to  $n$ . Sensitivity to  $\lambda$  was not significant for the clay soil (Table 3.2), but for the studied Danish soils, with sandy loam texture,  $\lambda$  was maintained as an optimization parameter.

The low sensitivity of  $\theta_r$  and  $\theta_s$ , added to the fact that they can be experimentally measured, made it advantageous to fix these parameters at their true values instead of inversely model them. Therefore, only parameters  $\alpha$ ,  $n$ ,  $\lambda$ , and  $K_s$  were optimized to obtain the soil water retention and hydraulic conductivity functions.

Table 3.2 RMSE and NSE of pressure heads obtained from simulations in sand, silt and clay soil (Table 3. 1) scenarios in 100 Monte Carlo realizations for each of the VG parameters. Average (and standard deviations between brackets) for pressure heads at three depths (7, 10 and 13 cm), compared to values obtained with the reference parameter set

Soil	Criteria	VG Parameters <sup>†</sup>					
		$\theta_r$	$\theta_s$	$\alpha$	$n$	$K_s$	$\lambda$
Sand	RMSE	1.2(0.0)	1.5(0.0)	25.2(0.7)	3.5(0.6)	9.2(0.5)	9.9(0.1)
	NSE	0.98(0.0)	0.97(0.0)	-5.38(1.8)	0.82(0.0)	0.09(0.1)	-0.38(0.3)
Silt	RMSE	0.7(0.0)	2.0(0.0)	21.9(2.0)	10.8(1.0)	10.9(0.6)	3.3(0.3)
	NSE	0.99(0.0)	0.95(0.0)	-3.04(1.2)	-0.04(0.1)	-0.19(0.0)	0.86(0.0)
Clay	RMSE	1.9(0.9)	1.7(1.1)	24.0 (12.5)	28.1(3.2)	13.6(6.5)	4.4(2.8)
	NSE	0.98(0.0)	0.98(0.0)	-2.2(1.9)	-3.6(1.8)	0.0(0.8)	0.88(0.1)

<sup>†</sup>  $\theta_r$ , residual volumetric water content;  $\theta_s$ , saturated volumetric water content;  $\alpha$ ,  $n$  and  $\lambda$ : fitting parameters;  $K_s$ , saturated hydraulic conductivity

Results of the 2-D sensitivity analyses are shown in (Figure 3.2). For  $n$  and  $\alpha$  (Figure 3.2a), any change in  $\alpha$  leads to large variation in the objective function however,  $n$  hardly affects the objective function and contours are parallel to the  $n$  axis. As a result,  $n$  is not sensitive to  $\alpha$  and the forward problem of ADI is highly sensitive to  $\alpha$ . This makes estimation of these parameters cumbersome, non-unique, when only pressure head data are used. The same applies to  $\lambda$  (Figure 3.2b) which is difficult to predict because the objective function approaches its minimum value when  $\alpha$  is close to its reference (0.0191 cm<sup>-1</sup>).

An increase in  $\alpha$  together with an increase in  $K_s$  leads to similar values for the objective function (Figure 3.2c). Consequently, the forward problem of ADI has a high sensitivity to either  $\alpha$  or to  $K_s$ . There is a larger sensitivity to  $n$ - $\lambda$ ,  $n$ - $K_s$  and  $K_s$ - $\lambda$  (Figure 3.2 d, e and f, respectively). Observing the  $n$ - $\lambda$  response surface, the objective function reaches a low value for  $n$  between 1.1 and 1.2, almost independent of  $\lambda$  between -3 and 3. Low values for the objective function also occur when  $\lambda$  is between -1.2 and -2 and  $n$  varies from 1.3 to 2.5. For the case of  $n$ - $K_s$  (Figure 3.2 f), there is a large area of insensitivity especially when both parameters are above their reference values (1.159 and 13.8 cm d<sup>-1</sup>, respectively). There is no specific pattern for the sensitivity of the problem to the simultaneous variation of  $K_s$ - $\lambda$  (Figure 3.2 f), however, low  $K_s$  with positive  $\lambda$  and high  $K_s$  with negative  $\lambda$  causes the objective function to increase.

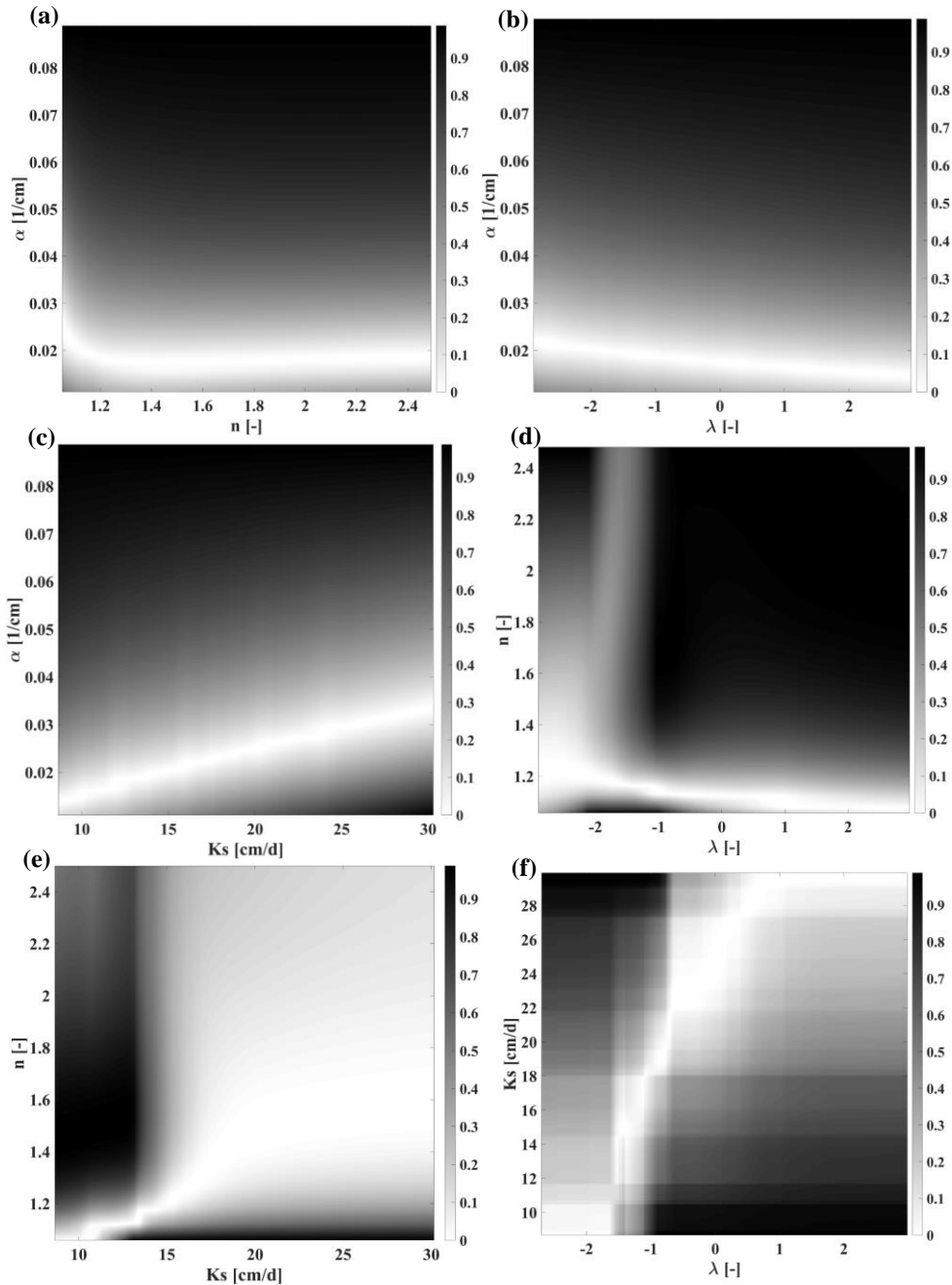


Figure 3.2. Response surfaces (2-D sensitivity analysis) of the objective function for pressure heads at three depths for parameter pairs (a)  $\alpha$ - $n$ , (b)  $\alpha$ - $\lambda$ , (c)  $\alpha$ - $K_s$ , (d)  $n$ - $\lambda$ , (e)  $n$ - $K_s$ , (f)  $K_s$ - $\lambda$

### 3.3.2 Inverse modeling using synthetic data

The synthetic data obtained by forward modeling of a hypothetical ADI experiment on the three soil types from Table 3.1 are shown in Figure 3.3 a. As expected, decrease in pressure head is faster and larger in the sandy soil. Temporal variation of pressure head measured by tensiometers is the typical output of ADI experiments (Figure 3.3 a), and is used in inverse

modeling to predict SHPs. Figure 3.3 b shows a simulated measurement error imposed as a stochastic bias added to the numerically synthesized pressure head data (ADI output) for the silt soil.

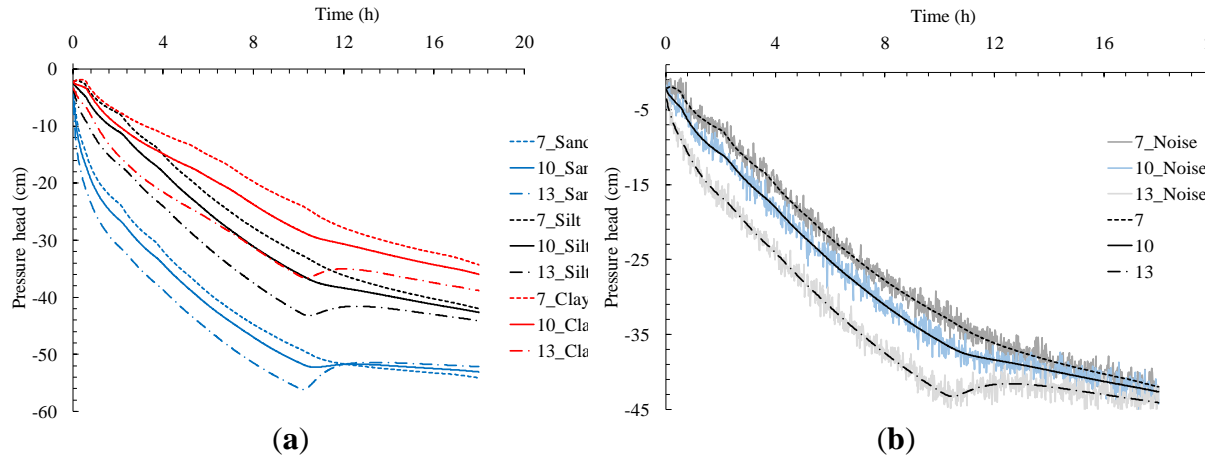


Figure 3.3. (a) Simulated pressure head over time at three depths in simulated ADI experiments for three soil types; (b) example of the imposed stochastic bias added to the pressure heads for the silt soil. Numbers in the legend represent the depth (cm) of the tensiometers

VG parameters estimated with and without added bias are shown in Table 3.1 together with their true values. The robustness of the proposed experiment to estimate SHPs is confirmed especially for sandy and clayey soils, with reference parameters equal or very close to estimated parameters (Table 3). As mentioned by Peters and Durner (2008), prediction of the hydraulic conductivity function is the most crucial part.

Adding a small bias to the input data (as illustrated in Figure 3.3 b) introduced some uncertainties in the estimated parameters as shown in Table 3.3, except for the silty soil parameters. Prediction of  $\lambda$  shows to be cumbersome, occasionally with major differences between simulations with and without bias (sand soil) as well as large CVs (clay soil).

Table 3.3. Soil hydraulic parameters estimated from synthesized data with and without added bias (standard deviation between parentheses if  $\geq 0.5\%$  of average value), together with true values for sand, silt and clay reference soils

Soil	Scenario	VG parameters				
		$\alpha$ ( $\text{cm}^{-1}$ )	$n$ (-)	$K_s$ ( $\text{cm d}^{-1}$ )	$\lambda$ (-)	$RMSE_h$ (cm)
Sand	True Value	0.0214	2.075	15.56	0.039	-
	Estimated	0.0214	2.075	15.54	0.038	0.002
	Estimated with bias	0.0213	2.10 (0.3)	15.06	0.000 (0.01)	1.013
Silt	True Value	0.0160	1.370	6.00	0.5	-
	Estimated	0.0172	1.361	6.678	-0.001	0.018
	Estimated with bias	0.0171	1.363	6.610	0.000	0.052
Clay	True Value	0.0191	1.152	13.80	-1.384	-
	Estimated	0.0191	1.152	13.80	-1.384	0.000
	Estimated with bias	0.0182	1.154	12.83 (1.27)	-0.975 (0.3)	0.036

†  $\theta_r$ , residual volumetric water content;  $\theta_s$ , saturated volumetric water content;  $\alpha$ ,  $n$  and  $\lambda$ : fitting parameters;  $K_s$ , saturated hydraulic conductivity

### 3.3.3 Pedotransfer function

The developed GPR-PTF did not show robust for the prediction of water contents at pF 1, but at pF 2, 3 and 4.2 well-trained GPR-PTFs were obtained (Table 3.4) with a low error and an  $R^2$  of 0.99 in the training data set. Feature selection of GPR based on kernel parameters allows to eliminate predictors without a considerable negative effect on response prediction (KOTLAR et al, 2019a). Therefore, to predict  $\theta_{pF2}$ ,  $\theta_{pF3}$  and  $\theta_{pF4.2}$ , two components of textural data (sand, sand/clay, or sand/silt content), organic matter content, and/or bulk density resulted as important predictors. Their predictive role was of similar importance for  $\theta_{pF2}$  and  $\theta_{pF3}$  (Table 3.4), however, the silt fraction plays a more predominant role in the prediction of  $\theta_{pF4.2}$ .

Table 3.4. Statistical indicators of performance of the GPR pedotransfer functions for the prediction of  $\theta_{pF1}$ ,  $\theta_{pF2}$ ,  $\theta_{pF3}$ ,  $\theta_{pF4.2}$  (volumetric water contents at pressure heads -0.1, -1, -10 and -158 m) for testing data and respective predictors (BD, bulk density; OM, organic matter content; sand, silt and clay contents)

	Targets			
	$\theta_{pF1}$	$\theta_{pF2}$	$\theta_{pF3}$	$\theta_{pF4.2}$
$R^2$	0.534	0.952	0.894	0.946
RMSE	0.035	0.019	0.026	0.012
Predictors (weight in prediction)	BD	BD (0.34)	BD (0.40)	Silt (0.79)
	(1.0)	Sand (0.34)	Sand (0.35)	OM (0.20)
		OM (0.31)	Clay (0.25)	Sand (0.01)

Given the observed performance of the four PTFs,  $\theta_{pF2}$ ,  $\theta_{pF3}$ ,  $\theta_{pF4.2}$  for each experimental ADI soil column were predicted with the trained GPR-PTF and used as additional data for the drier part in the inverse simulation. The use of both pressure heads and water content data improves the well-posedness of the inverse problem (KOOL; PARKER, 1988).

Considering the bad performance of the respective PTF,  $\theta_{pF1}$  data were not used. This, however, was acceptable as many data from the ADI experiments were already available for very wet soil conditions. The average and coefficient of variation of measured soil parameters and estimated water contents for the fifteen soil columns are given in Table 3.5.

Table 3.5. Average and coefficient of variation (CV) for measured soil physical and hydraulic properties and PTF-estimated water contents for the soil columns ( $n=15$ )

properties <sup>†</sup>	Sand	Silt	Clay	OM	BD	$K_s$	$\theta_{pF2}$	$\theta_{pF3}$	$\theta_{pF4.2}$
unit	(%)				(g cm <sup>-3</sup> )	log(cm d <sup>-1</sup> )			
Average	61.8	22.3	13.4	2.5	1.5	2.88	0.30	0.21	0.09
CV (%)	3.5	3.9	9.1	7.5	4.9	122	3.9	7.0	8.4

<sup>†</sup> sand, silt and clay fractions; OM, organic matter content; BD, bulk density;  $K_s$ , saturated hydraulic conductivity,  $\theta_{pF2}$ ,  $\theta_{pF3}$ ,  $\theta_{pF4.2}$ , volumetric water contents at -1, 10 and 158 m of pressure head predicted by PTF

### 3.3.4 Inverse modeling of actual measurements

Addition of the water content data obtained from the developed PTF to the pressure head data from ADI resulted in proper estimation of VG parameters as illustrated in Table 3.6. Although the columns were sampled from the same field, there is an extensive variation of VG parameters except for  $n$  (with a standard deviation of 0.08). Minimum and maximum values for  $\alpha$  are 0.014 and 0.052 (cm<sup>-1</sup>) and for  $\lambda$  are -1 to 24.4.

There was no agreement between values of observed and simulated  $K_s$ . It should be remembered that  $K_s^{sim}$  values were obtained by inverse modeling from unsaturated columns, so they refer to extrapolation, and are meant to be used for prediction of unsaturated  $K$  values.  $K_s^{obs}$  values (Table 3.6) were obtained from actual measurements in laboratory. Similar findings were discussed by Pinheiro et al. (2018). Optimized parameters should be used only in the range where they were determined, and any extrapolation outside that range (as towards saturation) will be associated to a high level of uncertainty. Furthermore, there is spatial variability of  $K_s$  over small distances due to variability and connectedness of macropores formed by root channel, earthworms or variability in bulk density (compaction) highlighted by

Ghanbarian et al. (2017) and Garcia-Gutierrez et al. (2018). According to Table 3.6, the columns with the largest BD ( $>1.6 \text{ g cm}^{-3}$ ) were columns 2, 3 and 15, corresponding to the lowest measured  $K_s$ . The highest values of  $K_s$  (9800, 5386 and  $4068 \text{ cm d}^{-1}$ ) belong to columns 13, 4 and 12 respectively with BD of  $1.45 \text{ g cm}^{-3}$  on average.

Table 3.6. Estimated parameters obtained from inverse modeling of ADI experiments in 15 soil columns, including GPR-PTF  $\theta(h)$  values. (Standard deviations between parentheses if  $\geq 0.5\%$  of true value)

Column number	parameter†						
	$\theta_s$	$\alpha \text{ (cm}^{-1}\text{)}$	$n$	$K_s^{sim} \text{ (cm d}^{-1}\text{)}$	$K_s^{obs} \text{ (cm d}^{-1}\text{)}$	$\lambda$	$BD \text{ (kg m}^{-3}\text{)}$
1	0.442	0.0360	1.342	186.8 (22.4)	532	5.9 (0.2)	1.48
2	0.381	0.0249	1.338	8.1 (0.2)	43	-0.02	1.64
3	0.381	0.0512	1.263	21.60	60	0.01	1.64
4	0.46	0.0515	1.269	29.6 (0.3)	5386.2	0.66	1.43
5	0.457	0.0141	1.552	5.9	2146	24.38 (1.5)	1.44
6	0.437	0.0391	1.275	7.1 (0.3)	845	0.001	1.49
7	0.479	0.0491	1.247	32.5 (0.2)	2680	-1.03	1.38
8	0.430	0.0360	1.372	9.6 (0.3)	494	0.02 (2.3)	1.51
9	0.415	0.0249	1.329	3.0 (0.2)	1447	0.02	1.55
10	0.453	0.0397	1.281	24.1 (1.8)	1735	-0.04	1.45
11	0.445	0.0395	1.298	75.6 (4.0)	834	1.14 (0.1)	1.47
12	0.456	0.0407	1.294	21.3 (1.7)	4068	3.10 (0.2)	1.44
13	0.445	0.0405	1.245	24.66 (1.0)	9829	-0.002 (0.2)	1.47
14	0.415	0.0379	1.251	20.9 (1.4)	373	0.001 (0.04)	1.55
15	0.392	0.0520	1.239	25.6	32	0.02	1.61

†  $\theta_s$ , saturated volumetric water content;  $\alpha$ ,  $n$  and  $\lambda$ : fitting parameters;  $K_s$ , saturated hydraulic conductivity; BD, bulk density

When using only pressure head values in inverse modeling, no reliable SHPs were obtained. Values of RMSE for  $\theta(h)$  are very high without employing the GPR-PTF and reduce to more acceptable values when including the GPR-PTF water contents (Table 3.7). As ADI data covered the wet range only, by excluding water content data no convergence was obtained for  $K(h)$  parameters and resulting retention parameters showed high errors in water content prediction (Table 3.7). In the predictions without GPR-PTF, unrealistic parameter prediction was frequently observed and inclusion of some water content values ( $\theta_{pF2}$ ,  $\theta_{pF3}$ ,  $\theta_{pF4.2}$ ) is required for proper estimation of  $\theta(h)$  and  $K(h)$ . Table 3.7 also evaluates the accuracy of simulated  $K(h)$  by Equation 3.3 in terms of RMSE and MSPE using the parameters in Table 3.6 in comparison to the observed values of  $K(h)$ . Small values of  $K(h)$  or the dry-end tail of the  $K(h)$  function

may be overestimated by the obtained SHPs. RMSE is less able to detect this, because absolute values of errors in the dry zone are small. The relative indicator MSPE showed more adequate to express this.

Small values of RMSE do not always indicate a proper prediction of  $K(h)$ . For example, columns 3, 7 and 10 correspond to similar values of RMSE but resulted in very different values of MSPE (126, 1519 and 131, respectively). Similarly, the lowest value of RMSE belongs to column 6 with MSPE equal to 260.

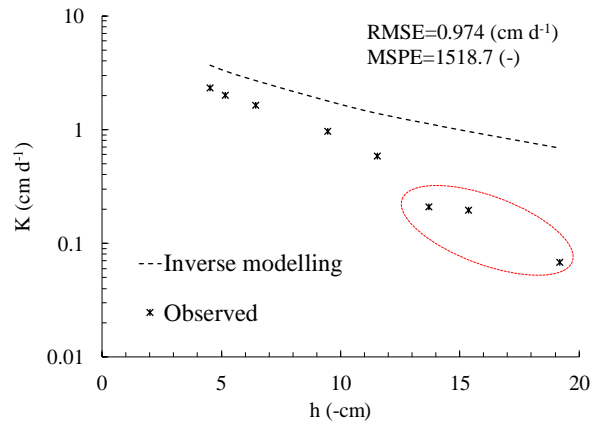
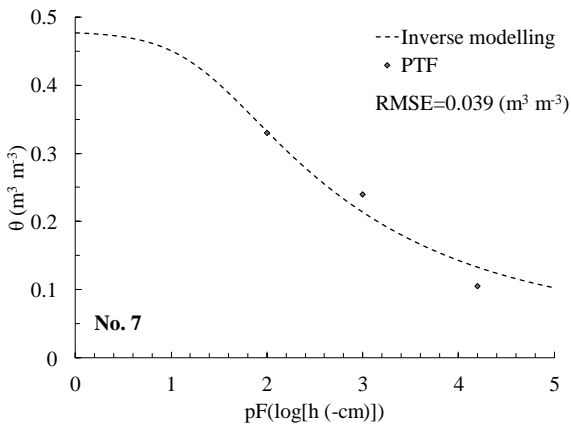
Table 3.7. Statistical indicators for the performance of  $\theta(h)$  prediction by inverse modeling of ADI experiments in 15 soil columns including GPR-PTF water contents and without GPR-PTF data

Column index	Including GPR-PTF			without GPR-PTF
	RMSE $K(h)$ (cm d <sup>-1</sup> )	MSPE $K(h)$	RMSE $\theta(h)$	RMSE $\theta(h)$
1	9.6	39	0.034	0.125
2	0.2	30	0.037	0.030
3	0.8	126	0.036	0.046
4	2.3	176	0.025	0.117
5	4.5	48	0.046	0.189
6	0.1	260	0.052	0.164
7	0.9	1519	0.039	0.043
8	0.5	93	0.044	0.063
9	0.5	13	0.022	0.231
10	0.8	131	0.021	0.041
11	3.5	54	0.035	0.030
12	0.0	5	0.021	0.080
13	0.5	50	0.024	0.191
14	0.9	65	0.065	0.079
15	0.3	14	0.038	0.049

\*for many cases VG parameters obtained from the scenarios without GPR-PTF did not result in reasonable values for  $K(h)$

Figure 3.4 shows the retention and hydraulic conductivity functions obtained in soil columns 7 and 12, the ones with the highest and lowest deviations, respectively, between values of  $K$  measured and those obtained by inverse modeling. In the retention graphs, the dashed line is obtained using the VG parameters from Table 3.6. In some cases, larger deviations occur between measured values of  $K$  and those obtained by inverse modeling, in their drier part. This is the case, for example, in soil column 7, indicated in Figure 3.4 a by the red circle.

(a)



(b)

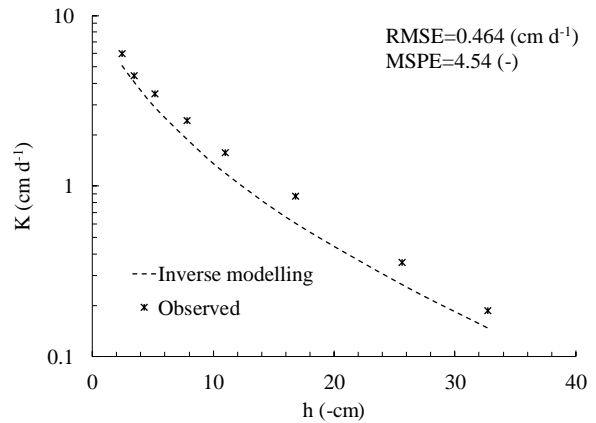
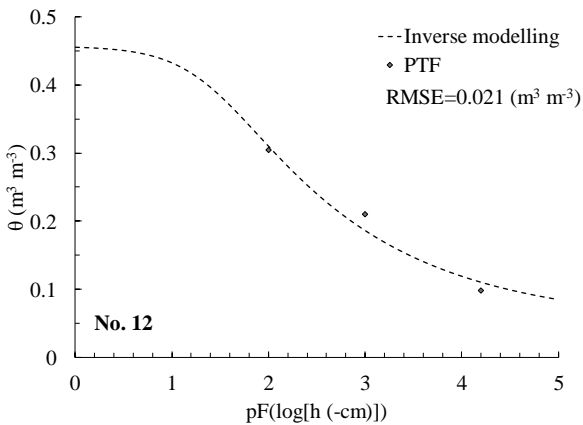


Figure 3.4. Retention and hydraulic conductivity functions obtained in (a) soil column 7, the column with the highest deviation between  $K$  measured and obtained by inverse modeling, and (b) soil column 12, with the lowest respective deviation. Red circle in (a) shows the high deviation for some of the observed values.

Finally, average and standard deviations of water retention data ( $\theta_s$ ,  $\theta_{\text{pF1}}$ ,  $\theta_{\text{pF2}}$ ,  $\theta_{\text{pF3}}$ ,  $\theta_{\text{pF4.2}}$ ) measured by steady state methods (SSM) on small rings with the obtained ones from inverse modeling of ADI+PTF performed on large columns are compared in Figure 3.5. The difference between measured and simulated water contents for the drier soil ( $\theta_{\text{pF3}}$  and  $\theta_{\text{pF4.2}}$ ) is larger than for the wetter values. The water contents estimated by SSM were higher than those inversely obtained from ADI experiments. Differences increased to about  $0.05 \text{ m}^3 \text{m}^{-3}$  in the drier region.

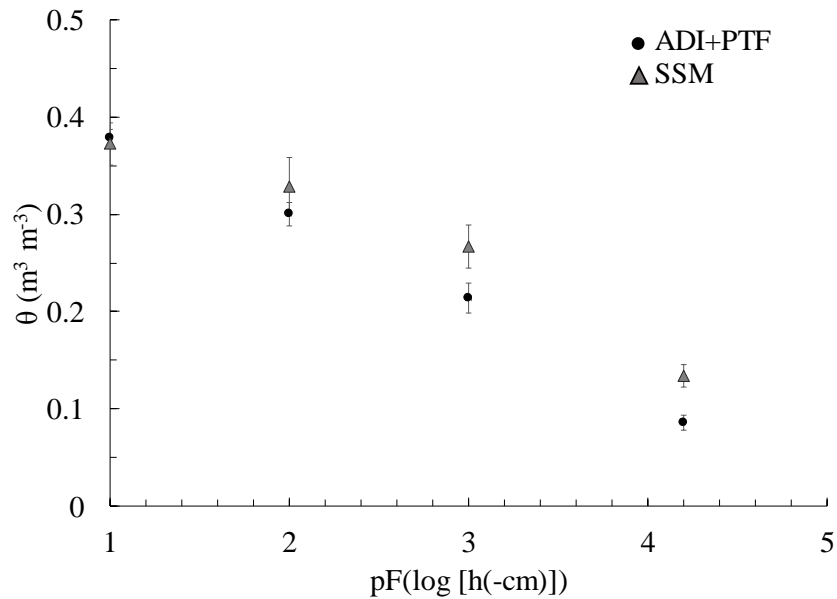


Figure 3.5. Average of water content at pF1, pF2, pF3 and pF4 obtained from SSM (steady state methods) versus corresponding values obtained from inverse modeling of ADI + PTF

### 3.4 Conclusions

The here performed evaluation of automated drip infiltrometer (ADI) scenarios in numerical and real experiments to obtain soil hydraulic parameters from inverse modeling allowed to conclude that:

- Evaluated for three reference soils, the inverse modeling of ADI experiments showed insensitive to residual and saturated water content. These parameters can better be measured or estimated than predicted from these experiments.
- A numerical simulation of automated drip infiltrometer scenarios ADI showed robust prediction of soil hydraulic parameters by inverse modeling. Introduction of a random error on input data did not affect the parameter estimation notably.
- Including water contents predicted for the drier soil by a Gaussian process regression PTF for the inverse modeling ADI data from 15 large undisturbed columns collected from the same field located in Denmark, Van Genuchten parameters  $\alpha$ ,  $K_s$ ,  $n$  and  $\lambda$  were uniquely identified and the unsaturated hydraulic conductivities calculated by these data were in a good agreement with measured  $K(h)$ . Not including the PTF water contents resulted in non-uniquely estimated van Genuchten parameters.

## References

ARORA, B.; MOHANTY, B. P.; MCGUIRE, J. T. Inverse estimation of parameters for multidomain flow models in soil columns with different macropore densities. **Water Resources Research**, v. 47, n. 4, 2011. DOI: 10.1029/2010WR009451.

BOUMA, J.; BAKER, F. G. **Measurement of water movement in soil pedons above the water table**. Madison, WI: University of Wisconsin, 1974.

DURNER, W.; PRIESACK, E.; VOGEL, H.-J.; ZURMÜHL, T.; VAN GENUCHTEN, M. T. **Determination of parameters for flexible hydraulic functions by inverse modeling**. Characterization and measurement of the hydraulic properties of unsaturated porous media. Riverside, CA: University of California, 1999. p. 817–829.

GARCIA-GUTIÉRREZ, C.; PACHEPSKY, Y.; MARTIN, M. Á. Saturated Hydraulic Conductivity and Textural Heterogeneity of Soils. **Hydrology and Earth System Sciences Discussions**, v. 22, p. 3923–3932, 2018.

GARDNER, W. R.; MIKLICH, F. J. Unsaturated conductivity and diffusivity measurements by a constant flux method. **Soil Science**, v. 93, n. 4, p. 271–274, 1962.

GHANBARIAN, B.; TASLIMITEHRANI, V.; PACHEPSKY, Y. A. Accuracy of sample dimension-dependent pedotransfer functions in estimation of soil saturated hydraulic conductivity. **Catena**, v. 149, p. 374–380, 2017.

GROH, J.; STUMPP, C.; LÜCKE, A.; PÜTZ, T.; VANDERBORGHT, J.; VERECKEN, H. Inverse estimation of soil hydraulic and transport parameters of layered soils from water stable isotope and lysimeter data. **Vadose Zone Journal**, v. 17, n. 1, 2018.

HOPMANS, J. W.; NIELSEN, D. R.; BRISTOW, K. L. How useful are small-scale soil hydraulic property measurements for large-scale vadose zone modeling? **Geophysical Monograph-American Geophysical Union**, v. 129, p. 247–258, 2002.

HUDSON, D. B.; WIERENGA, P. J.; HILLS, R. G. Unsaturated hydraulic properties from upward flow into soil cores. **Soil Science Society of America Journal**, v. 60, n. 2, p. 388–396, 1996.

IVERSEN, B. V.; KOPPELGAARD, M.; JACOBSEN, O. H. **An automated system for measuring air permeability and hydraulic conductivity in the laboratory on large soil cores**. Tjele, Denmark, 2004. 24 p. (DIAS Report, Plant Production, 111).

KELLEENERS, T. J.; SOPPE, R. W. O.; AYARS, J. E.; ŠIMŮNEK, J.; SKAGGS, T. H. Inverse analysis of upward water flow in a groundwater table lysimeter. **Vadose Zone Journal**, v. 4, n. 3, p. 558–572, 2005.

KOOL, J. B.; PARKER, J. C. Analysis of the inverse problem for transient unsaturated flow. **Water Resources Research**; v. 24, n. 6, p. 817–830, 1988.

KOOL, J. B.; PARKER, J. C.; VAN GENUCHTEN, M. T. Determining Soil Hydraulic Properties from One-step Outflow Experiments by Parameter Estimation: I. Theory and Numerical Studies 1. **Soil Science Society of America Journal**, v.49, n. 6, p. 1348–1354, 1985.

KOTLAR, A. M.; IVERSEN, B. V.; DE JONG VAN LIER, Q. Evaluation of Parametric and Nonparametric Machine-Learning Techniques for Prediction of Saturated and Near-Saturated Hydraulic Conductivity. **Vadose Zone Journal**, v. 18, n. 1, 2019a.

KOTLAR, A. M.; IVERSEN, B. V.; DE JONG VAN LIER, Q. Evaluation of parametric and nonparametric machine-learning techniques for prediction of saturated and near-saturated hydraulic conductivity. **Vadose Zone Journal**, v. 18, n. 1, 2019b.

KOTLAR, A. M.; IVERSEN, B. V.; DE JONG VAN LIER, Q. Machine Learning-Based Prediction of Drainage in Layered Soils Using a Soil Drainability Index. **Soil Systems**, v. 3, n. 2, p. 30, 2019.

LAMBOT, S.; HUPET, F.; JAVAUX, M.; VANCLOOSTER, M. Laboratory evaluation of a hydrodynamic inverse modeling method based on water content data. **Water Resources Research**, v. 40 (3), 2004.

LI, Y.B.; LIU, Y.; NIE, W.-B.; MA, X.-Y. Inverse Modeling of Soil Hydraulic Parameters Based on a Hybrid of Vector-Evaluated Genetic Algorithm and Particle Swarm Optimization. **Water**, v. 10, n. 1, p. 84, 2018.

LINDHARDT, B.; ABILDTRUP, C.; VOSGERAU, H.; OLSEN, P.; TORP, S.; IVERSEN, B. V.; GRAVESEN, P. **The Danish Pesticide Leaching Assessment Programme**. Site Characterization and Monitoring Design, GEUS, Copenhagen, Denmark, 2001.

MALLANTS, D.; MOHANTY, B. P.; VERVOORT, A.; FEYEN, J. Spatial analysis of saturated hydraulic conductivity in a soil with macropores. **Soil Technology**, v. 10, n. 2, p. 115–131, 1997.

MCKENZIE, N. J.; CRESSWELL, H. P.; RATH, H.; JACQUIER, D. Measurement of unsaturated hydraulic conductivity using tension and drip infiltrometers. **Australian Journal of Soil Research**, v. 39, n. 4, p. 823–836, 2001.

MORET-FERNÁNDEZ, D.; LATORRE, B.; PEÑA-SANCHO, C.; GHEZZEHEI, T. A. A modified multiple tension upward infiltration method to estimate the soil hydraulic properties. **Hydrological Processes**, v. 30, n. 17, p. 2991–3003, 2016.

PACHEPSKY, Y.; HILL, R. L. Scale and scaling in soils. **Geoderma**, v. 287, p. 4–30, 2017.

PARK, C.; APLEY, D. Patchwork kriging for large-scale Gaussian process regression. **The Journal of Machine Learning Research**, v. 19, n. 1, p. 269–311, 2018.

PETERS, A.; DURNER, W. Simplified evaporation method for determining soil hydraulic properties. **Journal of Hydrology**, v. 356, n. 1–2, p. 147–162, 2008.

PINHEIRO, E. A. R.; DE JONG VAN LIER, Q.; METSELAAR, K. A matric flux potential approach to assess plant water availability in two climate zones in Brazil. **Vadose Zone Journal**, v. 17, n. 1, 2018.

RASHID, N. S. A.; ASKARI, M.; TANAKA, T.; SIMUNEK, J.; VAN GENUCHTEN, M. T. Inverse estimation of soil hydraulic properties under oil palm trees. **Geoderma**, v. 241, p. 306–312, 2015.

RASMUSSEN, C. E.; WILLIAMS, C. K. I. **Gaussian processes for machine learning**. Cambridge, MA, The MIT Press, 2006.

RITTER, A.; HUPET, F., MUÑOZ-CARPENA, R.; LAMBOT, S.; VANCLOOSTER, M. Using inverse methods for estimating soil hydraulic properties from field data as an alternative to direct methods. **Agricultural Water Management**, v. 59, n. 2, p. 77–96. 2003.

ROMANO, N.; SANTINI, A. Determining soil hydraulic functions from evaporation experiments by a parameter estimation approach: Experimental verifications and numerical studies. **Water Resources Research**, v. 35, n. 11, p. 3343–3359. 1999.

SCHARNAGL, B.; VRUGT, J. A., VEREECKEN, H.; HERBST, M. Inverse modelling of in situ soil water dynamics: Investigating the effect of different prior distributions of the soil hydraulic parameters. **Hydrology and Earth System Sciences**, v. 15, n. 10, p. 3043–3059. 2011.

SCHELLE, H.; IDEN, S. C.; DURNER, W. Combined transient method for determining soil hydraulic properties in a wide pressure head range. **Soil Science Society of America Journal**, v. 75, n. 5, p. 1681–1693. 2011.

SIMUNEK, J.; VAN GENUCHTEN, M. T.; SEJNA, M. **The HYDRUS-1D software package for simulating the one-dimensional movement of water, heat, and multiple solutes in variably-saturated media**. Riverside, CA: University of California, 2005. 240 p. (Research Reports, 3).

SIMUNEK, J.; VAN GENUCHTEN, M. T.; WENDROTH, O. Parameter estimation analysis of the evaporation method for determining soil hydraulic properties. **Soil Science Society of America Journal**, v. 62, n. 4, p. 894–905, 1998.

ŠIMUUNEK, J.; ŠEJNA, M.; SAITO, H.; SAKAI, M.; VAN GENUCHTEN, M. T. **The HYDRUS-1D software package for simulating the movement of water, heat, and multiple solutes in variably saturated media, version 4.0**: HYDRUS Software Series 3. Riverside, CA: University of California, Department of Environmental Sciences, 2008.

VAN DAM, J. C.; STRICKER, J. N. M.; DROOGERS, P. Inverse method for determining soil hydraulic functions from one-step outflow experiments. **Soil Science Society of America Journal**, v. 56, n. 4, p. 1042–1050, 1992.

VAN DAM, J. C.; STRICKER, J. N. M.; DROOGERS, P. Inverse method to determine soil hydraulic functions from multistep outflow experiments. **Soil Science Society of America Journal**, v. 58, n. 3, p. 647–652. 1994.

VAN GENUCHTEN, M. T. A closed-form equation for predicting the hydraulic conductivity of unsaturated soils. **Soil Science Society of America Journal**, v. 44, n. 5, p. 892–898, 1980.

VRUGT, J. A.; BOUTEN, W.; WEERTS, A. H. Information content of data for identifying soil hydraulic parameters from outflow experiments. **Soil Science Society of America Journal**, v. 65, n. 1, p. 19–27, 2001.

WELLER, U.; IPPISCH, O., KÖHNE, M.; VOGEL, H.-J. Direct measurement of unsaturated conductivity including hydraulic nonequilibrium and hysteresis. **Vadose Zone Journal**, v. 10, n. 2, p. 654–661, 2011.

WENINGER, T.; BODNER, G.; KREISELMEIER, J.; CHANDRASEKHAR, P.; JULICH, S.; FEGER, K.-H.; SCHWEN, A. Combination of Measurement Methods for a Wide-Range Description of Hydraulic Soil Properties. **Water**, v. 10, n. 8, p. 1021, 2018.

WIND, G. P. **Capillary conductivity data estimated by a simple method**. Wageningen: International Association of Scientific Hydrology, 1969. 13 p.

YOUNG, M. H.; KARAGUNDUZ, A.; ŠIMUNEK, J.; PENNELL, K. D. A modified upward infiltration method for characterizing soil hydraulic properties. **Soil Science Society of America Journal**, v. 66, n. 1, p. 57–64, 2002.

ZHANG, Z. F.; WARD, A. L.; GEE, G. W. Estimating soil hydraulic parameters of a field drainage experiment using inverse techniques. **Vadose Zone Journal**, v. 2, n. 2, p. 201–211, 2003.

#### **4 Assessment of nitrogen fertilizer release half-life using crop modelling based experiments**

##### **Abstract**

Agricultural intensification to increase crop yield has been along with land use change and deforestation, especially in Brazil. However, proper nutrient, especially nitrogen delivery to plant can substantially boost crop productivity. Slow-release fertilizer using encapsulation of urea fertilizer is a suitable approach to improve nitrogen efficiency. This numerical study uses SWAP- N module crop model to assess the effect of hypothetical slow-release fertilizer with different half-lives 10, 20, 30 and 40 days. The soil hydraulic parameters of typical layered profiles nearby Piracicaba under cultivation of summer maize and the recommended  $180 \text{ kg N ha}^{-1}$  was considered as major input of the model. Typical urea fertilization to provide  $180 \text{ kg N ha}^{-1}$  was simulated and then SRFs were applied in two different ways first when the  $180 \text{ kg N ha}^{-1}$  was added on the sowing date and secondly we assumed the application of alleviated weight of SRFs to provide the plant with  $180 \text{ kg N ha}^{-1}$  during cropping period. The yield of maize under application of SRFs with half-lives of 30 and 40 days can increase up to  $200 \text{ kg N ha}^{-1}$  and leaching of nitrogen diminished by 30 to  $40 \text{ kg ha}^{-1}$ , unless bottom layers of the soil profile are very permeable. In both scenarios of SRF application and in all soils, SRF with half-life of 10 days resulted in more leaching and less uptake by the plant compared to typical fertilization scenario.

**Keywords:** slow release fertilizer, layered soil profiles, nitrogen leaching, nitrogen uptake, half-life

#### 4.1. Introduction

More fertile land may meet the increasing trend of food demand for worldwide population. This directs the agriculture industry in a way that water and nutrient use efficiency of crops should be optimized for enhancing productivity (TIMILSENA et al., 2015). The sustainable agricultural intensification optimizes the use of resources and management aiming to increase land productivity (YAMAMOTO et al., 2016). Slow-release fertilizers (SRFs) have been developed to boost nutrient crop availability and reduce environmental N loss from the soil system. SRFs are engineered fertilizers manufactured by covering e.g. urea with environmentally friendly coatings which extend active nutrient release time synchronized with plant root uptake (SAHA et al., 2018). This release is complex and depends on different factors including nature of coating material, climatic conditions, soil physics and chemistry and etc. SRFs are expensive however they are applied once usually on sowing date.

There have been numerous experimental studies committing to synthesis of SRFs and understand the nitrogen release and uptake. Inorganic materials especially sulfur has been suitable coating material as its low melting point, cost and being a secondary plant nutrient and fungicide (BLOUIN et al., 1971; ALLEN; MAYS, 1971; SALMAN et al., 1989; SHAVIV, 2001 and TANG et al., 2018). Later on polymer coating materials due to higher cost and slow degradable residues in soil were replaced by starch based alternatives (DEVASSINE et al., 2002 and MELLO et al., 2017). Lignin and cellulose were another interesting alternative for coating as its abundant in the pulp and paper industry wastes. Although various materials can be employed to coat fertilizer, they should be biodegradable and cheap in extraction and process.

The experimental studies in the application of SRFs from the batch experiments to field scale cases are of great importance, however, experiments required time, chemicals and human resources, thus often impossible to be implemented (NAZ; SULAIMAN, 2016). Mathematical modelling allows considering the effective factors such as coating thickness and materials, soil properties such as water content, pH and other boundary conditions in the mechanism of nutrient release without performing any experiments. Generally, the nutrient release has been modelled from a granule of SRF by mechanistic or empirical approaches. Mechanistic models are constructed taking Fickian diffusion laws into consideration. The empirical model presented by King et al. (2000) considered the effect of soil water content and seven-day dissolution amount. Fujinuma et al. (2009) developed a time, temperature and soil moisture-based empirical model for nitrogen release based on the results of field experiments.

A logistic growth-based model was constructed by Tong et al. (2009). Mechanistic models are generated for sulfur and polymer-based SRFs. The developed mechanistic model by Jarrell and Boersma (1980) described urea release from sulfur coated fertilizer did not consider the geometry, size and volume to surface ratio of SRF. However, Shaviv et al. (2003) improved the non-linearity nature of the release process from polymer coating by considering pressure-gradient-driven mass flow, dissolution, and chemical degradation of the coating. Nitrogen release was modelled using the finite element method in 2-D geometry and introducing urea diffusivity as a function of its concentration (TRINH et al., 2015).

Using a computer model now facilitates the prediction of SRF application under simulated field conditions. Development of the soil-plant-atmosphere models results in more reliable crop yield predictions that are requiring for many crop management and marketing policies. Simulation of crop growth considering under different parameters and complexities can decrease the need for expensive and long term field trials. From the crop simulation models; water oriented ones i.e. agrohydrological models give better results as the soil water dynamics is driven by numerical simulation of Richards' equation. SWAP (Soil; Water; Atmosphere and Plant) solves 1-D form of Richards' equation knowing boundary and initial conditions at field scale besides hydraulic properties of the soil including soil water retention and hydraulic conductivity function (KROES et al., 2009). World Food Studies (WOFOST) model is coupled with SWAP to model crop growth and its production based on the incoming photosynthetically active radiation absorbed by the crop canopy; its photosynthetic leaf characteristics; and accounting for water and salt stress on the crop (KROES et al., 2009). The most recent developed soil N module also enables the simulation of nitrogen fate in soil-plant due to the application of mineral fertilizer or organic matter decay. This complete modelling package abbreviated SWAP-N makes the evaluation of the influence of land use changes and fertilizer managements on crop yield or environmental factors. There are few studies that modelled cropping systems in the south and southeastern regions; however; only part of them considered WOFOST model coupled with SWAP and there is no study to perform crop simulation under coupling of newly developed Nitrogen module (GROENENDIJK et al., 2016).

An ideal SRF prolongs nitrogen release to meet crop requirement. To unify properties of slow-release fertilizer, the half-life of fertilizer can be used where longer half-life results in longer tailoring. Implementing these assumptions into SWAP-N, one can assess the effect of SRF on different crops and soils under different climatic conditions.

To the best of authors' knowledge, there is no research which numerically evaluates the fate of nitrogen released from SRF in the literature. Therefore, the objective of this study is to design and study the numerical experiments under application SRFs with different half-lives and maize cultivation under three typical soil profiles in the state of São Paulo, Brazil.

## 4.2. Materials and Methods

### 4.2.1. Soil and meteorological data

Data of three soil profiles within the distance of 50 kilometers from each other nearby Piracicaba, Brazil under maize cultivation were retrieved from de Jong van Lier (2017). For these layered soils, water retention data were obtained using undisturbed samples by tension table and pressure plates and internal drainage experiment was performed to measure unsaturated hydraulic conductivities. Hydraulic properties were described using van Genuchten (1980) equations and shown in Table 4.1

$$S_e(h) = \frac{\theta(h) - \theta_r}{\theta_s - \theta_r} = (1 + |\alpha h|^n)^{-m} \quad (4.1)$$

$$K(h) = K_s S_e^\lambda [1 - (1 - S_e^{1/m})^m]^2 \quad (4.2)$$

where  $S_e$  is the saturation degree,  $\theta_s$  and  $\theta_r$  are volumetric saturated and residual water contents, and  $\alpha$  ( $\text{cm}^{-1}$ ),  $m = 1 - 1/n$ , and  $\lambda$  are fitting parameters.

Table 4.1 Hydraulic parameters of the soils according to the van Genuchten (1980) equation

Soil	Layer (cm)	$\theta_r$	$\theta_s$	$\alpha$ ( $\text{cm}^{-1}$ )	$n$	$K_s$ ( $\text{cm d}^{-1}$ )	$\lambda$
(I) Sandy Clay Loam	0-20	0.186	0.436	0.0263	2.328	27.18	2.02
	20-30	0.179	0.332	0.0275	1.697	25.49	0
	30-40	0.202	0.293	0.0070	2.919	42.29	7.17
	40-50	0.186	0.350	0.0262	1.523	42.77	0
	50-60	0.218	0.333	0.0154	2.570	34.12	0
	60-70	0.184	0.303	0.0181	1.869	43.24	0
	70-80	0.179	0.408	0.0269	2.754	118.79	1.99
	80-100	0.169	0.353	0.0289	1.735	79.29	0
(II) Sandy Clay Loam	0-15	0.113	0.469	0.0593	1.608	38.20	-0.36
	15-30	0.138	0.362	0.0421	1.759	32.80	1.13
	30-45	0.112	0.332	0.0373	1.551	24.00	2.16
	45-60	0.144	0.329	0.0392	1.527	17.50	1.30
	60-100	0.142	0.351	0.0424	1.487	17.50	1.76
(III) Clay	0-20	0.275	0.463	0.0232	1.389	76.42	3.93
	20-40	0.290	0.447	0.0181	1.356	113.85	4.71
	40-60	0.287	0.444	0.0136	1.443	120.54	4.98
	60-80	0.270	0.506	0.0254	1.590	1352.34	4.96
	80-100	0.257	0.513	0.0265	1.583	2014.19	4.97

Daily meteorological data were obtained for a 38-year period (1990-2008) from the University of São Paulo weather station in Piracicaba, Brazil (22.703°S;47.624°W), representing the sub-tropical winter-dry climate (Koeppen Cwa) of southeast Brazil. Potential (reference) evapotranspiration for a hypothetical grass surface was calculated based on the Penman-Monteith ( $ET_{0P}$ ,  $\text{mm d}^{-1}$ ) equation (2.1) (ALLEN et al., 1998):

$$ET_{0P} = \frac{0.408\Delta(R_n - G) + \gamma \frac{900}{T_{ave} + 273} u_2 (e_s - e_a)}{\Delta + \gamma(1 + 0.34u_2)} \quad (4.3)$$

In equations (4.3),  $R_n$  and  $R_s$  are the net radiation at the crop surface and solar radiation ( $\text{MJ m}^{-2} \text{d}^{-1}$ ),  $G$  represents the soil heat flux density which is usually ignored in daily calculations ( $\text{MJ m}^{-2} \text{d}^{-1}$ ),  $T$  ( $^{\circ}\text{C}$ ) and  $u_2$  ( $\text{m s}^{-1}$ ) are mean temperature and wind speed at 2 m height,  $(e_s - e_a)$  is the vapour pressure deficit ( $\text{kPa}$ ),  $\Delta$  is the slope of the vapour pressure curve ( $\text{kPa } ^{\circ}\text{C}^{-1}$ ) and  $\gamma$  is the psychometric constant, equal to  $0.06317 \text{ kPa } ^{\circ}\text{C}^{-1}$  for the Piracicaba weather station.

#### 4.2.2. SWAP-1D numerical modelling

The SWAP-1D model numerically simulates the temporal and spatial changes in water content by the Richards' equation:

$$\frac{\partial \theta}{\partial t} = \frac{\partial}{\partial z} \left[ k(h) \frac{\partial h}{\partial z} - k(h) \right] - S(h, z, t) \quad (4.4)$$

In this equation,  $\theta$  is volumetric soil water content,  $t$  is time ( $d$ ),  $z$  is the vertical space coordinate ( $cm$ ),  $k$  is the hydraulic conductivity ( $cm d^{-1}$ ),  $h$  represents pressure head ( $cm$ ) and  $S$  is the sink term ( $d^{-1}$ ) accounting for the volume of water removed from the soil per unit of time due to crop water uptake and described by

$$S(h, z, t) = \alpha(h)S_p = \alpha(h)\beta(z, t)T_p \quad (4.5)$$

where  $S_p$  is the potential water uptake rate ( $d^{-1}$ ) calculated from the potential transpiration rate  $T_p$  ( $cm s^{-1}$ ) distributed over the root zone based on the normalized root density distribution function  $\beta(z, t)$  ( $cm^{-1}$ ).  $0 \leq \alpha(h) \leq 1$  is a dimensionless root water uptake stress reduction function

proposed by Feddes et al. (1978) defined by crop dependent parameters described for grass in (FEDDES; KOWALIK; ZARADNY, 1978).

Maize was simulated under rainfed conditions planted in the middle of October and harvested on February. Major required crop data in SWAP-N input were extracted from calibrated regional study (PINTO et al., 2019) and shown in Table 4.2.

Table 4.2. Main calibrated crop data parameters

Parameter; Description	Value	Unit
$H_{max}$ ; Plant maximum height	200	cm
$C_{ref}$ ; Reflection coefficient, Albedo	0.2	-
$RSC$ ; Minimum canopy resistance	131	s m <sup>-1</sup>
$T_{sum,ea}$ ; Temperature sum from emergence to anthesis	1000	°C
$T_{sum,am}$ ; Temperature sum from anthesis to maturity	1150	°C
$A_{max,d}$ ; Maximum CO <sub>2</sub> assimilation rate	35	kg ha <sup>-1</sup> d <sup>-1</sup>
$RLAI$ ; Maximum relative increase in LAI	0.012	m <sup>2</sup> m <sup>-2</sup>
$K_{dif}$ ; Extinction coefficient for diffuse visible light	0.60	-
$K_{dir}$ ; Extinction coefficient for direct visible light	0.75	-
$e_{ff}$ ; Light use efficiency	0.45	kg CO <sub>2</sub> j <sup>-1</sup>
$C_{vt}$ ; Assimilates conversion efficiency into leaves	0.68	kg kg <sup>-1</sup>
$C_{vo}$ ; Assimilates conversion efficiency into storage organs	0.67	kg kg <sup>-1</sup>
$C_{vr}$ ; Assimilates conversion efficiency into roots	0.29	kg kg <sup>-1</sup>
$C_{vs}$ ; Assimilates conversion efficiency into stems	0.66	kg kg <sup>-1</sup>
$R_{it}$ ; Relative increase in respiration rate with temperature	2.00	kg CH <sub>2</sub> O j <sup>-1</sup> d <sup>-1</sup>
$R_{ml}$ ; Relative maintenance respiration rate of leaves	0.03	kg CH <sub>2</sub> O j <sup>-1</sup> d <sup>-1</sup>
$R_{mo}$ ; Relative maintenance respiration rate of storage organs	0.01	kg CH <sub>2</sub> O j <sup>-1</sup> d <sup>-1</sup>
$R_{mr}$ ; Relative maintenance respiration rate of roots	0.015	kg CH <sub>2</sub> O j <sup>-1</sup> d <sup>-1</sup>
$R_{ms}$ ; Relative maintenance respiration rate of stems	0.015	kg CH <sub>2</sub> O j <sup>-1</sup> d <sup>-1</sup>
$P_{dl}$ ; Maximum relative death rate of leaves due to water stress	0.03	d <sup>-1</sup>
Critical pressure heads according to Feddes		
$h_1$	-10.0	cm
$h_{2u}$	-25.0	cm
$h_{2l}$	-25.0	cm
$h_{3h}$	-400.0	cm
$h_{3l}$	-500.0	cm
$h_4$	-10000.0	cm
$\alpha$ ; Interception coefficient	0.25	-
$R_{rd,i}$ ; Maximum daily increase in rooting depth	2.20	cm d <sup>-1</sup>
$R_{d,m}$ ; Maximum root depth	100	cm
$BC$ ; Below ground plant coverage	0.5	-

### 4.2.3. N module paramters and Fertilizer application

A soil nitrogen module (N- module) implemented in the SWAP model simulates the nitrogen fate in soil, plant and atmosphere due to fertilizer or organic matter decay. The ammonium balance is as

$$y_{ts}K_{sorb}\rho_d \frac{dC_{NH_4}}{dt} + \frac{d\theta C_{NH_4}}{dt} = q_{in}C_{NH_4;in} - q_{out}C_{NH_4;out} + R_{Nmin} - R_{NH_4;upt} - R_{nitr} \quad (4.6)$$

where  $C_{NH_4}$  is the concentration of  $NH_4$  in soil water ( $kg\ m^{-3}$ );  $C_{NH_4;in}$  is the concentration of  $NH_4$  in flowing water with flux  $q_{in}$  ( $m\ d^{-3}$ ) of and  $q_{out}$  is the flux of out-flowing water.  $K_{sorb}$  is linear sorption constant ( $m^3\ kg$ ) and  $\rho_d$  is dry bulk density ( $kg\ m^{-3}$ ).  $R_{NH_4;upt}$  and  $R_{nitr}$  are  $NH_4$  mineralization; uptake and nitrification rates ( $kg\ m^{-3}\ d^{-1}$ ). We assumed volatilization is zero. Similar to  $NH_4$  balance; nitrate balance is governed by

$$\frac{d\theta C_{NO_3}}{dt} = q_{in}C_{NO_3;in} - q_{out}C_{NO_3;out} + R_{nitr} - R_{NO_3;upt} - R_{denitr} \quad (4.7)$$

For establishing the nitrate uptake by plant roots ( $R_{NO_3;upt}$ ); two calculations of the mass conservation equation are performed. In the first calculation; the uptake is set equal to the demand of the crop; as calculated by the WOFOST model. In the second calculation;  $R_{NO_3;upt}$  is formulated as a first order term and it is assumed that the uptake is limited by the nitrate amount in soil.

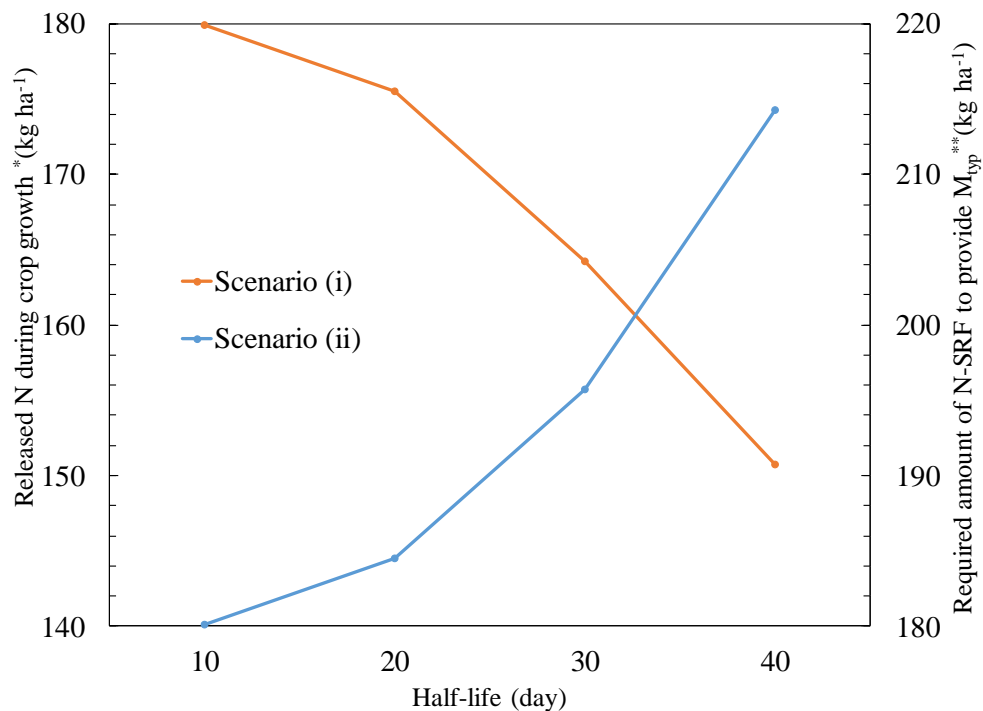
The soil N module requires parameters to model the nitrogen chain and fate. Firstly, the time of fertilization should be specified. Typical scenario usually done in the regional fields is  $180\ kg\ N\ ha^{-1}$  for maize (CANTARELLA et al., 1997), thus in this study we applied  $65\ kg\ Urea\ ha^{-1}$  on sowing day plus  $325\ kg\ Urea\ ha^{-1}$  at about V6 or 4 weeks later. However, for hypothetical SRFs we considered two scenarios. (i) SRFs with different half-lives (Half-life=10, 20, 30 and 40 days) should be applied in the same quantity as typical fertilizer ( $M_{typ}=180\ kg\ ha^{-1}$ ) in the sowing date. In this case, not all the nitrogen ( $390\ kg\ ha^{-1}$ ) will be released during 120-day crop growing and remaining part will be released after harvest so we assume that part is lost, so crop may tolerate nitrogen stress. In the second scenario (ii) the increasing initial amount of SRF was applied on the sowing date to provide crop all  $180\ kg\ N\ ha^{-1}$  during crop growth and the remaining part is again lost. This alleviated amount of fertilizer required to compensate nitrogen is calculated by

$$M_{sr} = \sum_{n=1}^m \frac{M_{req,n}}{2^n} \quad (4.8)$$

where  $m$  is the growing time divided by half-life of slow release fertilizer.

### 4.3. Results and Discussion

According to our assumptions for application of urea SRF, there is nitrogen loss for all half-lives except for the one with half-life of 10 days (Figure 4.1). Assuming the first scenario when  $180 \text{ kg N ha}^{-1}$  was applied, there could be 5, 16 and 29  $\text{kg N ha}^{-1}$  lack of nitrogen for plant uptake during growth time for SRFs with half-life of 20, 30 and 40 days. On the other hand, excessive application of urea when scenario (ii) was considered because this excessive amount guarantees delivering of  $180 \text{ kg Urea ha}^{-1}$  urea during plant growth, although the remaining should be considered as N loss when they are released after plant harvesting.



\*This is for the first scenario when  $180 \text{ kg N ha}^{-1}$  SRF was applied

\*\*this is for the second scenario when SRF applied to provide  $180 \text{ kg N ha}^{-1}$  urea

Figure 4.1 Quantification of released and required urea SRF applied in sowing date for scenario (i) and (ii)

The results of numerical simulation of assumptions in scenario (i) are shown in Figure 4.2. Note that as the amount of release for SRFs with half-lives of 10 and 20 days between scenario (i) and (ii) similar, their corresponding results are explained later. Different soils led to different fate of  $180 \text{ kg N ha}^{-1}$  with half-life of 30 and 40 days. Although 30 days' half-life did not significantly change nitrogen uptake it increased yield by about  $200 \text{ kg ha}^{-1}$  in soils I and II and  $20 \text{ kg ha}^{-1}$  nitrogen leaching reduction. When half-life increased to 40 days, more than  $250 \text{ kg ha}^{-1}$  yield reduction was observed in soil III while still yield in the other two soils improved. Indeed, considering scenario (i) the availability of nitrogen diminished by increasing half-life so there is high nitrogen stress in years with intense rainfall in the early days of plant growth when more nitrogen is released.

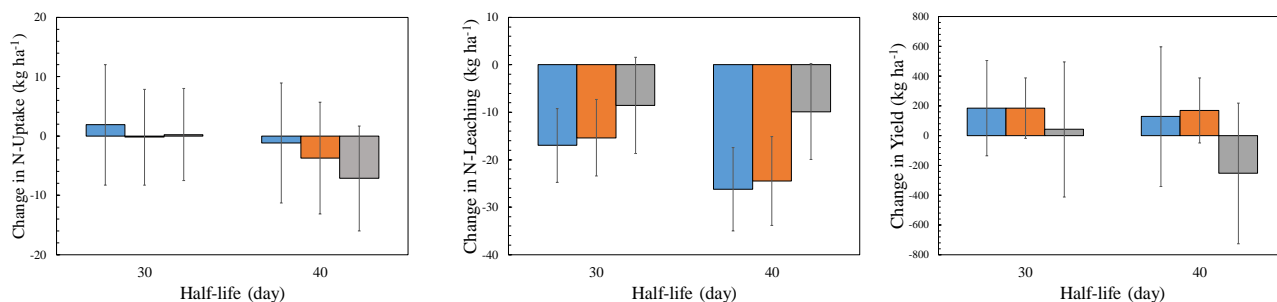


Figure 4.2. Changes in nitrogen uptake and leaching as well as yield under application of different SRFs with half-life of 10, 20, 30 and 40 days with the same weight of typical fertilizer compared to the corresponding values using typical

The uptake and leaching of nitrogen besides grain yield of simulated maize are plotted in Figure 4.2. Generally, increase in half-life resulted in increase in nitrogen uptake and yield, however leaching of nitrogen was reduced, regardless of inherent 25 and 50 kg nitrogen loss of slow release fertilizers with half-life of 30 and 40 days. Nitrogen uptake increased more by increasing half-lives for soils (II) and (III) where 7 and 10  $\text{kg ha}^{-1}$  rise in N uptake was observed in using SRF with 40 days' half-life compared to typical urea fertilizer. However, in soil (I), no improvement in nitrogen uptake between SRF with half-life of 20, 30 and 40 days occurred. A very permeable layer in soil (III) can affect in a way that no more nitrogen is taken up by plant due to increasing half-life. This simulated maize has 60 cm rooting depth on average within the first 30 days and in this depth soil hydraulic conductivity is extremely large in this soil, thus movement of water in lower depths are faster than root uptake. Therefore, soils with permeable layers at the bottom could entirely react in a different way with SRFs. In soil (III),

no significant change between nitrogen leaching and yield were observed along with half-life increasing, confirming that during plant growth extension of half-life will. In soil (II) and (III), using SRF with longer half-lives can reduce nitrate leaching by more  $10 \text{ kg ha}^{-1}$ , however SRF with half-life of 10 days resulted in increase in leaching by 10 and  $6 \text{ kg ha}^{-1}$  compared to the typical fertilizer (half-life of zero). In these soils (II and III), SRF with 40 days' half-life led to 350 and  $400 \text{ kg ha}^{-1}$  yield increase in comparison to application of typical fertilizer.

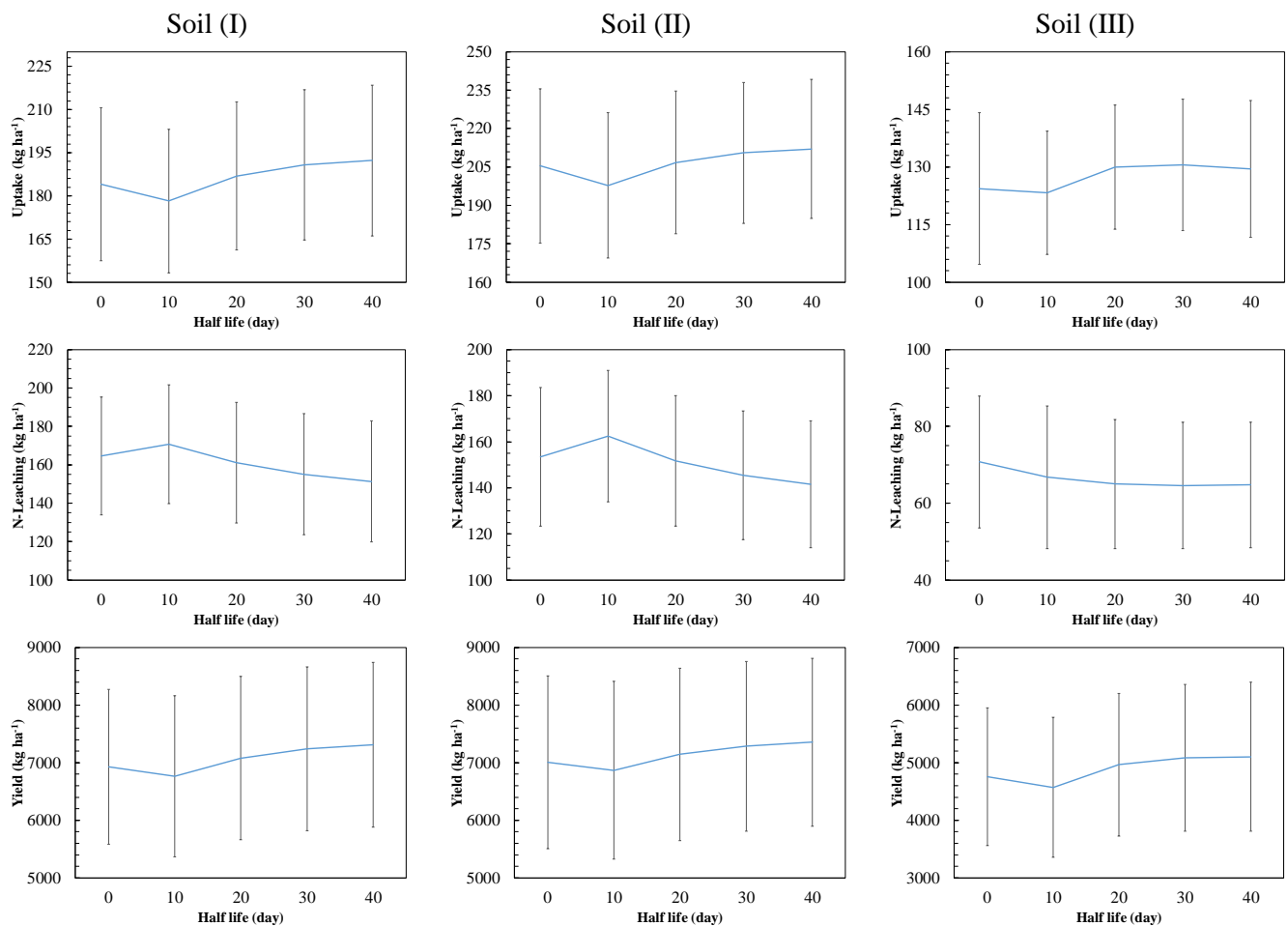


Figure 4.3 Nitrogen uptake and leaching as well as grain yield of maize under application of different SRFs with half-life of 10, 20, 30 and 40 days and typical fertilizer with zero half-life

#### 4.4. Conclusion

Synchronized nitrogen delivery to plant with plant growth is the most optimal management practice, however this task depends on the complex system of soil plant atmosphere. In this study, we demonstrated that using numerical experiments the fate of

nitrogen from hypothetical slow release fertilizers with half-life of 10, 20, 30 and 40 days can be traced within the media. Short time slow release fertilizer did not provide required amount of nitrogen for maize, however, SRF with longer half-life increased nitrogen uptake by plant. Using slow release fertilizer with half-life between 20 to 40 days for maize cultivation in Sao Paulo, Brazil, 200 to 400 kg ha<sup>-1</sup> yield increase and 10 kg ha<sup>-1</sup> nitrogen leaching reduction can be expected.

## References

ALLEN, R. G.; PEREIRA, L. S.; RAES, D.; SMITH, M. **Crop evapotranspiration**. Guidelines for computing crop water requirements. Rome: FAO, 1998. 300 p. (FAO Irrigation and Drainage Paper, 56).

ALLEN, S. E.; MAYS, D. A. Sulfur-coated fertilizers for controlled release. Agronomic evaluation. **Journal of Agricultural and Food Chemistry**. v. 19, p. 809–812, 1971.

BLOUIN, G. M.; RINDT, D. W.; MOORE, O. E. Sulfur-coated fertilizers for controlled release. Pilot-plant production. **Journal of Agricultural and Food Chemistry**. v. 19, p. 801–808, 1971.

CANTARELLA, H.; RAIJ B VAN, C. **Recomendações de adubação e calagem para o estado de São Paulo**. Cereais. 2. ed. Campinas, SP: Instituto Agronômico de Campinas (IAC), 1997. (Boletim Técnico 100).

DE JONG VAN LIER, Q. Field capacity, a valid upper limit of crop available water? **Agricultural water management**, v. 193, p. 214–220, 2017.

DEVASSINE, M.; HENRY, F.; GUERIN, P.; BRIAND, X. Coating of fertilizers by degradable polymers. **International Journal of Pharmaceutics**, v. 242, p. 399, 2002.

FEDDES, R. A.; KOWALIK, P. J.; ZARADNY, H. **Simulation of field water use and crop yield**. New York: Wiley, 1978. (Simulation Monographs).

FUJINUMA, R.; BALSTER, N. J.; NORMAN, J. M. An improved model of nitrogen release for surface-applied controlled-release fertilizer. **Soil Science Society of America Journal**. v. 73, p. 2043–2050, 2009.

GROENENDIJK, P.; BOOGAARD, H.; HEINEN, M.; KROES, J. G.; SUPIT, I.; DE WIT, A. **Simulation nitrogen-limited crop growth with SWAP/WOFOST**: process descriptions and user manual. Wageningen, Wageningen Environmental Research, 2016. (Report, 2721).

KING, K. W.; BALOGH, J. C. Development of a nitrogen-release algorithm for slow-release fertilizers. **Transactions of the ASAE**, v. 43, p. 661, 2000.

KROES, J. G.; VAN DAM, J. C.; GROENENDIJK, P.; HENDRIKS, R. F. A.; JACOBS, C. M. J. SWAP version 3.2. Theory description and user manual. Wageningen: Alterra, 2009. (Alterra Report, 1649).

MELLO, T.; BUZETTI, S.; TEIXEIRA FILHO, M. C. M.; GALINDO, F. S.; NOGUEIRA, L. M. Residual effects of nitrogen fertilizer with polymer-coated urea in a corn crop. **Revista Caatinga**, v. 30, p. 586–594, 2017.

NAZ, M. Y.; SULAIMAN, S. A. Slow release coating remedy for nitrogen loss from conventional urea: a review. **Journal of Controlled Release**, v. 225, p. 109–120, 2016.

PINTO, V. M.; VAN DAM, J. C.; DE JONG VAN LIER, Q.; REICHARDT, K. Intercropping Simulation Using the SWAP Model: Development of a 2X1D Algorithm. **Agriculture**, v. 9, p. 126, 2019.

SAHA, B. K.; ROSE, M. T.; WONG, V. N. L.; CAVAGNARO, T. R.; PATTI, A. F. Nitrogen Dynamics in Soil Fertilized with Slow Release Brown Coal-Urea Fertilizers. **Scientific Report**, v. 8, art. 14577, 2018.

SALMAN, O. A.; HOVAKEEMIAN, G.; KHRAISHI, N. Polyethylene-coated urea. 2. Urea release as affected by coating material, soil type and temperature. **Industrial & Engineering Chemistry Research**, v. 28, p. 633–638, 1989.

SHAVIV, A.; RABAN, S.; ZAIDEL, E. Modeling controlled nutrient release from polymer coated fertilizers: Diffusion release from single granules. **Environmental Science & Technology**, v. 37, p. 2251–2256, 2003.

TANG, J.; HONG, J.; LIU, Y.; WANG, B.; HUA, Q.; LIU, L.; YING, D. Urea Controlled-Release Fertilizer Based on Gelatin Microspheres. **Journal of Polymers and the Environment**. v. 26, p. 1930–1939. 2018.

TIMILSENA, Y. P.; ADHIKARI, R.; CASEY, P.; MUSTER, T.; GILL, H.; ADHIKARI, B. Enhanced efficiency fertilisers: a review of formulation and nutrient release patterns. **Journal of the Science of Food and Agriculture**, v. 95, p. 1131–1142, 2015.

YAMAMOTO, C. F.; PEREIRA, E. I.; MATTOSO, L. H. C.; MATSUNAKA, T.; RIBEIRO, C. Slow release fertilizers based on urea/urea-formaldehyde polymer nanocomposites. **Chemical Engineering Journal**, v. 287, p. 390–397, 2016.

ZHENG, T.; LIANG, Y.; YE, S.; HE, Z. Superabsorbent hydrogels as carriers for the controlled-release of urea: Experiments and a mathematical model describing the release rate. **Biosystem Engineering**, v. 102, p. 44–50, 2009.

## 5 Nitrate leaching from layered double hydroxides in tropical and temperate soils <sup>3</sup>

### Abstract

We evaluate layered double hydroxide (LDH) as a potential alternative for nitrate slow release fertilizer. Synthesized Mg-Fe-NO<sub>3</sub> LDH particles with Mg:Fe (2:1) were synthesized by coprecipitation and characterized by ICP-OES, XRD, FTIR and TGA analyses. Batch experiments with LDH particles containing 0.5, 0.1 or 0.01 M of KCl, K<sub>2</sub>SO<sub>4</sub> or CaCl<sub>2</sub> showed that 60 to 100% of intercalated nitrate is exchanged by anions within a few hours. Soil column studies with soils from temperate (Denmark) and tropical (Brazil) regions confirmed rapid release of nitrate from LDH. A reduction of 22% in nitrate leaching was the best result obtained for LDH applied to the Danish soils. The highest X-ray fluorescence spectroscopy (XRF) intensities of Fe and Mg were recorded at the top 0.5 cm of tropical soil columns, showing the high retention of LDH residues at soil surface. Application of LDH to a soil profile with bulk density of 1300 kg m<sup>-3</sup>, 0.3 m rooting depth and a typical rate of field nitrogen application (120 kg ha<sup>-1</sup>) caused accumulation of 400 to 1050 kg Mg and 230 to 478 kg of Fe or Al depending on type of LDH. This high load of residual metals may restrain the use of the LDH as slow release nitrate source.

Keywords: Layered double hydroxide; sustained release fertilizer; nitrate leaching; unsaturated soil column

---

<sup>3</sup> Kotlar, A.M., De Carvalho, H. W. P., Iversen, B.V., De Jong van Lier, Q. Nitrate leaching from layered double hydroxides in tropical and temperate soils. *Applied Clay Science*, 184, 2020. DOI: 10.1016/j.clay.2019.105365

## 5.1. Introduction

One of the main challenges of the fertilizer industry consists in raising efficiency of its products (AZIZ et al., 2015; SAHA et al., 2018). Due to competing condition of soil and plant for nutrients, any type of fertilizer improvement or field activities by farmers must aim at facilitating plant nutrient uptake within this competing system (KOTTEGODA et al., 2011).

Nitrogen emissions due to human activities receives much attention and the nitrogen footprint is used by policy makers to assess sustainability of resource use (GALLOWAY et al., 2014). Agricultural activity is one of the main sources of nitrogen emissions to the environment (XIAN et al., 2019). The main forms of nitrogen fertilizers used in agriculture are urea, ammonium, and nitrates. After field broadcasting, nitrogen may be lost by volatilization, immobilization, denitrification and leaching. Especially nitrate, which is negatively charged, does not readily bind to soil minerals and is therefore susceptible to leaching, possibly accumulating in groundwater and the surface waters. It may contaminate and cause eutrophication of lakes and coastal marine ecosystems, representing a significant economic loss for farmers and society (TORRES-DORANTE et al., 2008) and a risk of oxygen depletion of water bodies. Nitrate can also be converted to nitrous oxides, a greenhouse gas, and be lost via volatilization (ZHANG et al., 2015).

Improved management with a proper selection of fertilizer type, rate, placement, and timing can diminish such losses. Among the management options, fertilizers with controlled or slow release properties have been extensively studied (TIMILSENA et al., 2015, NAZ; SULAIMAN, 2016; GIROTO et al., 2017 and LI et al., 2018). Encapsulation and coating technologies diminish dissolution rate of fertilizer and reduce leaching of nitrate making it longer available to plants. Slow and controlled release of nitrate from fertilizer, particularly in well-drained weathered tropical soils with excess rainfall, may prevent nitrate loss and maintain more available nitrate for plants, resulting in higher yields and reduced greenhouse gas emissions and leaching (NYAMANGARA et al., 2003).

Layered double hydroxides (LDHs) are natural or synthetic layered mineral compounds with a structure identical to the mineral brucite  $Mg(OH)_2$ ; chemical formula of  $[M_{1-x}^{2+}M_x^{3+}(OH)_2]A_{x/m}^{m-}nH_2O$ ; where  $M^{2+}$  and  $M^{3+}$  are divalent and trivalent metals;  $A^{n-}$  is the interlayer anion and  $x=M^{3+} / (M^{3+} + M^{2+})$ .

In terms of agrochemical application; the positive charge bared by LDH has been explored as a carrier for anionic nutrients and herbicides (GILLMAN, 2005; BRUNA et al., 2009; BENICIO et al., 2015). Several parameters in the synthesis process and adsorption-desorption experiments could affect the sustainable release of interlayered anions. For example; Halajnia et al. (2012) concluded that one gram of low charge density of Mg-Al LDH ( $x=0.25$ ) adsorbed 38.4 mg of nitrate which was twice of the amount incorporated by  $x=0.33$ ; illustrating higher nitrate affinity for LDH metal layers dominated by divalent cation (EVERAERT et al., 2016). However; the maximum nitrate adsorption for the LDH in which Fe is used as trivalent cation was roughly equal for either LDH with  $x=0.25$  or  $0.33$  (HALAJNIA et al., 2016); which was 67% of adsorption capacity of the same LDH reported in (SASAI; NORIMATSU; MATSUMOTO, 2012). Therefore; metal types and ratios could change adsorption capacity of nitrate. The highest adsorption capacity of nitrate 67.73 mg/g LDH has been revealed in a study done by Tong et al., (2017) with the Mg- Al- Fe (3- 0.1-0.9) LDH.

Results from a batch study by Olfes et al. (2009) showed that 100% of nitrate intercalated in Mg- Al LDH exposed to different anionic environments left the LDH in an hour equilibrium experiment. Urena-Amate et al. (2011) showed that unmodified granules Mg-Al LDH released more than 90% of its intercalated nitrate less than 10 h. However; the modification of LDH by hydroxypropyl methylcellulose could increase nitrate buffer capacity.

The literature presents many studies regarding nitrate adsorption by LDH, however less attention is dedicated to the release rate of nitrate used in fertilizer. Additionally, current available studies do not focus on the applicability of LDH as a slow release fertilizer. Apparently, in most cases nitrate release or anion exchangeability is fast, of the order of magnitude of hours, and the low loading capacity of nitrogen provided by LDH does not seem to be adequate for crop uptake and agricultural applications. More importantly, there is lack of soil column studies testing the fate of LDH components and intercalated nitrate, especially under unsaturated flow conditions which are most common in the field.

The main objective of this study was therefore to evaluate the nitrate release from synthesized LDH particles under kinetic and equilibrium batch (soilless) and unsaturated flow (soil column) conditions using soil material from temperate and tropical regions. The fate of the cationic component of LDH particles was also studied.

## 5.2. Materials and Methods

### 5.2.1. Synthesis of Mg-Fe-NO<sub>3</sub> LDH

The chemicals required for the synthesis of the nitrate form of LDH, including nitrate salts of Mg, Fe and KOH with purity of 99%, were purchased from Merck, Germany. Magnesium (II) nitrate hexahydrate and iron (III) nitrate nanohydrate were dissolved in 100 ml of degassed deionized water (DDW) yielding a solution with a Mg:Fe molar ratio of 2. This solution was added to a reactor equipped with a pH meter dropwise and under rigorous magnetic stirring, purging nitrogen gas in order to prevent carbonate contamination. The increase of pH of the resultant slurry caused by the metal addition in the reactor was controlled to remain between 10 to 10.5 by the adding of a 2 M KOH solution during the synthesis. The coprecipitation product was aged for 24 hours followed by three times subsequent washing with DDW water and centrifuging (10 minutes at 2000 rpm). The resulting solids were dried at 70°C overnight, milled and passed through a 0.5 mm mesh sieve.

### 5.2.2. Characterization of LDH

The chemical composition of synthesized LDH was determined by inductively coupled plasma optical emission spectrometry (ICP-OES; Perkin Elmer Optima 3300 DV) through acid digestion (20% HNO<sub>3</sub>). Powder X-ray diffraction scans were performed using a Philips PW 1877 diffractometer; with Ni-filtered Cu- K $\alpha$  radiation; a 0.02° step size and one second counting time. The scan ranged from 3° to 90°. Fourier Transform Infrared (FT-IR) spectra were recorded on a Shimadzu IRPrestige-21 spectrometer. Spectra were recorded by accumulating 50 scans in the 4600–400 cm<sup>-1</sup> spectral range in absorbance mode with a resolution of 2 cm<sup>-1</sup>. Approximately 0.50 mg of sample was homogenized in 250 mg of spectroscopic-grade KBr and pressed into a pellet for analysis. Samples were analyzed immediately after preparation in a nitrogen atmosphere. Thermogravimetric analyses (TGA) were carried out with a DTG-60H-Simultaneous DTA-TG; Shimadzu; Kyoto; Japan. The scans were performed from room temperature to 1200 °C; heating rate 10 °C min<sup>-1</sup> in a nitrogen atmosphere.

### 5.2.3. Nitrate release batch experiments

Different background electrolytes ( $\text{CaCl}_2$ ;  $\text{KCl}$  and  $\text{K}_2\text{SO}_4$ ) were tested in order to assess nitrate exchangeability by common counter-anions. For equilibrium experiments; 50 milligrams of milled as-synthesized LDH was dispersed in 20 ml of solutions containing 0.5; 0.1 and 0.01 mol  $\text{L}^{-1}$  of  $\text{CaCl}_2$ ;  $\text{KCl}$  and  $\text{K}_2\text{SO}_4$  in centrifuge tubes. Three replicate samples were subsequently shaken during 2 h followed by centrifugation at 2000 rpm for 3 minutes. Kinetic experiments of nitrate release were performed using 0.01 mol  $\text{L}^{-1}$  of  $\text{CaCl}_2$ ;  $\text{KCl}$  and  $\text{K}_2\text{SO}_4$ . In these experiments; the nitrate concentration at different times was measured by the extraction of supernatants. For both equilibrium and kinetic batch experiments; the relative amount of released nitrate (nitrate concentration in extracted supernatants relative to the initial nitrate concentration in the batch) was reported.

### 5.2.4. LDH dissolution experiment

A LDH dissolution experiment was conducted by dispersing 500 mg of LDH powder in 50 ml of solutions with different pH (between 3-9) synthesized by  $\text{H}_2\text{SO}_4$  or  $\text{KOH}$  carried out under end over end mixing for 24 hours. The pH; ranging from moderately acid to slightly alkaline; corresponds to values typically found in soils. After shaking; samples were centrifuged for 10 minutes at 3000 rpm and the supernatant was withdrawn for determination of dissolved Mg and Fe by atomic adsorption spectroscopy. The release fraction of the components is the ratio of the concentration of Mg or Fe in the supernatant at each pH relative to the total concentration of the metal in the LDH.

### 5.2.5. Soil column study

Soil column experiments were performed with material from temperate soils from Denmark and tropical soils from Brazil, with selected properties given in Table 1. Columns with temperate soils were larger (9.6 cm diameter) in order to obtain transport parameters, while smaller columns (diameter of 2.5 cm) with tropical soil material were used for X-ray fluorescence spectroscopy (XRF) line scan. The height of columns in both experiments was 8 cm.

To evaluate how fast nitrate is released from LDH under flow conditions, two replicates from each of the larger soil column with temperate soil material from Denmark were physically and chemically equilibrated by running a flow of  $0.01 \text{ mol L}^{-1} \text{ CaCl}_2$  for 6 hours. In sequence, the soil surface in the column was covered by a thin layer of 3 g LDH, uniformly applied and avoiding about a few mm nearby the column walls, and flow was run again. The concentration of nitrate was measured in collected leachate. Although there is a variety of methods to perform LDH transport experiments at column scale, for the purpose of this study the surface application matches most with reality as mineral fertilizers are typically spread on the soil surface. Another advantage of surface application resides in the possibility of performing the nitrate transport experiment before and after addition of LDH. LDH amended soil prohibits the possibility of establishing in advance equilibrium condition, consequently the soil free of LDH should be used. One could consider mixing a thin layer of soil with LDH particles, but this would cause a loss in uniformity and continuity, especially important under unsaturated flow conditions.

The soil column study was designed to explore the fate of nitrate in cases where LDH particles are used as nitrate source. In order to verify the capability of LDH to perform retention of nitrate from an external source, a pulse of  $\text{KNO}_3$  was applied before and after covering the surface of the column with LDH. Subsequently, the leaching of intercalated nitrate was investigated after the added nitrate from  $\text{KNO}_3$  was completely washed from the soil column. Finally, when the nitrate from the previous step was totally washed away, another pulse of  $\text{KNO}_3$  was applied to investigate to what extent the remaining LDH particles were capable to retain the nitrate. Breakthrough curves (BTCs: relative solute concentration versus relative time) of nitrate were obtained for all steps and compared to assess nitrate retention by LDH particles.

Soil column studies with tropical soil material were designed to better explore the fate of added cationic LDH components. In Brazil, 58% of territory is covered by highly weathered Oxisols and Ultisols which are rich in Fe and Al (hydr)oxides. Management practices to rise pH (mainly by liming) are widely used to reduce the availability and toxicity of these elements and enhance the availability of anions like phosphates. Therefore, addition of any mineral fertilizer composed of Fe or Al to these soils would be a countersense. The smaller columns with tropical soil material were physically and chemically equilibrated like the temperate soil columns. A pulse of nitrate tracer was applied and LDH was added on top in four steps, adding 20, 50, 100 and 100 mg. Each adding was done when all nitrate from the previous step had been removed from the column, warranted by allowing enough time of washing with the background

solution at known concentrations. Finally, a pulse of nitrate was applied to assess the nitrate adsorption of remaining LDH particles.

After finishing the leaching experiments in the columns with tropical soil material, they were cut longitudinally into two hemicylinders which were dried at 45°C for a week. In order to trace the diffusion of LDH along the soil column, the hemicylinders were line-scanned by X-ray fluorescence (XRF) spectroscopy. XRF scanning is noninvasive and generates high resolution records of elemental variations of unprocessed samples (CHAWCHAI et al., 2016). The XRF intensity of Mg and Fe were monitored using a 1 mm X-ray beam under vacuum conditions. The measurements were performed using a benchtop  $\mu$ -XRF system (Orbis PC EDAX, United States) furnished with a Rh anode operating at 400  $\mu$ A of tube current beside 40kV. The Si-SDD detector worked at 20 s dwell time.

Table 5.1. Some properties of temperate (Denmark) and tropical (Brazil) soils used in soil column experiments

sample	Region and column size	clay (%)	Silt (%)	Sand (%)	OM (%)	BD (g cm <sup>-3</sup> )	texture
S(S) <sup>†</sup>		0	0	100	0	1.41	Sand
S(L) <sup>††</sup>		0	0	100	0	1.39	Sand
Fensholt	Denmark Ø 9.6 cm height 8 cm	19.8	17.2	57.1	5.9	1.35	Sandy clay loam
Foulum		10.8	8.7	79	1.5	1.44	Sandy loam
Aarslev		11.2	18.6	72.7	2.5	1.41	Sandy Loam
B1	Brazil Ø 2.5 cm height 8 cm	55	16	29	1	1.65	Clay
B2		17	12	71	5	1.75	Sandy Loam

<sup>†</sup> 0.9-1.6 mm grain diameter <sup>††</sup> 0.18-0.5 mm grain diameter

### 5.2.6. Solute Transport Parameters Estimation

The data from obtained BTCs of temperate soils were fitted to the dimensionless advection dispersion equation (ADE) Equation 5.1 to obtain the respective soil transport parameters and to assess the changes in these parameters caused by the addition of LDH:

$$R \frac{\partial c}{\partial T} = \frac{1}{P} \frac{\partial^2 c}{\partial X^2} - \frac{\partial c}{\partial X} \quad (5.1)$$

where  $T(=v.L/t)$  and  $X(=x/L)$  are the dimensionless time and distance ( $L$ : length of soil column and  $v$  is pore water velocity ) and  $c$  is the normalized concentration representing reduced

volume averaged solute concentration and R is retardation factor. The Peclet number; ( $P = L/\lambda$ ); where  $\lambda$  is the length of flow path ( $\lambda = D/v$ ) and D is effective dispersion coefficient [ $ML^{-2}$ ]; allows to assess which mechanism of transport (advection or diffusion) dominates the flow. Larger values of the Peclet number indicate domination of advection dispersion transport to diffusion. If the equilibrium model (Equation 5.1) failed to describe BTCs; a two region non-equilibrium model; Equation 5.2; was used which takes into account mobile and stagnant water:

$$\beta R \frac{\partial c_m}{\partial T} = \frac{1}{P_m} \frac{\partial^2 c_m}{\partial X^2} - \frac{\partial c_m}{\partial X} - \omega(c_m - c_{im}) \quad (5.2)$$

$$(1 - \beta)R \frac{\partial c_{im}}{\partial T} = \omega(c_m - c_{im}) \quad (5.3)$$

where m and im subscripts refer to the mobile and immobile phase;  $\beta$  a dimensionless non-equilibrium partitioning coefficient varies from 0 (all non-equilibrium) to 1 (all equilibrium) and; and  $\omega$  is a dimensionless mass transfer coefficient determining the rate of exchange between mobile and immobile fluid regions.

### 5.3. Results and Discussion

#### 5.3.1. LDH Characterization

ICP-OES revealed an experimental Mg:Fe molar ratio of 2.13 (or:  $x = 0.32$ ) which confirmed the prior assumption regarding the value of  $x$ , showing correct elemental composition. Sharp and asymmetrical peaks at low  $2\theta$  values and only some asymmetrical peaks at high angles for XRD pattern (shown in Figure 5.1) are typical pattern of the formation of the good crystalline LDH materials (FERREIRA et al., 2004; SASAI et al., 2012). Layered structures with a basal distance ( $d_{003}$ ) of 8.07 obtained from Bragg's law with peak occurring at  $11.01^\circ$  which is similar to the values reported by Chao et al. (2008) and Nejati et al. (2011). Consequently, lattice parameters including  $c (=3 \times d_{003}) = 24.21 \text{ \AA}$  and  $a (=2 \times d_{110}) = 3.11 \text{ \AA}$  are therefore compatible with results from Halajnia et al. (2012) and Shafigh et al. (2019). Considering  $4.8 \text{ \AA}$  as constant layer thickness of brucite, resulting interlayer thickness was  $3.27 \text{ \AA}$ , capable of allocating nitrate ( $2.76 \text{ \AA}$ ) and water inside. The same results were reported by Imran et al. (2016) and Olfes et al. (2009) under very similar synthesis conditions. Note that basal spacing for nitrate intercalated LDH, mostly synthesized by Mg and Al, were reported between  $7.8$  to  $8.8 \text{ \AA}$  due to varying effective parameters such as

type of cation,  $x$  and pH (OLANREWAJU et al., 2000; UREÑA-AMATE et al., 2011; HALAJNIA et al., 2012; EVERAERT et al., 2016).

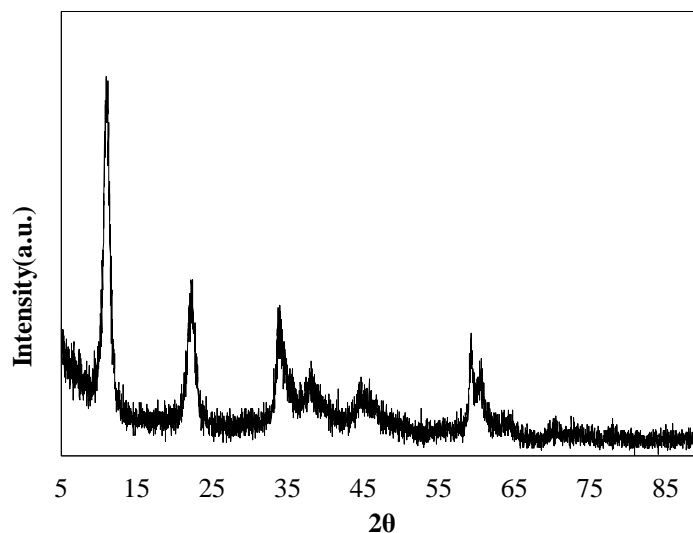


Figure 5.1 XRD patterns of synthesized LDH

Infrared analyses of synthesized LDH allowed to verify the nitrate intercalation by detecting a typical vibrational band profile of anionic clay materials. FTIR spectra (Figure 5.2) at low wavelength ( $<600\text{ cm}^{-1}$ ) were attributed to the vibration of metal oxygen (MOM; OM; and OMO). As an example; the spike at  $567\text{ cm}^{-1}$  was due to  $\text{FeO}_6$  and  $\text{MgO}_6$  octahedral bonds and are typical of LDH solid materials as mixed oxides were precipitated (OLFS et al., 2009; BERBER et al., 2014). However; the shoulder at  $1070\text{ cm}^{-1}$  is assigned to N-O stretching bands besides the most intense and striking absorption band at  $1384\text{ cm}^{-1}$  ( $\nu_3$ ); which proved incorporation of free nitrate anion in interlayer of LDH. The presence of the band centered at  $827\text{ cm}^{-1}$  is caused by ( $\nu_4$ ) mode of the same anion (WANG; WANG, 2007; YANG et al., 2015). A small shoulder occurred at around  $3000\text{ cm}^{-1}$  because of hydrogen bonding between water and intercalated anion (CAVANI et al., 1991). OH stretching ( $\nu_{\text{O-H}}$ ) from both water molecules and hydroxyl groups were characterized by a broad band at  $3435\text{ cm}^{-1}$  followed by an adsorption band at  $1635\text{ cm}^{-1}$ ; indicating the presence of interlamellar water and angular deformation of water molecules connected to nitrate anions in interlayers (BENSELKA-HADJ ABDELKADER et al., 2011; BENICIO et al., 2017).

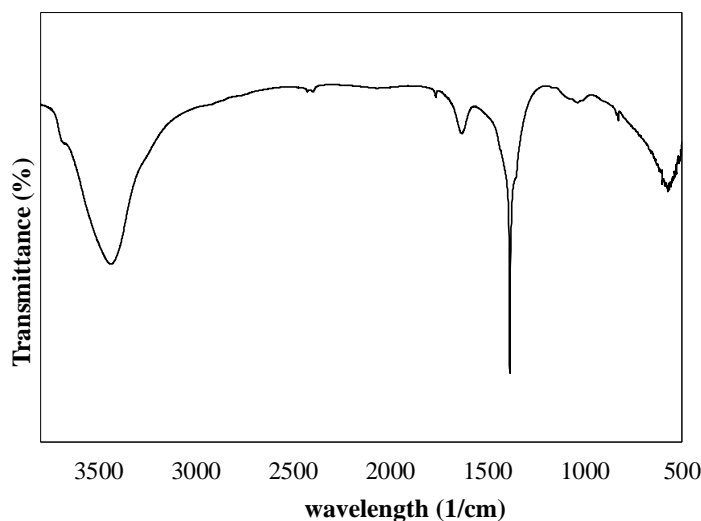


Figure 5.2 FTIR spectra of synthesized LDH

The thermogravimetric analysis (TGA) is a robust tool to estimate the total water content (both adsorbed and interlayer) and to observe the hydroxyl group plus anion loss at higher temperature. The TGA curve (Figure 5.3) showed the final remaining residue to represent 57.36% of the initial mass (36.785 mg) under 1200°C. 19.2% mass was lost up to 303°C, which corresponds to the surface adsorption and interlayer water loss, by which the number of water molecules was determined. Two endothermic effects within this temperature range confirmed total water loss (BENÍCIO et al., 2017). Increasing temperature to 730 °C caused a decrease of sample mass by 20.1%, assigned to the loss of nitrate anions (decomposed to NO<sub>2</sub>) and dehydroxilation of brucite layers followed by an endothermic event in the DTA curve (NAKAGAKI et al., 2016). By the end of TGA, 56.35% of LDH had left as metal oxides and the small exothermic effect after 745 °C was attributed to formation of metal oxides as MgO and probably MgFe<sub>2</sub>O<sub>4</sub>, as demonstrated by Ferreira et al. (2004), Olf et al. (2009) and Abdelkader et al. (2011). Given these results, including  $x=0.32$  and calculation of water content through TGA analysis, the chemical formula of the synthesized LDH was concluded to be  $[Mg_{0.68}Fe_{0.32}(OH)_2](NO_3)_{0.32} \cdot 1.17H_2O$ . The ratio of Mg and Fe cations in the solid particles was equal to that of the initial solution.

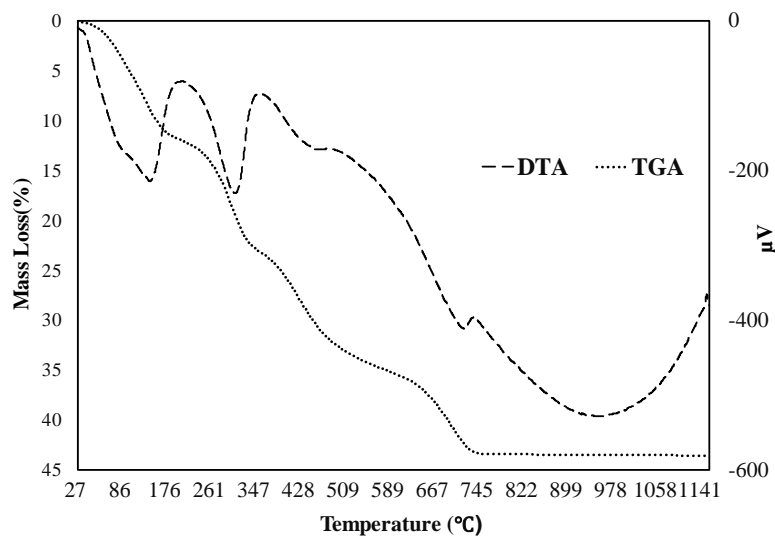


Figure 5.3 TGA and TDA curves of synthesized LDH

### 5.3.2. Nitrate release studies

Figure 5.4 **Error! Reference source not found.** shows how the nitrogen was released from the milled LDH particles in different solutions. It was calculated that 4.11 wt. % of LDH was composed of nitrogen, similar to findings by Noh et al. (2015). There was high affinity for LDH to release the nitrogen equilibrated with chloride or sulphate (Figure 5.4 a) as the fraction of nitrate released was always high in the equilibrium experiments. These results were in good agreement with Komarneni et al. (2003) and Olf et al. (2009), who concluded that the total amount of nitrate in LDH synthesized by  $x=0.33$  was exchanged by sulphate or chloride rapidly. The type of background electrolyte effectively changed the release of nitrate from LDH as Cl from  $\text{CaCl}_2$  was replaced by total nitrate inside the LDH in all ionic strengths. The behavior of nitrate release was evaluated under two conditions: lower (0.01 M) and higher (0.1 and 0.5 M) ionic strength (Figure 5.4 a). According to the results reported by Noh et al. (2015), the presence of Cl<sup>-</sup> in the electrolyte facilitated nitrate to leave LDH types with a high charge density (like in our case,  $x=0.33$ ). This is illustrated in Figure 5.4 a for an ionic strength of 0.01 M. For higher ionic strengths (0.1 and 0.5 M), it seems there was a relation between the mass of anions in the electrolyte solutions and release of nitrate from LDH, as nitrate release increased in the order  $\text{CaCl}_2 > \text{K}_2\text{SO}_4 > \text{KCl}$ , corresponding to an increase in the mass ratio of anion to total background electrolyte mass from 0.47 to 0.55 and 0.64, respectively. This finding is opposite to previous ideas that higher charge density of anion increases their adsorption by LDH.

The fraction of released nitrate from the 0.01 M CaCl<sub>2</sub>, K<sub>2</sub>SO<sub>4</sub> and KCl solutions measured at 15, 30, 60, 90, 120, 180 and 240 minutes is shown in Figure 5.4 b. This figure shows that an exponential function could predict the nitrate release fraction with RMSE of 0.015, 0.03 and 0.02, respectively, while obtained K values for the exponential function were 0.01, 0.015 and 0.017, respectively, for the nitrate desorption from LDH suspended in solutions of KCl, K<sub>2</sub>SO<sub>4</sub>, and CaCl<sub>2</sub>. The nitrate release sharply increased with time up to the second hour, until equilibrium was reached. The initial rapid step (the first two hours) illustrates the fast exchange between nitrate and chloride or sulphate, where sulphate is replaced faster. This implies that in the case of a soil solution composed of a variety of anions, nitrate retention in LDH will be very low.

Consequently, the release of nitrate loaded in LDH particles is fast, occurring in less than 4 hours in batch experiments, and therefore may not be expected to provide slow release conditions for uptake by plant roots. Moreover, LDH contain no more than ca. 5 wt. % of nitrogen (KOMARNENI et al., 2003) and around 30 to 50% of Mg, Al or Fe, all heavy metals which are potentially toxic contaminants.

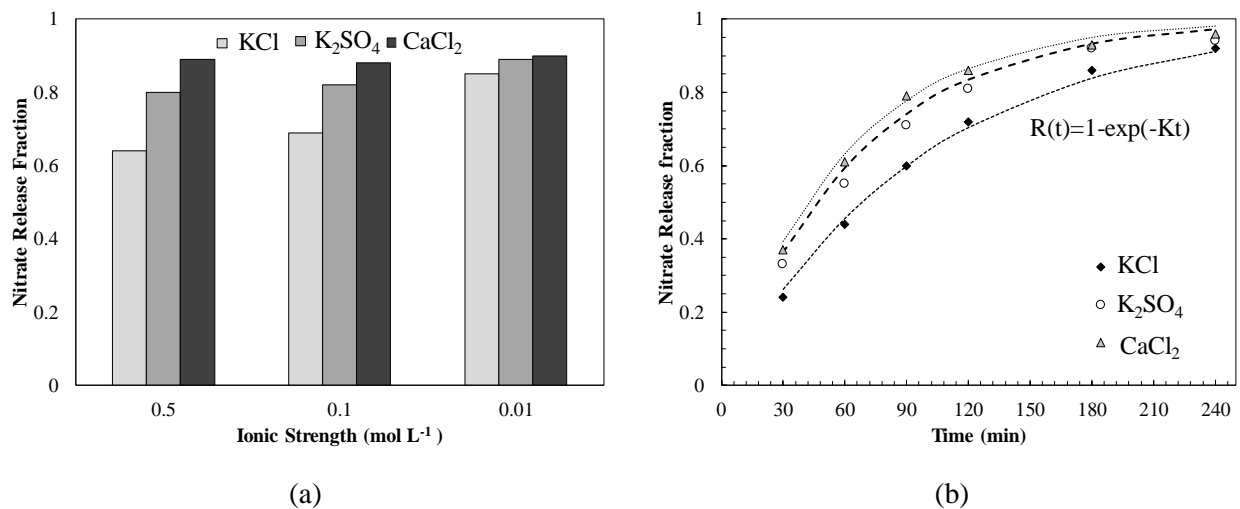


Figure 5.4 Nitrate release fraction from LDH particles dispersed in of KCl, K<sub>2</sub>SO<sub>4</sub>, and CaCl<sub>2</sub> solutions with 0.01, 0.1 and 0.5 mol L<sup>-1</sup> ionic strength performed in the equilibrium (a) and in time dependent (kinetic) experiments (b)

### 5.3.3. LDH dissolution

Although LDHs are stable at pH values normally found in soils; one should consider that acidic root exudates can decrease locally the pH (JOBÁGY; REGAZZONI, 2011). Dissolved fraction of Mg in suspensions with different initial mass and pH is shown in Figure 5.2. No dissolved Fe was observed in any scenario. Up to pH 4; less than 5% of Mg was dissolved in suspensions with higher initial mass (0.01; 0.1 and 0.2 g) while twice as much was dissolved in a suspension with 0.05 g LDH. At pH 3; 25% of total Mg in LDH was dissolved in  $\text{H}_2\text{SO}_4$  (2M) when 0.05 g LDH was initially mixed. However; Mg dissolution in concentrated suspension (0.2 g LDH) did not exceed more than 5% within the range of pH used in our experiments. The cation dissolution is associated with proton consumption. The Fe(III) (hydroxide) enriched material precipitated within the whole range of pH (3-9) because of extremely low dissolution rate considering solubility product ( $K_{sp}$ ) of  $\text{Fe}(\text{OH})_3$  equal to  $-37$  (MEIGHAN et al., 2008). Hence dissolution of LDH is non stoichiometric and governed by Mg dissolution (SCHECKEL et al., 2000).

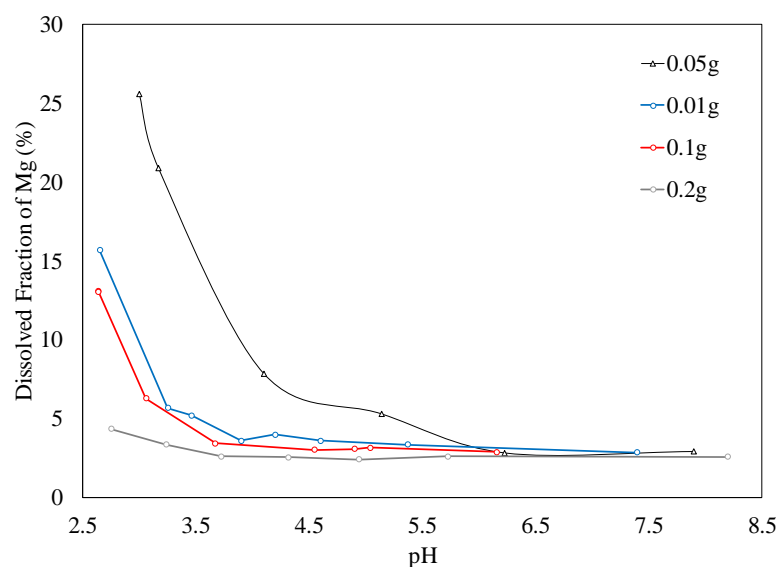


Figure 5.5 Dissolved fraction of Mg of LDH as a function of initial mass of LDH and pH of electrolyte background

### 5.3.4. Breakthrough curve analysis of temperate soils

In soil columns, the fast release of loaded nitrate in LDH, representing 4% of total LDH mass, was confirmed by the early peak of relative mass shown in Figure 5.5. The earliest peaks of relative mass, at about 0.5 relative pore volume, were observed in columns filled with Aarslev and Fensholt soil material. Generally, the asymmetric shape of the BTCs associated with a long tail for the Fensholt soils is probably related to their higher organic matter content and smaller sand fraction (Table 5.1). Intense organic farming in Fensholt region increases its organic matter content. BTC of columns from Foulum and large-grain sand (L) were alike, with fast recovery in the sandy Foulum soils.

It can be inferred that soil type and field management are determining factors for the retardation of nitrate leaching, more impacting than the use of LDH particles, because soils with higher organic matter contents showed longer tails in their BTC, in agreement to results by Jin et al. (2016). The total amount of intercalated nitrate available in the surface spread LDH was removed after washing with 1.5 to 2 pore volumes, therefore LDH particles seem inefficient as slow release fertilizer. The concentration of Mg in the collected leachates were below the limit of detection, which agrees with the result of the batch experiments where a low dissolution rate of Mg in an environment at medium pH (5.8 to 7.2) was observed (Figure 5.5).

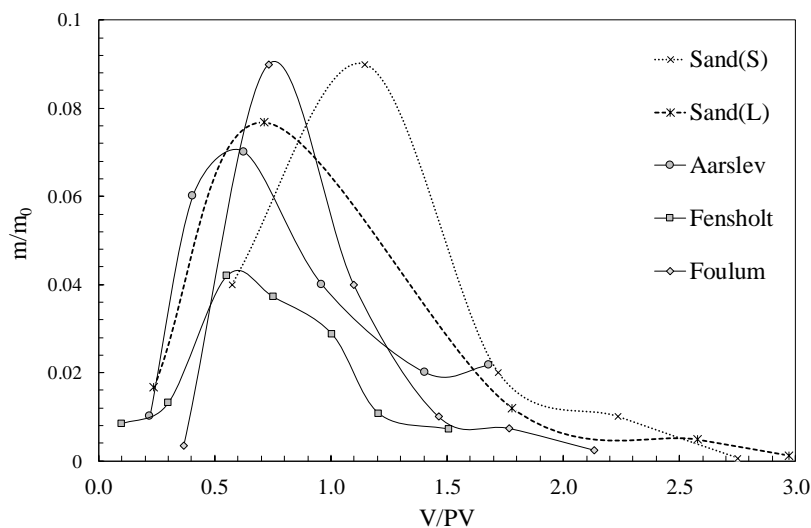


Figure 5.6. Breakthrough curves showing the relative loaded nitrate concentration ( $m/m_0$ ) as a function of the amount of leachate collected relative to the total pore volume ( $V/PV$ ) after applying 3 g of LDH on the soil surface of columns with material from five Danish soils

For the second purpose of study, determining the retardation of nitrate by LDH particles, Figure 5.7 demonstrates the breakthrough curves of nitrate applied before and after addition of LDH, where Figure 5.7 a just gives information about the columns filled with pure small and large-grain sands (S and L) and Figure 5.7 illustrates BTCs for soils collected from fields in Denmark. A good agreement was obtained for the shape of replicate BTCs.

Results obtained using STANMOD (VAN GENUCHTEN et al., 2012) used to estimate equilibrium or non-equilibrium transport parameters are shown in Table 2. Symmetrical BTCs are typical in scenarios with a conservative tracer at steady rate in the absence of an immobile phase or a physical non-equilibrium. Sand columns (S and L) showed bell-shaped BTCs because of their high mobile water content, which results from low structural heterogeneity (GONZÁLEZ-DELGADO; SHUKLA, 2014). In these columns,  $(C/C_0)_{\max}$  occurs at about 1.1-1.3  $V_R$  for both the small and large grain size sands (S and L). After the addition of LDH on the surface of these sand columns, the reduction in  $(C/C_0)_{\max}$  was just 3.5 and 6.8%, respectively. The reduction of nitrate leaching reported in this study, and also Halajnia et al. (2016) using LDH particles, is smaller than the strong nitrate removal ability of Purlite resin (GUPTA et al., 2012) or high capacity of nitrate reduction by Fe nanoparticles (KIM et al., 2012). Equilibrium ADE perfectly describes the BTCs while LDH addition increases dispersivity ( $\lambda$ ) by respectively 0.13 and 0.03 cm in both sand types S and L (Table 5.2).

Characteristics of BTCs were different in columns with real soil material which present a non-uniform particle size distribution and contains organic matter. In field soil scenarios, nitrate retention did not change significantly as  $(C/C_0)_{\max}$  declined by 5, 6 and 9 % for Aarslev, Fensholt and Foulum, respectively. This small reduction was not caused by the LDH, as the  $\text{Fe}(\text{OH})_3$  enriched materials and Mg are accumulated on the soil surface and were never transported down for more than a few millimeters. However, the high sand content in Foulum soils made their BTC shape and trend similar to the pure sands (L) and (S), with a sharp peak and short tail. Recovery of nitrate in this column after LDH application was reduced by 14%, whereas dispersivity increased from 0.064 to 0.079 cm (Table 5.2).

The asymmetry in BTCs for Aarslev and Fensholt soil columns is probably caused by preferential flow and the presence of immobile water. Nitrate transport in Fensholt and Aarslev is limited by diffusion, as their dispersivity is larger than in Foulum soil and the pure sands, resulting in a flow dominated by advection (Table 5.2). In the Fensholt soil, with 5% of organic matter, the peak was observed earlier than 1 relative pore volume due to anion exclusion

because of negatively charged particle surfaces (PIÑÓN-VILLARREAL et al., 2013). As a result, this soil did not show a significant reduction in nitrate loss because recovery was constant (Table 5.2). Nevertheless, LDH reduced the recovery of nitrate by 13% in the Arslev soil, and its BTC was skewed to the right resulting in an increase in  $V_{R\ BT10}$  and  $V_{R\ BT50}$  (relative pore volume when 10 and 50% of accumulated  $C/C_0$  occurred) by 0.1 and 0.3 (Table 5.2). Hence, non-equilibrium CDE explained the variation of  $C/C_0$  for this soil with non-equilibrium ( $\beta$ ) and mass transfer ( $\omega$ ) coefficients of 0.35 and 0.09 when LDH had been applied (Table 5.2). A similar tail on the right side of the BTC and also 15% reduction in  $(C/C_0)_{\max}$  was observed by Sepasbaksh et al. (2007) in a saturated condition column experiment filled with loamy soils amended with  $8\text{ g kg}^{-1}$  zeolite. The average pH of the collected leachate was  $6.4\pm 0.3$ , causing positive sites for nitrate adsorption. Long tail and larger residence times are other characteristics of these BTCs.

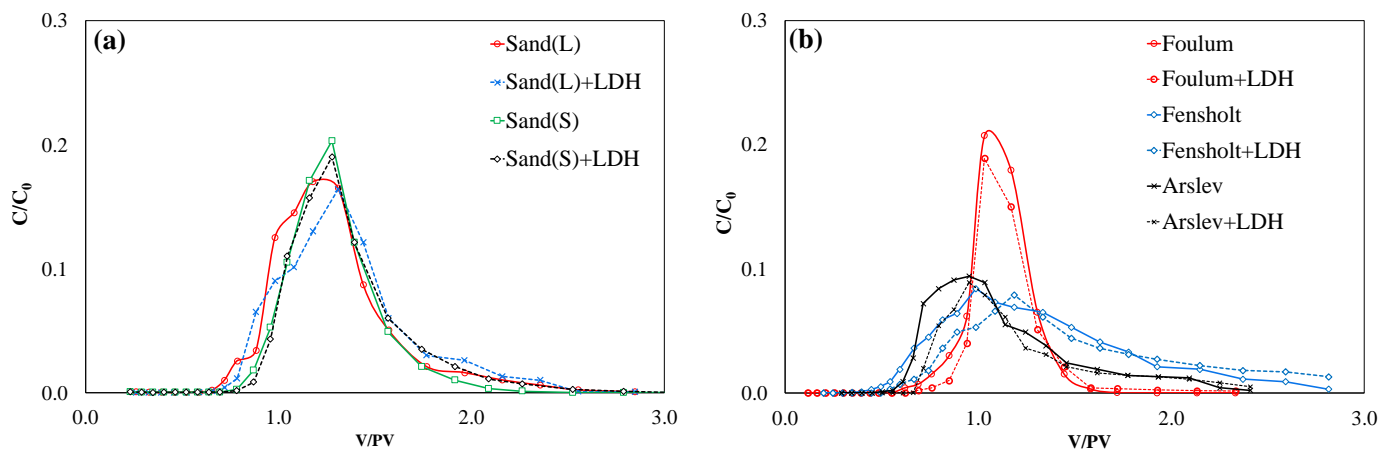


Figure 5.7 Breakthrough curves of (a) sand (L; large sand, S: small sand) and (b) real soil packed columns (with the name of locations as mentioned in Table 5.1), showing the relative loaded nitrate concentration ( $C/C_0$ ) as a function of the amount of leachate collected relative to the total pore volume ( $V/PV$ ) after applying 3 g of LDH on the soil surface of columns with material from five Danish soils before and after addition of LDH

Table 5.2. Transport parameters obtained with STANMOD for temperate soil columns with and without (control) LDH

Soil		$(C/C_0)_{\max}$	Recovery	$V_{R(C/C_0)_{\max}}$	$V_{R_{BT10}}$	$V_{R_{BT50}}$	$V(\text{cm/h})^\dagger$	$\lambda(\text{cm})^\dagger$	$\beta^\dagger$	$\omega^\dagger$	$R^2$
Sand(L)	Control	0.17	100±0.02	1.18	0.92	1.18	2.72	0.184	-	-	0.978
	LDH	0.13	96±0.04	1.31	0.92	1.27	2.52	0.312	-	-	0.966
Sand(S)	Control	0.20	100±0.009	1.28	0.98	1.20	2.29	0.105	-	-	0.989
	LDH	0.18	100±0.004	1.28	1.00	1.24	2.20	0.134	-	-	0.982
Foulum	Control	0.21	95±0.04	1.03	0.89	1.06	2.54	0.064	-	-	0.981
	LDH	0.18	81±0.06	1.03	0.95	1.12	2.64	0.079	-	-	0.923
Fensholt	Control	0.08	100±0.08	0.99	0.73	1.15	2.36	0.77	-	-	0.975
	LDH	0.07	98±0.04	1.18	0.85	1.33	2.02	0.78	-	-	0.957
Arslev	Control	0.09	80±0.03	0.95	0.74	1.13	2.29	0.48	0.56	0.05	0.884
	LDH	0.08	67±0.04	0.95	0.83	1.43	1.32	0.31	0.35	0.09	0.986

V: average pore water velocity (cm/h);  $\lambda$ : dispersivity (cm);  $\beta$ : non-equilibrium partitioning coefficient;  $\omega$ : mass transfer coefficient

### 5.3.5. Breakthrough curve analysis of tropical soils

The experiments performed in columns with tropical soil material from Brazil (Figure 5.8) agreed with those carried out with Danish soils, suggesting that the LDH does not provide a gradual release of nitrate. The experiments with material from two soils of clayey (B1) and sandy loam (B2) textures started with tracer application and an almost full recovery of nitrate was observed (95% in the clay soil 98% in the sandy loam soils, Figure 5.8). Subsequently, LDH was applied to the soil surface. Differences between relative concentrations of replication in Figure 5.8 a (soil B1) when 20, 50 and 100 mg of LDH was added was due to large resolution measurement of nitrate in the collected pore volumes however both replicates behave in the same way in terms of nitrate mass balance in these steps. It should be noted that the CDE curve fitting was not carried out for these experiments because soils columns were small and the wall effect would be significant.

There was an insignificant change in relative pore volume (less than  $0.3 V_R$ ) required to remove nitrate tracer between initial and end (the first and last five  $V_R$  in Figure 5.8) of nitrate application, while the recovery of nitrate was around 4% lower for the latter. Recovery of removed intercalated nitrate was  $94\pm 2\%$  on average for the sandy loam soil in all steps.

The nitrate mass balance after LDH application observed for the clay soil (Figure 5.8b) was 86, 82 and 84% respectively when 20, 50 and 100 mg LDH was spread. The ending tracer run was associated with  $(C/C_0)_{\max}$  of 83%, which is 12% less than corresponding value for the primary tracer test. Removal of nitrate from each step in clay soils required on average 2.1, 2.2, 2.7 and 3.2  $V_R$  respectively for 20, 50, 100 and 100 mg of LDH and there was about 1.8  $V_R$  increase in removal of the last nitrate tracer compared to the initial nitrate tracer application.

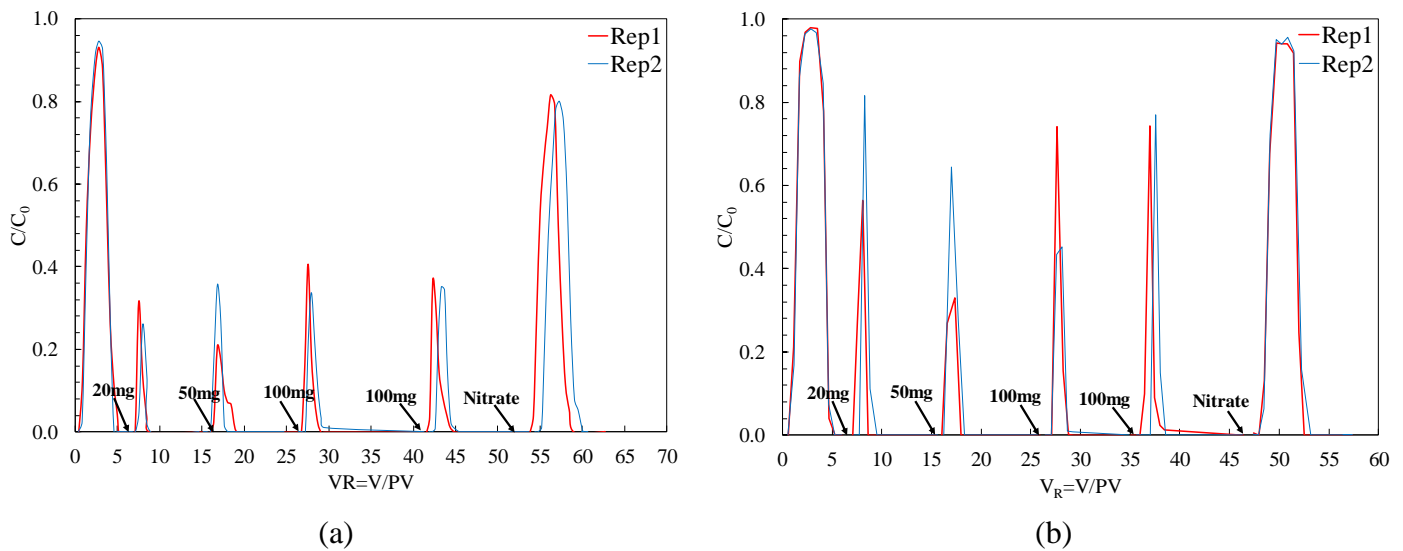


Figure 5.8 Relative nitrate concentration ( $C/C_0$ ) as a function of the amount of leachate collected relative to the total pore volume ( $V/PV$ ) after application of different doses of LDH (arrows show when and how many mgs of LDH was applied) in various steps in clay (B1: a) and loamy sandy soil (B2: b)

Figure 5.9 **Error! Reference source not found.** shows XRF intensity counts of Mg and Fe s, detected by scanning of three lines for each soil column filled with tropical soil material. High surface accumulation of LDH cationic components was expected, firstly because a very low dissolution rate of Mg and Fe was already verified in batch experiments (Figure 5.5) and secondly because of the implementation of experimental measures similar to field conditions, including step addition of LDH on the surface and establishment of an unsaturated zone.

On average, the highest peaks of intensities for either Fe or Mg were found in the top first cm of the soil column, around 5 mm, showing a strong retention of LDH particles at the end of the leaching experiment after applying about 55 pore volumes. A high retention of metal components of LDH particles added to soil columns was recently reported by Jiang et al. (2019), especially when ionic strength for potassium increased from 1 to 100 mM. A very low vertical

transport of iron was observed by Al-Sid-Cheikh et al. (2019) using  $\mu$ XRF line scanning when nano magnetite particles were applied with water flow on top of soil columns filled with wetland organic-rich soil. In case of long term penetration of the remained amorphous form of iron oxyhydroxides, they can be accumulated on root surfaces creating a barrier for elemental adsorption (TRIPATHI et al., 2014). The net intensity of Mg was lower than Fe due to intrinsic elemental sensitivity (RODRIGUES et al., 2018). The clay fraction of weathered tropical soils is mainly composed of 1:1 clay minerals and iron and aluminum oxides and hydroxides, explaining the intensities for Fe recorded for clay soil (Figure bottom) to be higher than the in sandy soil material (Figure 5.9: top) (PEREIRA et al., 2019).

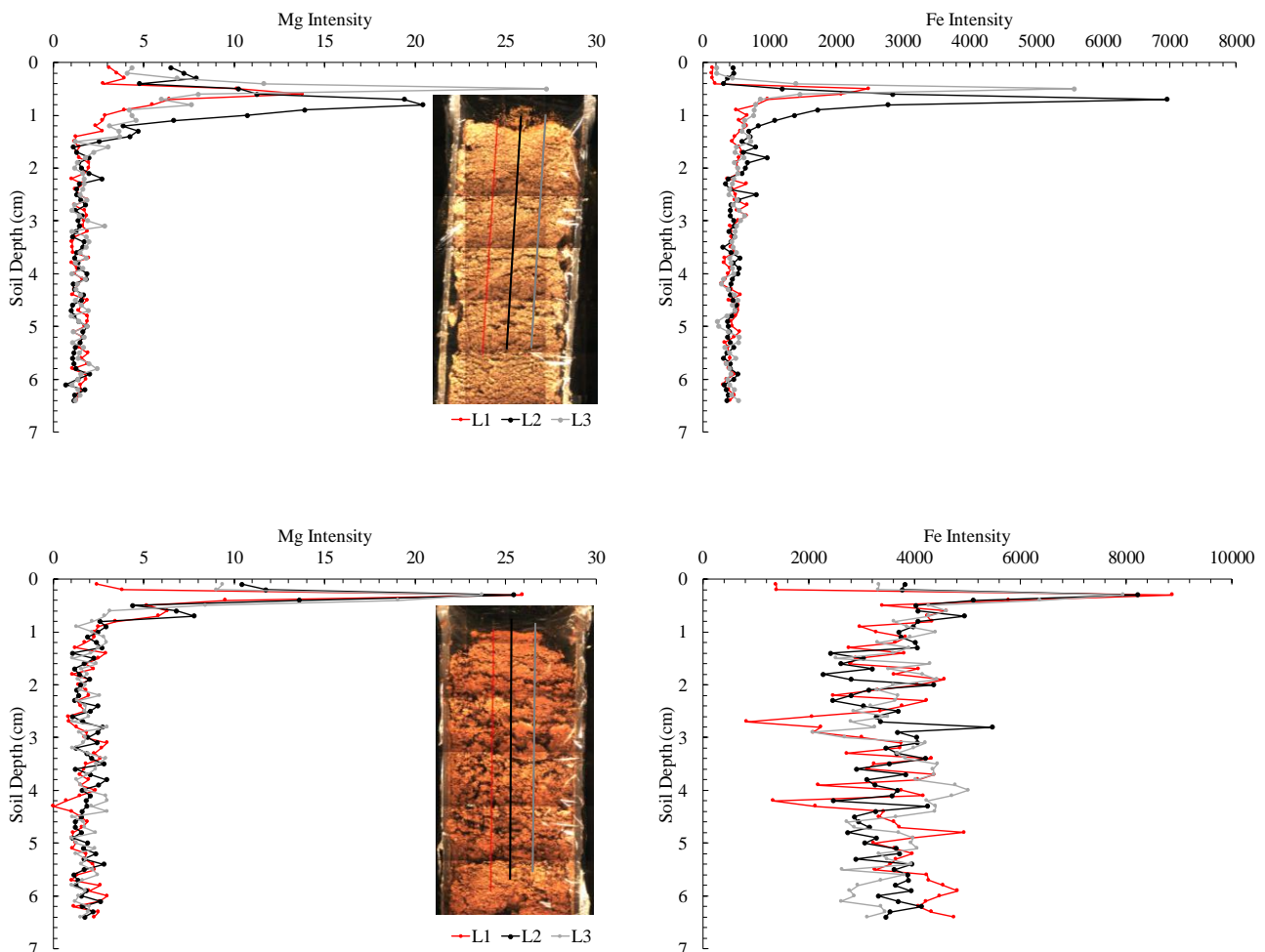


Figure 5.9. Mg (left) and Fe (right) intensities obtained from line scanning of two soil columns; sandy loam (B1: top) and clay (B2: bottom) by EDXRF; (L1; L2 and L3 are scanned lines)

### 5.3.6. LDH in practice

Recalling the chemical composition of LDH ( $[M_{1-x}^{2+}M_x^{3+}(OH)_2]A_{x/m}^{m-}nH_2O$ ); containing Mg; Al or Fe and nitrate with  $0.167 \leq x \leq 0.33$  and  $0 \leq n \leq 5$  (water molecule numbers); the ratio of nitrogen; divalent and trivalent cations to the whole mass of LDH are shown in Table 5.3. The most optimally synthesized LDH contains a maximum of 6% (mass-based) of nitrogen; whereas Mg and Al represent about 50%. These high contents of Mg and Al represent a problem; as they may cause very strong fixation of nutrients like phosphate (VILLEGAS et al., 2003; TEZUKA et al., 2004; GÉRARDIN et al., 2005; MA et al., 2019).

Table 1. LDH components ratio to the total mass of LDH

LDH	N/LDH	M(II)/LDH	M(III)/LDH
Mg-Fe-NO <sub>3</sub>	2.6-5.2	13.6-27.4	10.5-20.8
Mg-Al-NO <sub>3</sub>	2.8-5.8	14.7-29.3	5.3-11.3

In conventional fertilization; around 120 kg N ha<sup>-1</sup> is annually applied on farmlands. Considering a soil bulk density of 1300 kg m<sup>-3</sup> and a rooting depth of 30 cm; this amount is equivalent to 31 mg N kg<sup>-1</sup>. Applying the same amount of N in the form of LDH; either Mg-Fe or Mg-Al based; requires in between 2 to 4 tons LDH ha<sup>-1</sup>; thus introducing 400 to 1050 kg Mg and 230 to 478 kg of Fe or Al; depending on  $x$  of LDH with no intercalated water.

An 80% reduction in nitrate leaching reported in Torres-Dorante et al. (2009) and Halajnia et al. (2016) due to application of 10 and 20 g LDH kg<sup>-1</sup> is on one hand in contrast to our findings that show only a 10 to 30% reduction due to tracer like behavior of nitrate and inactivity of LDH residues. On the other hand; 10-20 g LDH per kg of soil is equivalent to application of 39 to 78 ton LDH for a one-hectare field with 30 cm root zone which is associated with metal accumulation and the cost of LDH synthesis become significant at larger scales. Accumulation of large amount of metals as byproduct of LDH and their possible leaching depending on soil structure and rainfall intensity to groundwater along besides increasing phosphate fixation potential due to the increase of Al or Fe contents in the soils are possible negative effects. Compared to the inexpensive or even free sources of nitrogen fertilizer as

manure or urea from livestock; the justification of using LDH as promising material for large-scale use in agriculture apparently cannot be confirmed based on leaching reduction and needs more investigation.

#### 5.4. Conclusion

The application of layered double hydroxide as potential slow release fertilizer is discussed in this study through batch and soil column experiments with soils from temperate and tropical areas. The results for case studies here provided main conclusions:

- (i) nitrogen loading capacity of LDH is between 3 to 7 % of the total mass of LDH.
- (ii) More than 90% of the whole nitrate loaded in LDH particles composed of Fe and Mg is released less than 4 hours confirmed by kinetic and equilibrium batch experiments.
- (iii) Regardless of concentration of LDH in acid solution with pH between 2.5 to 5; Fe cannot be dissolved and at most 25% of the total Mg in LDH can be dissolved.
- (iv) The maximum leaching mitigation of nitrate due to surface application of LDH was 14% in sandy loam temperate soils (Denmark) and no change in recovery of nitrate was observed in tropical soil by addition of LDH.
- (v) High surface accumulation of LDH iron rich residues was confirmed in the top few millimeters of column by line scanning of soil columns after multi step application of LDH.

#### References

AZIZ; T.; MAQSOOD; M. A.; KANWAL; S.; HUSSAIN; S.; AHMAD; H. R.; SABIR; M. Fertilizers and environment: issues and challenges. In: HAKEEM, K. (Ed.). **Crop production and global environmental issues**. Cham: Springer, 2015. p. 575–598.

BENICIO; L. P. F.; SILVA; R. A.; LOPES; J. A.; et al: Layered Double Hydroxides: Nanomaterials for Application in Agriculture; **Revista Brasileira de Ciência do Solo**, v. 39, n. 1, p. 1–13, 2015.

BENÍCIO; L. P. F.; CONSTANTINO; V. R. L.; PINTO; F. G.; VERGÜTZ; L.; TRONTO; J.; DA COSTA; L. M.: Layered double hydroxides: new technology in phosphate fertilizers based on nanostructured materials. **ACS Sustainable Chemistry & Engineering**, v. 5, n. 1, p. 399–409, 2017.

BENSELKA-HADJ ABDELKADER, N.; BENTOUAMI, A.; DERRICHE, Z.; BETTAHAR, N.; DE MÉNORVAL, L. C. Synthesis and characterization of Mg-Fe layer double hydroxides and its application on adsorption of Orange G from aqueous solution. **Chemical Engineering Journal**, v. 169, n. 1–3, p. 231–238, 2011.

BERBER, M. R.; HAFEZ, I. H.; MINAGAWA, K.; MORI, T. A sustained controlled release formulation of soil nitrogen based on nitrate-layered double hydroxide nanoparticle material. **Journal of Soils and Sediments**, v. 14, n. 1, p. 60–66, 2014.

BRUNA, F.; CELIS, R.; PAVLOVIC, I.; BARRIGA, C.; CORNEJO, J.; ULIBARRI, M. A. Layered double hydroxides as adsorbents and carriers of the herbicide (4-chloro-2-methylphenoxy) acetic acid (MCPA): Systems Mg-Al; Mg-Fe and Mg-Al-Fe; **Journal of Hazardous Materials**, v. 168, n. 2–3, p. 1476–1481, 2009.

CAVANI, F.; TRIFIRÒ, F.; VACCARI, A. Hydrotalcite-type anionic clays: Preparation; properties and applications. **Catalysis Today**, v. 11, n. 2, p. 173, 1991.

EVERAERT, M.; WARRINNIER, R.; BAKEN, S.; GUSTAFSSON, J. P.; DE VOS, D. E.; SMOLDERS, E. Phosphate exchanged Mg-Al Layered Double Hydroxides: a new slow release phosphate fertilizer. **ACS Sustainable Chemistry & Engineering**, v. 4, p. 4280, 2016.

VAN GENUCHTEN, M. T.; ŠIMUNEK, J.; LEIJ, F. J.; TORIDE, N.; ŠEJNA, M. STANMOD: Model use; calibration; and validation; **Transactions of the ASABE**, v. 55, n. 4, p. 1355–1366, 2012.

GÉRARDIN, C.; KOSTADINOVA, D.; SANSON, N.; COQ, B.; TICHIT, D. Supported metal particles from LDH nanocomposite precursors: control of the metal particle size at increasing metal content; **Chemistry of Materials**, v. 17, n. 25, p. 6473–6478, 2005.

GILLMAN, G. Environmentally manageable fertilizers: A new approach. **Environmental Quality Management**, v. 15, p. 59–70, 2005.

GIROTO, A. S.; GUIMARÃES, G. G. F.; FOSCHINI, M.; RIBEIRO, C. Role of slow-release nanocomposite fertilizers on nitrogen and phosphate availability in soil. **Scientific Reports**, v. 7, art. 46032, 2017.

HALAJNIA, A.; OUSTAN, S.; NAJAFI, N.; KHATAEE, A. R.; LAKZIAN, A. The adsorption characteristics of nitrate on Mg-Fe and Mg-Al layered double hydroxides in a simulated soil solution; **Applied Clay Science**, v. 70, p. 28–36, 2012.

HALAJNIA, A.; OUSTAN, S.; NAJAFI, N.; KHATAEE, A. R.; LAKZIAN, A. Effects of Mg-Al Layered Double Hydroxide on Nitrate Leaching and Nitrogen Uptake by Maize in a Calcareous Soil. **Communications in Soil Science and Plant Analysis**, v. 47, n. 9, p. 1162–1175, 2016.

IMRAN, A.; LÓPEZ-RAYO, S.; MAGID, J.; HANSEN, H. C. B. Dissolution kinetics of pyroaurite-type layered double hydroxide doped with Zn: Perspectives for pH controlled micronutrient release, **Applied Clay Science**, v. 123, p. 56–63, 2016.

JOBÁGY, M.; REGAZZONI, A. E. Dissolution of nano-size Mg--Al--Cl hydrotalcite in aqueous media, **Applied Clay Science**, v. 51, n. 3, p. 366–369, 2011.

KOMARNENI, S.; NEWALKAR, B. L.; LI, D.; GHEYI, T.; LOPANO, C. L.; HEANEY, P. J.; POST, J. E. Anionic Clays as Potential Slow-Release Fertilizers: Nitrate Ion Exchange. **Journal of Porous Materials**, v. 10, n. 4, p. 243–248, 2003.

KOTTEGODA, N.; MUNAWEERA, I.; MADUSANKA, N.; KARUNARATNE, V. A green slow-release fertilizer composition based on urea-modified hydroxyapatite nanoparticles encapsulated wood; **Current Science**, v. 101, n. 1, p. 73–78, 2011.

LI, Y.; JIA, C.; ZHANG, X.; JIANG, Y.; ZHANG, M.; LU, P.; CHEN, H. Synthesis and performance of bio-based epoxy coated urea as controlled release fertilizer; **Progress in Organic Coatings**, v. 119, p. 50–56, 2018.

MA, J.; DUAN, P.; REN, D.; ZHOU, W. Effects of layered double hydroxides incorporation on carbonation resistance of cementitious materials. **Journal of Materials Research and Technology**, v. 8, n. 1, p. 292–298, 2019.

MEIGHAN, M.; MACNEIL, J.; FALCONER, R. Determining the solubility product of  $\text{Fe}(\text{OH})_3$ : an equilibrium study with environmental significance; **Journal of Chemical Education**, v. 85, n. 2, p. 254, 2008.

NAKAGAKI, S.; MANTOVANI, M. K.; SIPPEL MACHADO, G.; DIAS DE FREITAS CASTRO, A. K.; WYPYCH, F. Recent Advances in Solid Catalysts Obtained by Metalloporphyrins Immobilization on Layered Anionic Exchangers: A Short Review and Some New Catalytic Results. **Molecules**, v. 21, n. 3, 2016.

NAZ, M. Y.; SULAIMAN, S. A. Slow release coating remedy for nitrogen loss from conventional urea: a review. **Journal of Controlled Release**, v. 225, p. 109–120, 2016.

NOH, Y. D.; KOMARNENI, S.; PARK, M. Mineral-Based Slow Release Fertilizers. **Korean Journal of Soil Science and Fertilizer**, v. 48, n. 1, p. 1–7, 2015.

NYAMANGARA, J.; BERGSTROM, L. F.; PIHA, M. I.; GILLER, K. E. Fertilizer use efficiency and nitrate leaching in a tropical sandy soil. **Journal of Environmental Quality**, v. 32, n. 2, p. 599–606, 2003.

OLANREWAJU, J.; NEWALKAR, B. L.; MANCINO, C.; KOMARNENI, S. Simplified synthesis of nitrate form of layered double hydroxide. **Materials Letters**, v. 45, n. 6, p. 307–310, 2000.

OLFS, H. W.; TORRES-DORANTE, L. O.; ECKELT, R.; KOSSLICK, H. Comparison of different synthesis routes for Mg-Al layered double hydroxides (LDH): Characterization of the structural phases and anion exchange properties. **Applied Clay Science**, v. 43, n. 3–4, p. 459–464, 2009.

SAHA, B. K.; ROSE, M. T.; WONG, V. N. L.; CAVAGNARO, T. R.; PATTI, A. F. Nitrogen Dynamics in Soil Fertilized with Slow Release Brown Coal-Urea Fertilizers. **Scientific Report**, v. 8, art. 14577, 2018.

SASAI, R.; NORIMATSU, W.; MATSUMOTO, Y. Nitrate-ion-selective exchange ability of layered double hydroxide consisting of Mg II and Fe III. **Journal of Hazardous Materials**, v. 215–216, p. 311–314, 2012.

SCHECKEL, K. G.; SCHEINOST, A. C.; FORD, R. G.; SPARKS, D. L.: Stability of layered Ni hydroxide surface precipitates - a dissolution kinetics study. **Geochimica et Cosmochimica Acta**, v. 64, n. 16, p. 2727–2735, 2000.

TEZUKA, S.; CHITRAKAR, R.; SONODA, A.; OOI, K.; TOMIDA, T. Studies on selective adsorbents for oxo-anions. Nitrate ion-exchange properties of layered double hydroxides with different metal atoms. **Green Chemistry**, v. 6, n. 2, p. 104–109, 2004.

TIMILSENA, Y. P.; ADHIKARI, R.; CASEY, P.; MUSTER, T.; GILL, H.; ADHIKARI, B. Enhanced efficiency fertilizers: a review of formulation and nutrient release patterns. **Journal of the Science of Food and Agriculture**, v. 95, n. 6, p. 1131–1142, 2015.

TONG, X.; YANG, Z.; XU, P.; LI, Y.; NIU, X. Nitrate adsorption from aqueous solutions by calcined ternary Mg-Al-Fe hydrotalcite. **Water Science and Technology**, v. 75, n. 9, p. 2194–2203, 2017.

TORRES-DORANTE, L.; LAMMEL, J.; KUHLMANN, H.; WITZKE, T.; OLFS, H. W. Capacity; selectivity; and reversibility for nitrate exchange of a layered double-hydroxide (LDH) mineral in simulated soil solutions and in soil. **Journal of Plant Nutrition and Soil Science**, v. 171, p. 777, 2008.

TORRES-DORANTE, L.; LAMMEL, J.; KUHLMANN, H. Use of a layered double hydroxide (LDH) to buffer nitrate in soil: long-term nitrate exchange properties under cropping and fallow conditions. **Plant and Soil**, v. 315, n. 1–2, p. 257–272, 2009.

UREÑA-AMATE, M. D.; BOUTARBOUCH, N. D.; SOCIAS-VICIANA, M. DEL M.; GONZÁLEZ-PRADAS, E. Controlled release of nitrate from hydrotalcite modified formulations. **Applied Clay Science**, v. 52, n. 4, p. 368–373, 2011.

VILLEGAS, J. C.; GIRALDO, O. H.; LAUBERND, K.; SUIB, S. L., New layered double hydroxides containing intercalated manganese oxide species: synthesis and characterization. **Inorganic Chemistry**, v. 42, n. 18, p. 5621–5631, 2003.

WANG, S. L.; WANG, P. C. In situ XRD and ATR-FTIR study on the molecular orientation of interlayer nitrate in Mg/Al-layered double hydroxides in water. **Colloids and Surfaces A: Physicochemical and Engineering Aspects**, v. 292, n. 2–3, p. 131–138, 2007.

WU, Q.; SJÅSTAD, A. O.; VISTAD, Ø. B.; KNUDSEN, K. D.; ROOTS, J.; PEDERSEN, J. S.; NORBY, P. Characterization of exfoliated layered double hydroxide (LDH; Mg/Al= 3) Nano sheets at high concentrations in formamide. **Journal of Materials Chemistry**, v. 17, n. 10, p. 965–971, 2007.

YANG, Z.; ZHANG, L.; XU, P.; ZHANG, X.; NIU, X.; ZHOU, S. The adsorption of nitrate from aqueous solution onto calcined Mg/Fe hydrotalcite. **Desalination and Water Treatment**, v. 54, n. 12, p. 3400–3411, 2015.

ZHANG, X.; DAVIDSON, E. A.; MAUZERALL, D. L.; SEARCHINGER, T. D.; DUMAS, P.; SHEN, Y. Managing nitrogen for sustainable development. **Nature**, v. 528, n. 7580, p. 51, 2015.

## 6 Final Remarks

In conventional agriculture, the fast-downward movement of nitrate into the soil makes farmers applying fertilizers more frequently to supply soil demands, which results in groundwater contamination. But what if the required amount of nitrate for plant is released steadily or synchronized with crop demand? This is the main idea of slow release fertilizer, where the compounds are supposed to be released at a much slower rate, so the farmer can avoid waste of resources and environmental contamination. However, in this technique important factors that influence the release, including spatial and temporal variability of soil hydraulic and chemical properties and variable climatic conditions are mostly neglected. Slow release fertilizers with variety types of organic and chemical coating materials are designed under laboratory conditions and then applied to field to be validated. As this process can be costly, using calibrated computer models can cut the cost of experimental trials or at least provide a reliable experimental design considering more influential parameters that can be controlled directly in the field. Therefore, in this thesis, we firstly discussed the importance of soil hydraulic properties on drainage under rainfed farming, upon understanding this importance we presented machine learning models combined with inverse modelling to obtain soil hydraulic properties. Later on we showed how numerical modeling using SWAP extended with a nitrogen module can be used to design numerical experiments in order to determine the best possible slow release fertilizer adopted to local soil hydraulic properties and climatic conditions. Finally, layered double hydroxide particles loaded with nitrate as future slow release fertilizers were synthesized and used for batch and soil column experiments filled with soils from temperate and tropical areas to explore their nitrate retention capacity especially under flow condition. These consecutive steps during this PhD project concluded in the below results:

- A soil drainability index (SDI) was established that could be a possible indicator to predict annual drainage from bare soils in the state of Sao Paulo. This index estimates bottom drainage using soils hydraulic function and saturate water contents of different layers in soil profile. SDI, precipitation and reference evapotranspiration together can be used to accurately predict monthly drainage of the bare soil using random forest method. This robust prediction of monthly drainage using machine learning methods can be obtained under planting while using SDI, precipitation and potential transpiration as predictors.
- The use of an automatic drip infiltrometer (ADI) allows a quick method to estimate soil hydraulic functions, especially in the wet range. The experimental observations of ADI including hydraulic conductivity at different pressure heads ( $K(h)$ ) were combined with the water contents of the drier range ( $h < -100$  cm) of the water retention curve estimated using machine learning method inversely modelled with Hydrus 1D. The final soil hydraulic properties of soil columns were mostly in good agreement with observed values.

- The SWAP 1D model extended with a nitrogen module allowed to evaluate the efficiency of application of slow release fertilizer (SRF) with different half-lives (10, 20, 30 and 40 days) for cultivation of summer maize in Piracicaba. The numerical modeling results showed that variation in yield and leaching depends on soil type and climatic condition. For example, SRF with a half-life of 40 days on average reduced the yield for maize cultivated in clay soils by about 300 kg ha<sup>-1</sup>.
- The nitrate contained in layered double hydroxides (LDH) can be released within a few hours under conditions of soil water flow. The remaining metal components may then be accumulated on top of the soil profile, potentially to be washed by erosion and end up in surface water. LDHs are also not able to retain the external nitrate sources added to soil through fertilization, as other competitive anions are likely to occupy the available sites. Therefore, potential application in agricultural management of LDH-based fertilizers seems cumbersome.

There are several possible follow-ups of this thesis research in order to assess the potentials of slow release fertilizers and influential factors. On the other hand, layered double hydroxides are a trending topic requiring more attention and systematic research depending on the target of LDH usage. At the end, some recommendations for future studies are:

- Applying ADI experiments for Brazilian soils using large samples to incorporate structure of the soil in soil hydraulic properties measurement.
- Generating maps of soil hydraulic properties using the dataset collected in the first recommendation in order to perform numerical experiments using SWAP to model crop cultivation in the region under various hypothetical nitrogen fertilizer application including slow release fertilizer.
- Performing of finite element Monte Carlo numerical simulation of hypothetical slow release fertilizers defined by their diffusion coefficient and coating thickness in order to explore the release of nutrients out of fertilizers granules.
- Investigating the available organic matter compounds instead of mineral elements to coat nitrate fertilizer synthesizing slow release fertilizer and determining its sensitive parameters such as thickness of coating, and effect of soil water content and soil chemical composition on the release of nitrate under field trials.